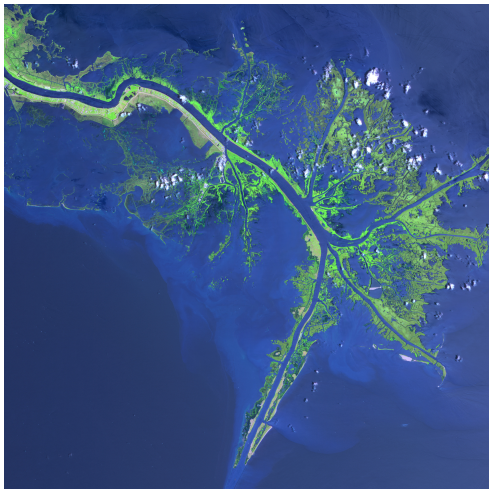

Delft University of Technology

Faculty of Civil Engineering and Geosciences

Department of Hydraulic Engineering

MSc. Thesis

Sediment Management in the Mississippi River

Impact of sediment diversions on the Lower Mississippi River

Author:

Hinnerk Fuhrhop

Graduation Committee:

Prof. W.S.J. Uijttewaal	Delft University of Technology
Dr. ir. C.J. Sloff	TU Delft, Deltares
Dr. ir. M. van Ledden	Delft University of Technology
Dr. E.A. Meselhe	TWIG, Louisiana State University

November 21, 2013

To bestinha and my family.

Acknowledgements

A lot of people contributed to a successful completion of this work with suggestions, comments and support.

First, I would especially like to thank the members of my graduation committee, Wim Uijttewaal, Kees Sloff, Mathijs van Ledden and Ehab Meselhe for their guidance. They were always available for discussing questions and gave important feed-back during committee meetings. A continuous process of exchange and communication helped to improve both scope and quality of the work and, moreover, created an inspiring environment.

At Deltares, several people were involved. I would like to thank Mohamed Yossef who was a great support when it came to establishing the right connections with the Lousiana State University and TWIG and preparing the formulation of the research proposal. Furthermore, I thank Bert Jagers for his support during the implementation of new Delft3D modules and the entire ZWS/RIV department including my fellow students for their support and fruitful discussions.

At LSU/TWIG, I would like to thank the staff for their support and cooperation. I had a very pleasant stay and highly appreciated to be able to work near the Mississippi River. In particular, I would like to thank Hoonshin Jung, Joao F. Pereira, Kazi Sadid, Mead Allison and Clinton Willson.

Last but not least, I want to thank my girlfriend, my friends and my family. They gave me strength and motivation throughout all the time and showed a great understanding for me hiding behind literature and laptop most of the time.

Abstract

The Mississippi River is one of the most engineered rivers in the world. Levees, bank revetments and training dikes ensure navigability and safety against flooding. Construction of dams in the upstream branches led to a decay in sediment supply of 70% during the last 100 years. Due to man-made constrictions, more sediment is spilled out in the Gulf of Mexico.

In this Master Thesis, the Lower Mississippi River is subject to morphodynamic modeling with Delft3D to find answers for the question, if there is a feasible way to restore the deltaic wetlands that suffer from high land loss rates due to land subsidence and sea-level rise without putting navigation at stake.
In delta restoration plannings, sediment diversions play an important role as they convey sediment laden water to the marsh areas and, this way, largely contribute to new land-building.
Several approaches are tested with the created model to understand the effect of altered flow and sediment discharge distributions on the morphology of the main channel.
For a good approximation and description of the physical processes, the model comprises important factors such as dredging activities, diversion sites, salt water intrusion, and quasi-steady discharge periods.

Several scenarios were tested, e.g. different operation modes of planned sediment diversions and discharge distributions at Old River Control Structure. From the model outcome the conclusions can be drawn that a combination of a pulsed operation of ORCS and large-scale diversions as proposed by Parker et al. seems to be the most effective solution for wetland restoration in the

model domain as it only leads to similar deposition rates upstream of Venice, only slightly higher dredging volumes in the downstream reach and high sediment diversion, whereas the implementation of multiple diversions seems to be more feasible, as they are already considered in the CWPPRA Masterplan. Moreover, it was found that additional groin fields can help to ensure navigability downstream of sediment diversions and thus mitigate negative morphological effects in the main channel.

In the end, it must be emphasized that the application of additional diversions can stabilize local delta regions, but without higher sediment supply from upstream, the diverted amount of sediment is not sufficient for wetland restoration on a larger scale.

Contents

List of Figures

List of Tables

1 | Introduction and Research Question

1.1 The Mississippi River

The Mississippi is the largest riverine system in North America and one of the most engineered rivers in the world [5]. Its basin drains water from 31 US states and 2 Canadian provinces and therewith covers about $3,225,000\ km^2$. In the delta region, the Lower Mississippi (without Atchafalaya) has an average discharge of $15,000\ m^3/s$. In comparison, even the River Rhine appears small with only 6% of the basin area and 13% of the annual average discharge [14].

The Mississippi basin is presented in the below figure together with an overview of the modeling area reaching from upstream of New Orleans to the branches of the Mississippi Birdfoot Delta.

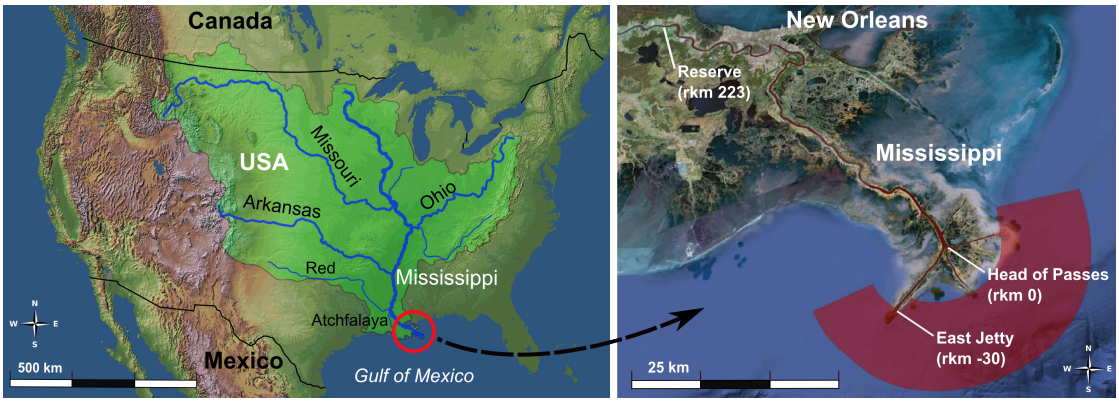

Figure 1.1: The Mississippi River Watershed and Area of Interest. The left figure shows the catchment and its major tributaries: Missouri, Arkansas, Red and Ohio River. At rkm 537, the flow from Upper Mississippi and Red River is diverted by the Old River Control Structure with a 70/30 ratio to the Lower Mississippi and to the Atchafalaya, respectively. The right figure shows the area of interest from Reserve (rkm 223) to East Jetty (rkm -30) and the Gulf of Mexico (red overlay). Adapted from NWAS and Google Earth [33].

As many other low-lying areas, the Mississippi Delta suffers from high land loss rates due to relative sea level rise. In addition to the eustatic sea level rise in the order of 2 mm/year, the effects of land subsidence play an important role, ranging up to 23 mm/year. As a matter of fact, human interventions along the Mississippi River and its tributaries largely contributed to this development. Reservoirs and dams at the Missouri and Arkansas Rivers as well as several hydraulic structures along the Mississippi River, such as levees or dikes and improved land management led to a decrease in suspended sediment load [10].
Since 1850, up to 70% reduction of suspended sediment is estimated [63]. However, it is questionable, if the reference sediment load is representative for the river system as initial changes in land use and the New Madrid earthquakes 1811-1812 led to a high sediment input [63, 73].

The Lower Mississippi River is vital for the economic development of the USA. Navigation is an important function and navigational depths have to be guaranteed by regularly dredging the fairway. Efficient use of the dredged material can be made by dumping or conveying extracted material into areas where sediment supply is needed for land-building purposes and stabilization of the wetlands that surround the Mississippi Delta.

However, with ongoing land losses, there have been a number of studies and measures to develop new approaches for wetland restoration. One possible solution is to reconnect the leveed river to its former floodplain by means of river diversions. This way, the wetlands could be supplied with sediment again.

Blum and Roberts (2009) [10] came to the conclusion that restoring the pre-dam sediment load of the Lower Mississippi would raise the sediment load from 205 to about 450 million tons per year. With the higher sediment input and depending on the scenario of relative sea-level rise, loss of deltaic wetlands could be counteracted or at least slowed down. Although river diversions showed to be promising for wetland restoration [39], Blum and Roberts indicate that these projects may fail due to a lack of sediment input.

Moreover, there is also an interaction of the river diversions and the main channel. Water withdrawal may lead to a decreasing sediment transport capacity of the river and,

consequently, to downstream deposition. In order to increase the sediment concentration in the diversions and to mitigate negative effects on navigation, additional dredging and pipeline conveyance might have to be considered [6].

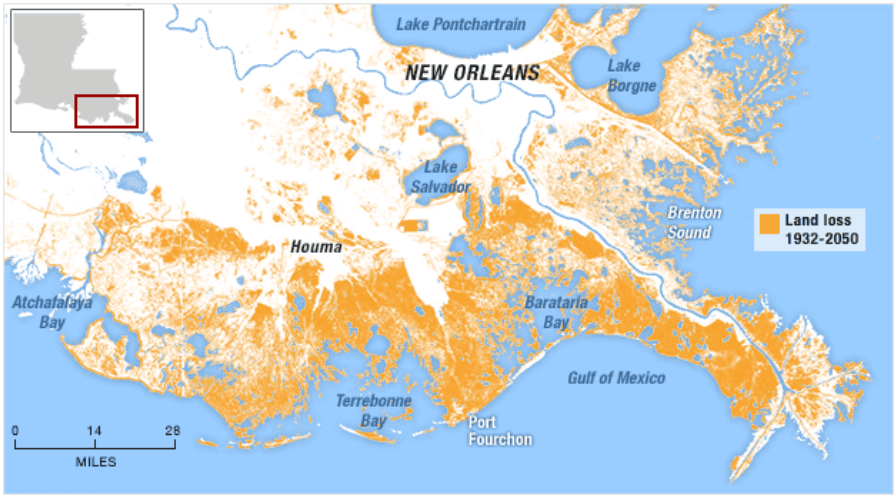

Figure 1.2: Historical and Predicted Land Loss. Source: Office of the Governor - Coastal Activities.

1.2 Starting Point

The study from Blum and Roberts shows that wetland restoration could be more efficient for an increased sediment input. In addition, various authors (e.g. Parker et al. [40] or CWPPRA [19]) proposed locations and dimensions of sediment diversions to convey sediment-laden water to the wetlands.

However, little is known about the effects of altered sediment and discharge regimes on the morphology of the Lower Mississippi River and also the impact of the proposed sediment diversions has to be evaluated.

As already mentioned, navigation plays an important role. It is yet unknown, if safe navigation and affordable dredging activities might be at stake.

Furthermore, more research has to be done on location, design and operation of the river diversions to achieve an effective sediment withdrawal.

1.3 Objective

1.3.1 Primary Research Question

The research question is posed based on the elaborated aspects above and reads:

How does the operation of sediment diversions influence the morphodynamics in the Lower Mississippi River from Reserve (rkm 223) to the Gulf (rkm -30) for changes in water and sediment supply?

With the results from this research, we want to evaluate the feasibility of higher sediment inputs to make wetland restoration more effective without increasing dredging activities to an unaffordable level.

1.3.2 General aspects

The research question comprises a number of physical, economic and ecological aspects whose importance for an accurate analysis has to be evaluated. Aspects playing a major role in the model area are listed below:

- Changes in sediment supply
- Distribution of water and sediment
- Location, design and operation of diversions
- Dredging operations and safe navigation
- Salt water intrusion
- Sea-level rise and land subsidence

1.3.3 Focus

It is not feasible to treat all the above mentioned aspects in detail. Accordingly, we choose to focus on the following aspects:

- **Criteria for location, design and operation of river diversions considering navigability**
  What are the available quantities of sediment for wetland restoration activities? What are the implications for navigation? Is it possible to keep the dredging activities affordable? What is the best operation mode?

- **The effect of altered upstream water and sediment input on morphology**
  How would a higher sediment input affect the bed levels of the Lower Mississippi River? How does the salt wedge interact with changes in sediment input and discharge variations due to operation of diversions? Where does the sediment settle in general and for altered sediment input?

1.4 Methodology

In this study we intend to develop and apply a two-dimensional morphodynamic Delft3D model of the Lower Mississippi River that can serve as an analytical tool to investigate the research questions.
Data has to be acquired and implemented before it can be calibrated for hydrodynamics and morphodynamics.
In order to achieve reliable results a step-wise evolution with increasing complexity is conducted. Starting from the data acquisition and some analytical estimates, a two-dimensional hydrodynamic model is created. The areas of salt water influence are subsequently taken from the output of a three-dimensional hydraulic model and implemented in the two-dimensional morphodynamic model.

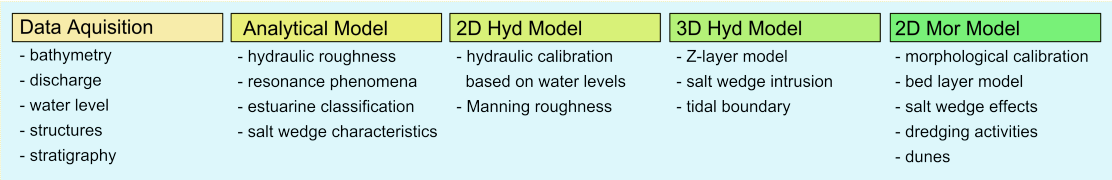

Figure 1.3: Calibration Procedure. Subsequent calibration of hydrodynamics, salinity and morphodynamics as carried out in Chapter 2.

The hydraulic calibration is carried out in 2D based on given water levels. The applied 2DH Delft3D model resolves the horizontal plane with a curvi-linear grid but has only a single vertical layer. The two-dimensional simulation leads to a significant reduction of computational time compared to a three-dimensional simulation. In order to deal with effects that are not uniform over the depth, empirical relations and parameters are used, e.g. for secondary flow.

Due to the size of the domain and the time-scales that are anticipated (up to 50 years), a two-dimensional morphodynamic is chosen.

In order to get a realistic behavior regarding salt intrusion, a Z-layer model with strictly horizontal layers is applied.
Due to a cut-cell approach at the bottom, it is possible to avoid a stair case and to achieve a relatively smooth bed shear stress.

Comparisons are carried out with the σ-layer model. However, in case of a weakly forced estuary, the Z-layer model will most likely lead to better results.

The model is ought to run for a longer period of between 10 to 50 years to find answers to the research questions. Various scenarios can be tested concerning different water and sediment discharges.
Dredging operations and different strategies can be included. Moreover, in order to distribute higher sediment inputs, the creation of additional sediment diversions may be required. Location, design and operation have to be established and evaluated.

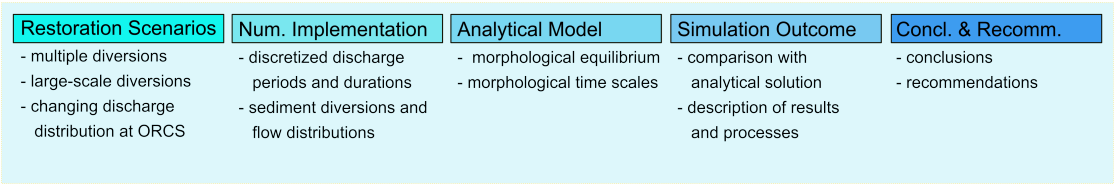

Figure 1.4: Modeling Procedure. Presentation of restoration scenarios, numerical implementation, analytical assessment, simulation outcome and conclusions & recommendations. The presented steps are carried out in Chapter 3 to 7.

2 | Delft3D Model

2.1 Model Overview

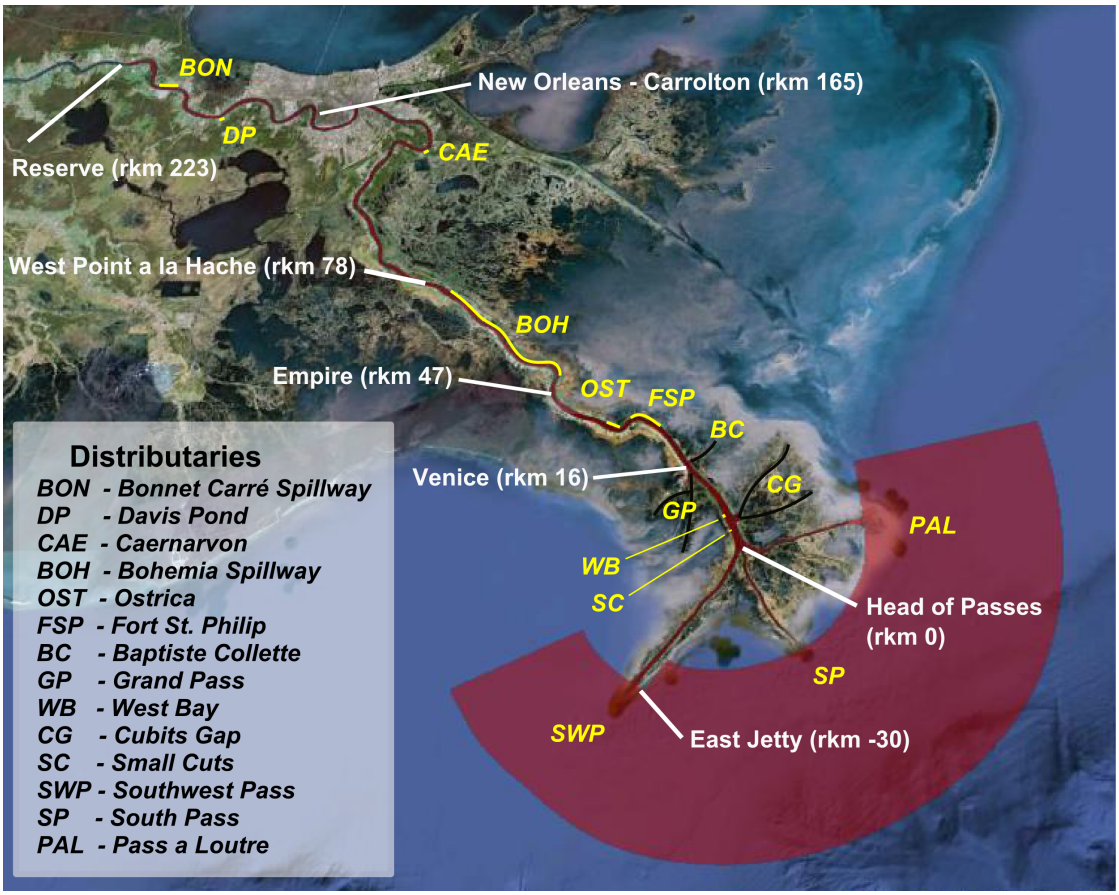

Figure 2.1: Model Overview. Distributaries and model area including domains of Gulf of Mexico only applied in three-dimensional simulations. Adapted from Google Earth [33].

The model starts at rkm 223 (Reserve, upstream of New Orleans) and comprises the trifurcation including Southwest Pass, South Pass and Pass a Loutre as well as other important diversions and spillways. An overview of the model is shown in figure 2.1.
Setting up a model requires the acquisition of basic data such as discharge, water levels, bathymetry and hydraulic structures. In the following, the implementation of the data that is relevant for a hydraulic simulation is presented.

Remark:
In more advanced simulation including salinity and morphology more information is required. Descriptions and concepts are available in the corresponding chapters as well as in the annex.

2.2 Grid Creation

The grid was created by the RGFGRID Delft3D module. The boundaries of the domains, i.e. the river banks were created in Google Earth and imported to Delft3D. The entire model is composed of three domains which are connected by "domain decomposition". This technique allows for parallel processing of various domains and facilitates grid creation as it enables a transition of grids with different resolutions. More information about this technique can be found in the Delft3D Manual [22].
Due to the geometry of the river system, it was decided to create a single grid for the main channel and the tributaries of the birdfoot delta. Segments of the most important tributaries and diversions upstream were added, as well. In downstream direction, the grid extends approximately 25 km into the Gulf of Mexico. This domain called MR is composed of approximately 20,000 cells.

Remark:
The two-dimensional model is based on this domain only. In order to better simulate salinity and tide, two grids covering the adjacent Gulf of Mexico are connected to the grid of the Lower Mississippi River in case of three-dimensional simulations and are called GOM 1 and GOM 2.

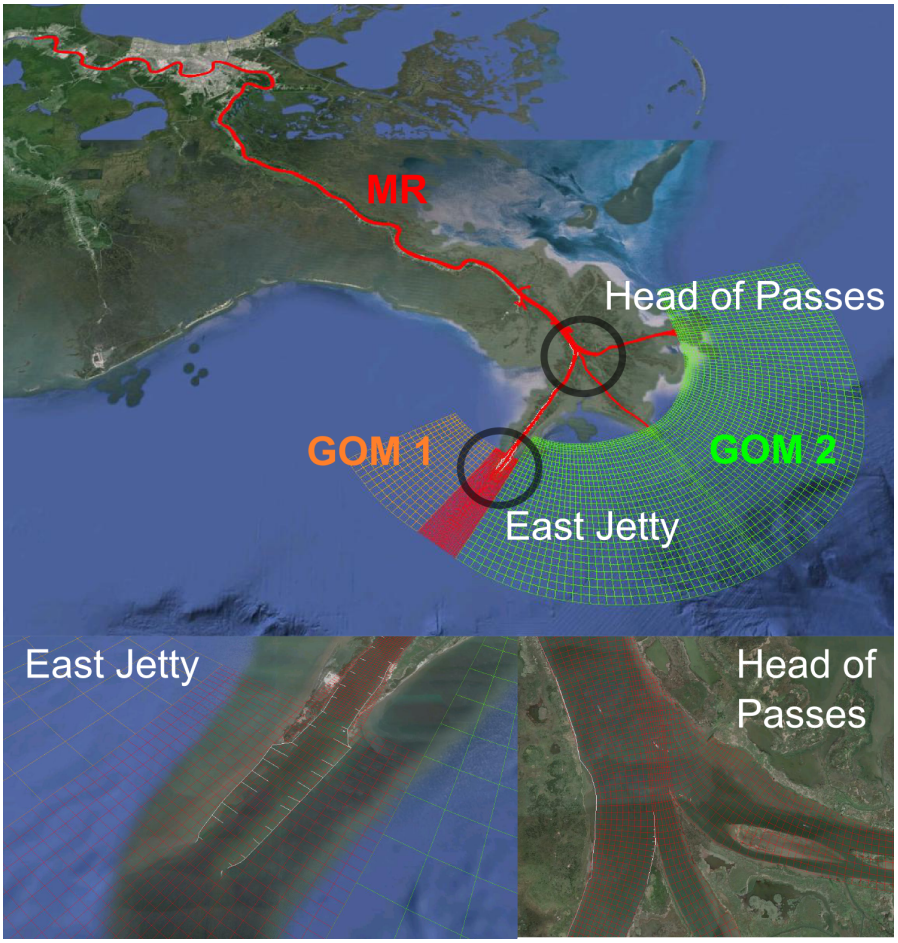

Figure 2.2: Grid Overview. The figure shows the different domains created for numerical simulations with Delft3D. Adapted from Google Earth.

2.3 Data Acquisition

2.3.1 Structures

Especially in the Southwest Pass structures, e.g. groin fields and jetties, are widespread and have to be taken into account (see also East Jetty in figure 2.2).
Dimensions and locations were obtained from Google Earth and transferred to the numerical grid. Depending on the model they were implemented as 2D weirs or as 3D local weirs, respectively. The Delft 3D manual states that weirs are
"[...] commonly used to model [...] groynes in simulation models of rivers" [22].

Moreover, revetment along the river banks, usually consisting of concrete mats, has to be taken into account. A GIS data set provided by TWIG reaching from Old River Control Structure (ORCS) to Venice was used for that purpose.

2.3.2 Bathymetry

The elevation data stems from the ADCIRC model (SL16).

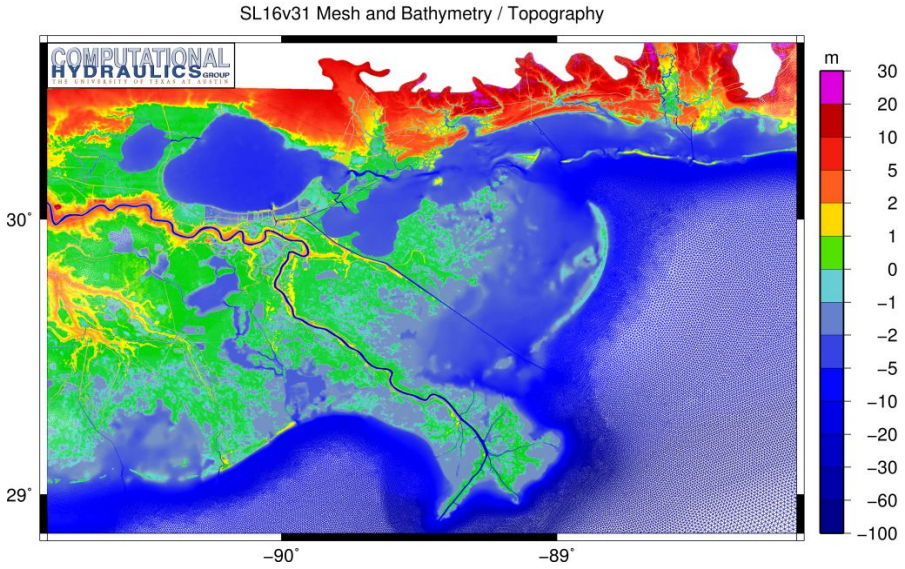

Figure 2.3: Digital Elevation Model (DEM) SL16. The figure shows the topography and bathymetry of the Southern Louisiana coast and the Mississippi delta, Source: Casey Dietrich.

Other digital elevation models (DEM) were compared to the present data set, e.g. a 2010 DEM from NOAA, which revealed strong local deviations. For consistency reasons it was decided to use the SL16 DEM with corrections for areas that were subject to human interventions, for example West Bay Diversion.

2.3.3 Discharge Data

The discharge data was obtained from the gage station at Tarberts Landing. It comprises a 23-year record (1990-2012) of daily discharge measurements.

The data can be used to determine the probability of exceedance of certain discharges. This probability can also be expressed in terms of days per year.
Moreover, in order to shorten the simulation time, the choice is made to discretize the discharge into eight periods of constant discharge. This was also recommended by Bos (2011) [12]. Hence, the discharges of 10, 20 and 33 thousand m^3/s were chosen based on previous considerations. In order to get a good correspondence to the exceedance curve, intermediate discharge periods were fitted. This way, the discharge periods were determined to be 7, 10, 13, 16, 20, 24, 28 and 33 thousand m^3/s.

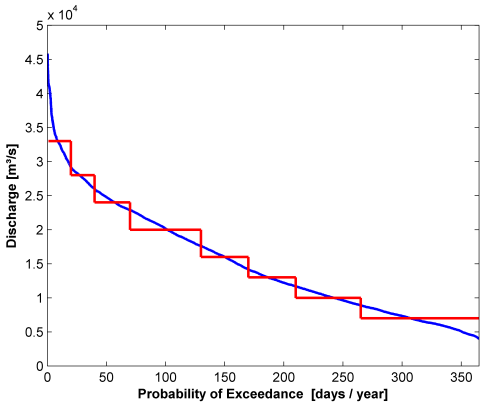

Figure 2.4: Discharge Discretization. Exceedance curve of discharge at Tarbert Landing from 1990 to 2012 and discretized fitted periods of constant discharge. Both curves integrate to 479 $km^3/year$.

In order to reduce the simulation time, the discharge curve is discretized into periods with constant discharge. Of course, the discretized discharges have to meet certain requirements.

- The annual water discharge has to correspond to the annual discharge obtained from the daily measurements
- The annual sediment transport has to correspond to the annual sediment transport obtained from the daily measurements

The second aspect will be treated separately in the morphological calibration. First, the focus lies on the hydrodynamics.

The average of the 23-year record of daily discharge measurements yields an average of 479 $km^3/year$ at Tarbert Landing (rkm 492) [5]. This values closely corresponds to

the flood year 2009 (October, 1st 2008 to September, 30th 2009), which shows the same annual discharge.

Based on local water levels and upstream discharge measurements, Allison et al. (2012) [5] estimated the corresponding discharges of various tributaries and diversions at the Mississippi Delta by means of rating curves.
The available data from this analysis were used during the discretization of the model to obtain the discharge distributions for eight constant periods of constant upstream inflow. Downstream discharges were related to discharges of 7000, 10000, 13000, 16000, 20000, 24000, 28000 and 33000 m^3/s within a 5% tolerance margin.
The absolute and relative distributions are presented below:

Table 2.1: Absolute Discharge Distribution with Q_{nom} in m^3/s

Q_{nom}	BON	CAE	DP	BOH	OST	FSP	BC	GP	WB	SC	CG	SWP	SP	PAL	Q_{eff}
7000	0	35	20	0	0	26	612	806	430	305	422	1299	708	851	5516
10000	0	67	56	0	0	318	926	1085	629	314	824	2577	970	1016	8781
13000	0	58	52	0	0	618	1199	1327	802	321	1173	3685	1197	1160	11591
16000	0	105	43	0	0	898	1454	1553	963	328	1500	4721	1409	1294	14268
20000	0	90	38	0	0	1327	1844	1899	1210	338	1998	6305	1733	1500	18283
24000	0	163	37	0	486	1611	2126	2150	1389	345	2360	7453	1968	1649	21738
28000	15	158	38	109	1348	1846	2486	2469	1617	355	2820	8914	2268	1838	26280
31532	115	156	57	421	1560	2220	2944	2876	1907	367	3406	10775	2649	2079	31839

Table 2.2: Relative Discharge Distribution in % of Effective Discharge with Q_{nom} in m^3/s

Q_{nom}	BON	CAE	DP	BOH	OST	FSP	BC	GP	WB	SC	CG	SWP	SP	PAL	Q_{eff}
7000	0.0	0.6	0.4	0.0	0.0	0.5	11.1	14.6	7.8	5.5	7.7	23.6	12.8	15.4	100
10000	0.0	0.8	0.6	0.0	0.0	3.6	10.5	12.4	7.2	3.6	9.4	29.3	11.0	11.6	100
13000	0.0	0.5	0.4	0.0	0.0	5.3	10.3	11.4	6.9	2.8	10.1	31.8	10.3	10.0	100
16000	0.0	0.7	0.3	0.0	0.0	6.3	10.2	10.9	6.8	2.3	10.5	33.1	9.9	9.1	100
20000	0.0	0.5	0.2	0.0	0.0	7.3	10.1	10.4	6.6	1.8	10.9	34.5	9.5	8.2	100
24000	0.0	0.7	0.2	0.0	2.2	7.4	9.8	9.9	6.4	1.6	10.9	34.3	9.1	7.6	100
28000	0.1	0.6	0.1	0.4	5.1	7.0	9.5	9.4	6.2	1.3	10.7	33.9	8.6	7.0	100
33000	0.6	0.5	0.2	1.3	4.9	7.0	9.3	9.1	6.0	1.2	10.8	34.2	8.4	6.6	100

The tables show that the distribution of discharge varies depending on the upstream flow. Some tributaries receive relatively more water during high discharge and vice versa, e.g. Southwest Pass and Cubit's Gap, while also the opposite is found, for example at Baptiste Collette, South Pass and Pass a Loutre.

Another important aspect is the difference between the upstream inflow and the cumulative discharge of all tributaries. Hence the individual discharges are expressed relative to their sum and not relative to the nominal discharge.
Especially during low discharges, the amount of water deviates significantly. Considering the relative increase of smaller tributaries and diversions for low discharges, a reason might be that not all smaller diversions were included in the analysis. Moreover, infiltration along the thalweg might be another factor.
In order to account for these water losses, the upstream boundary condition was changed to the cumulative discharge (last column in the above tables, Q_{eff}). This results in an effective discharge as stated below. For the sake of stringency, the nominal discharge periods will be used further on.

Table 2.3: Nominal and Effective Discharges

Q_{nom} $[m^3/s]$	Q_{eff} $[m^3/s]$
7000	5516
10000	8781
13000	11591
16000	14268
20000	18283
24000	21738
28000	26373
33000	31839

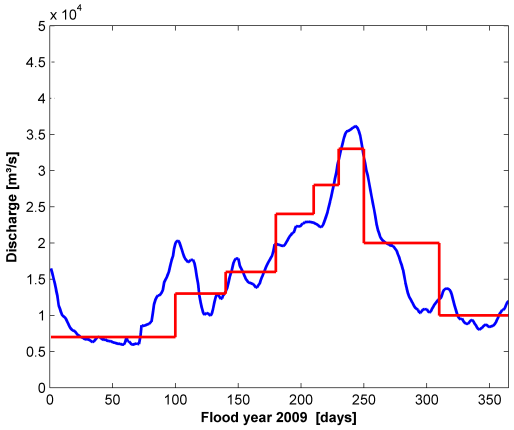

Figure 2.5: Schematized Flood Year 2009 at Tarbert Landing. Schematization and discharge hydrograph integrate to 479 m^3/s.

2.3.4 Water Level Data

Water level data is provided by United States Army Corps of Engineers (USACE) for several gage stations along the Lower Mississippi River.
The hydraulic calibration of the model comprises the comparison with water levels obtained from local water gages along the area of interest. The chosen stations are Reserve (rkm 223), New Orleans (Carrolton) (rkm 165), West Point a la Hache (rkm 78), Empire (rkm 47), Venice (rkm 16), Head of Passes (rkm 0) and East Jetty (rkm -30).
Because the stations can be subject to land subsidence, it is questionable whether especially older data is sufficiently accurate. Moreover, conversion to the actual vertical datum NAVD88 (North American Vertical Datum, introduced 1988) becomes necessary. The subsidence hardly follows a linear trend and is not considered in the transformation to the new vertical datum NAVD88 [62].
In the year of the bathymetric measurements, 2004, significant discharge peaks are missing. Also preceding years showed rather low flood peaks.
Due to Hurricane Katrina the water levels records at some stations show missing data between 2005 and 2007.
Analysis using only data since 2008 with NAVD88 datum led to quite different statistical properties than larger periods, e.g. the 23-year span.
This may partly be explained with the above mentioned factors. Furthermore, the Lower Mississippi River has also been subject to additional construction works, for example the West Bay Diversion. Especially the water levels in the area downstream of Venice where the Mississippi flow starts to separate might have changed throughout the years due to varying discharge distribution.

Under the circumstance that the used discharge distribution and the discharge discretization resemble the 2009 flood year, it was decided to use the entire water level data set from 1990 to 2012 only for the upstream area of the model (Reserve, New Orleans, West Point a la Hache, Empire) and to focus on recent data from 2008 to 2012 for the downstream area (Venice, Head of Passes, East Jetty).

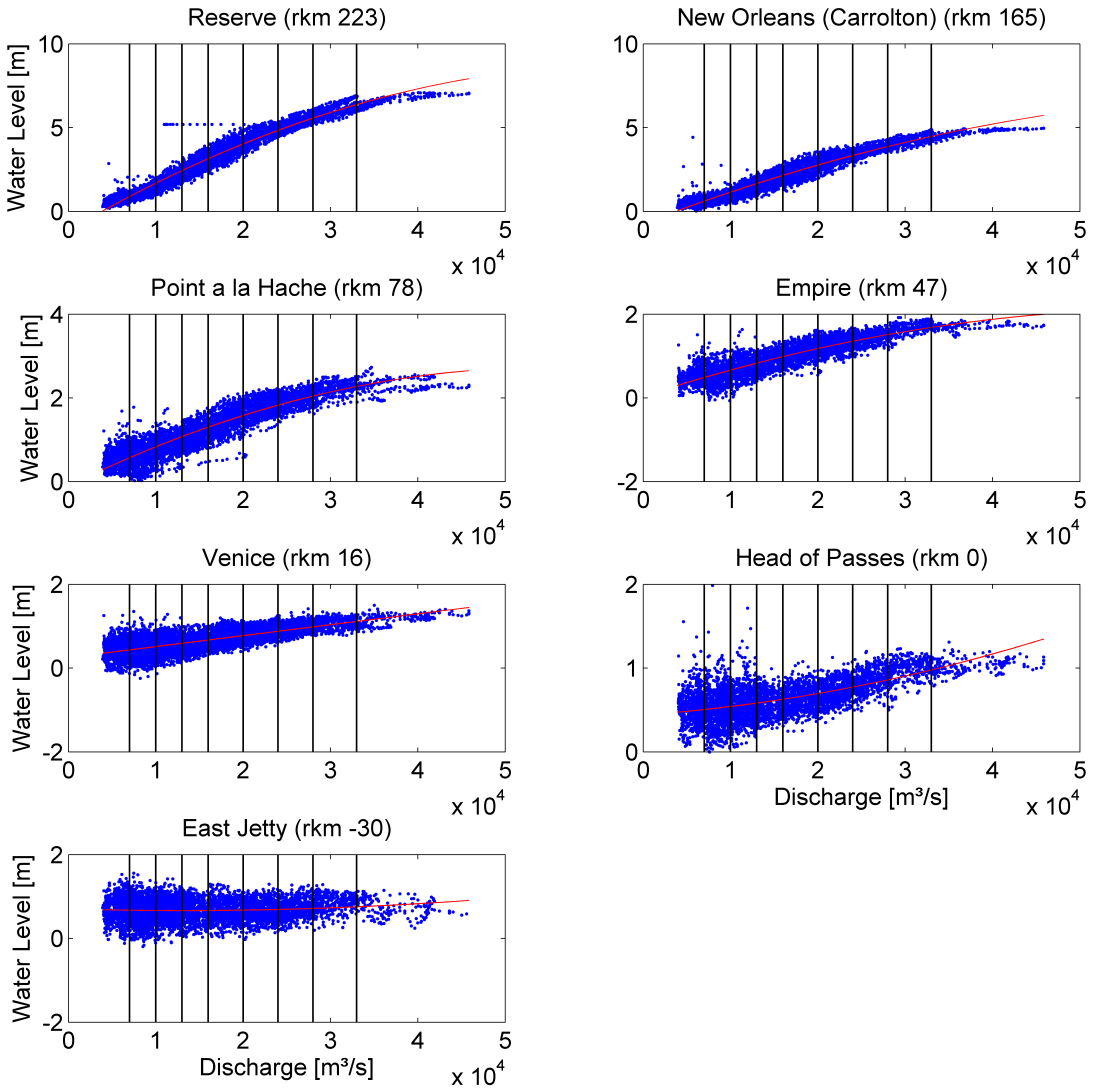

Figure 2.6: Water Level Data from 1990 to 2012 Converted to NAVD88. The black vertical lines represent the chosen periods of constant discharge. The red line is a 3rd order polynomial fitting. Source: USACE [80].

For the discretized discharge periods, corresponding water levels were filtered out and averaged. The margin for including water levels was set to 2% of the discharge period which generated a sufficient amount of data.

The water levels used for calibration including their standard deviations are shown below:

Table 2.4: Water Level Reference for Hydraulic Calibration in m w.r.t. NAVD88 and Q_{nom} in m^3/s

Q_{nom}	7000	10000	13000	16000	20000	24000	28000	33000
Reserve	0.91	1.52	2.28	3.10	4.18	4.94	5.61	6.30
Point a la Hache	0.61	0.82	1.00	1.27	1.61	1.88	2.09	2.30
Empire	0.52	0.63	0.75	0.96	1.21	1.37	1.51	1.74
Venice	0.52	0.45	0.62	0.67	0.80	0.95	1.06	1.17
Head of Passes	0.60	0.53	0.63	0.58	0.56	0.74	0.75	1.04
East Jetty	0.42	0.31	0.49	0.50	0.49	0.57	0.66	0.70

Table 2.5: Standard Deviations of Water Level References in m w.r.t. NAVD88 and Q_{nom} in m^3/s

Q_{nom}	7000	10000	13000	16000	20000	24000	28000	33000
Reserve	0.15	0.17	0.33	0.36	0.32	0.21	0.24	0.30
Point a la Hache	0.22	0.19	0.21	0.21	0.29	0.18	0.17	0.12
Empire	0.19	0.21	0.21	0.16	0.23	0.16	0.12	0.08
Venice	0.25	0.31	0.23	0.19	0.18	0.11	0.08	0.11
Head of Passes	0.22	0.21	0.23	0.14	0.12	0.09	0.16	0.06
East Jetty	0.23	0.24	0.25	0.27	0.23	0.12	0.14	0.06

The obtained values are expected to show a decrease from upstream to downstream stations. For the high discharge periods this is the case. The lower discharge periods, however, are more irregular and have stronger deviations. It is thus difficult to find the correct water levels based on this data. A first approach would be to focus on the higher discharges and apply the calibration parameters on the lower discharges, as well.

Table 2.6: Applied Downstream Boundary Conditions for 2D Calibration in m w.r.t. NAVD88 for Upstream Discharges Q_{nom} in m^3/s

Q_{nom}	7000	10000	13000	16000	20000	24000	28000	33000
East Jetty	0.40	0.40	0.50	0.50	0.50	0.57	0.66	0.70

Analyzing the downstream water levels at East Jetty revealed a dependence on the river discharge. It was decided to extend the model into the Gulf of Mexico with a discharge-independent mean water level. For 3D simulations with salinity, the water

level is set to 0.2 m at the downstream boundary in the Gulf of Mexico. It is expected that the water levels at the East Jetty station will vary due to salt intrusion when different river discharges are applied.

2.3.5 Tidal Boundary

The Mississippi Delta experiences a diurnal tide with a maximum amplitude of approximately 30 cm. It consists of several constituents whose most important components are K1, O1, P1 and Q1.
The data were obtained from the gage station at East Jetty provided by USACE.
For modeling purposes, the signal has to be discretized. The model is constructed such that a morphological factor can be applied in a two- or three-dimensional morphodynamic model to speed up the simulation.
Therefore, only discharge periods during full tidal cycles are used.
It was decided to model the tidal signal as a simple sinusoidal signal with an amplitude of 0.30 m and a frequency of 1/day.
Although one can argue that this might introduce shortcomings, e.g. no asymmetry/ altered impact on morphology, this decision can be justified by the relatively low tidal amplitude and, consequently, its small impact. This can also be derived from the delta classification presented in the Annex (A.1, p. 103). In this work, we mainly focus on the river itself and have to keep the model relatively simple and the computational costs affordable for long-term simulations.

Remark:
During morphological calibration, the impact of a tidal signal imposed at East Jetty turned out to have a negligible effect on the outcome of the two-dimensional model. Hence it was decided to not implement a tidal signal. For further details, see Annex C.3.3, p. 151.

2.3.6 Salt Wedge Intrusion Length

The intrusion length of the toe of the salt wedge is based on the work of Soileau et al. (1989) [65]. Other authors (Allison, USACE, Bos) refer to this analysis directly or indirectly. Soileau et al. presented a figure showing the intrusion length as a function of

river discharge. For $Q < 8,500\ m^3/s$ the salt wedge extends into from Southwest Pass into the Mississippi River and for $Q < 3,000\ m^3/s$ even up to New Orleans.

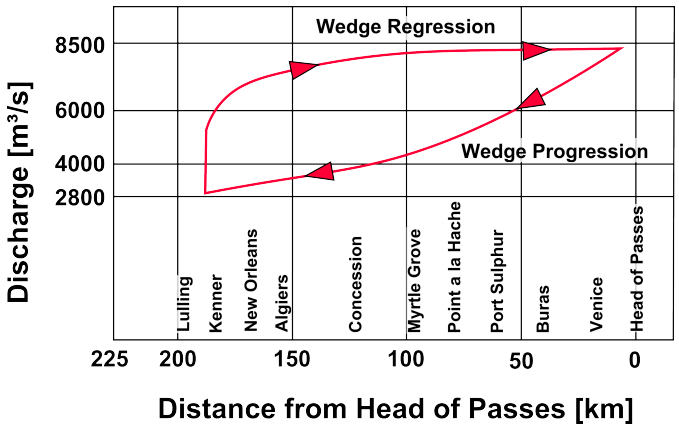

Figure 2.7: Location of the Toe of the Salt Wedge vs. River Discharge. Adapted from Soileau (1989) [65].

However, the publication is already 24 years old. As seen before, new diversions were constructed, dredging activities proceeded and, consequently, geometry and discharge distribution has changed.

During low river discharges, the operation of fresh water intakes in the region of New Orleans can become problematic due to raising salinity concentrations. However, the bathymetry allows for the construction of a saltwater barrier sill without interfering with navigation. The sill was constructed twice, in 1988 and in 1999 at rkm 116 [3].

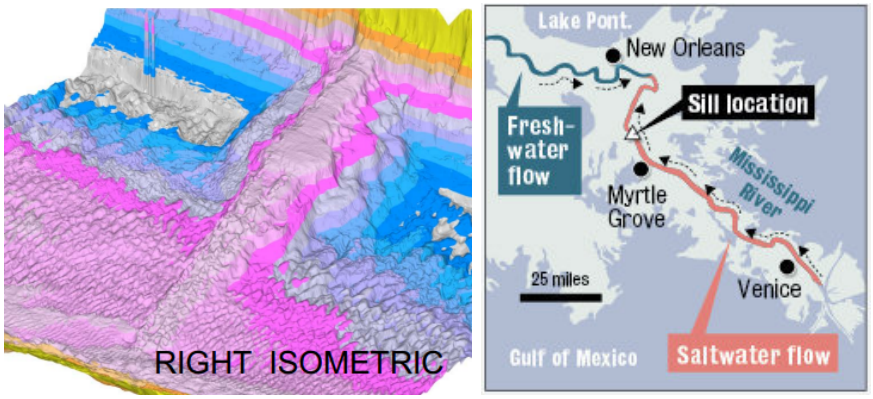

Figure 2.8: Saltwater Barrier Sill at rkm 116. Source: Propeller Club NOLA and The Watchers.

2.3.7 Grain Size Distribution

Samples collected by Allison (2010) [3] show the median sand diameter along the Lower Mississippi River. Measurements were taken in sandy areas between rkm 126 and rkm 0 (Head of Passes) in November 2003 and indicated a decrease of the median diameter from 0.265 mm to 0.180 mm at Head of Passes.

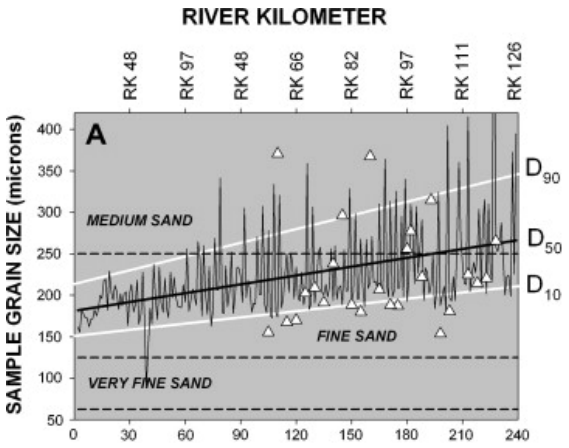

Figure 2.9: Grain Size Distribution Along Model Domain. Samples between rkm 126 (English Turn) and rkm 0 (Head of Passes). Source: Allison (2010) [3].

It was decided to use two sand fractions to simulate this spatially varying median grain diameter as obtained from sand bed samples by Allison (2010). In addition, the information was extrapolated to obtain values downstream of rkm 0 and upstream of rkm 165. This yielded a median grain size of 0.310 mm at Reserve (rkm 223) which linearly decreased to 0.160 mm at East Jetty. The bed composition could now be adjusted such that the average diameter of the sand layers corresponded to the median grain size.
The sand fractions where chosen to be Medium Sand with $D_{50} = 0.345\ mm$ and Fine Sand with $D_{50} = 0.125\ mm$.
Including estimated standard sizes for silt and clay particles, this led to the following median grain diameters:

Table 2.7: Median grain diameters for used sand and mud fractions

Fraction	D_{50} $[\mu m]$
Medium Sand	345
Fine Sand	125
Silt	16
Clay	2

Remark:
During the morphological calibration, it was also tried to run simulations with a single sand fraction with a median diameter of $D_{50} = 0.200\ mm$. This, however, led to negative effects for bed stability and behavior of the sediment introduced at the upstream boundary as the median sand diameter in suspension is clearly smaller than 0.200 mm (pers. comm. Ehab Meselhe, 22.08.2013). For more information see Annex C.3.7, p. 153.
From literature, the suspended sand load is in the order of 0.125 mm (Meselhe et al. 2012) [46]. Consequently, it was decided to use two sand fractions to simulate both the suspended load and the variations of the median grain size along the domain.

2.3.8 Bed Composition

The Lower Mississippi River shows an irregular and inconvenient bathymetry: The bed level decreases in upstream direction with deep pits up to 60 m below NAVD88 in river bends above Venice.
River training acting against the natural estuarine development might be one reason for this. In general, the river upstream of Head of Passes and in our area of interest has no significant floodplains. Revetments along the river and a decay in sediment supply from upstream due to dams in the main tributaries might have led to increased erosion as the river incised to find a new equilibrium.
According to Parker, the Lower Mississippi River can be divided into three sections:[53] There is a transition from an alluvial river with a relatively high sediment availability due to interaction between floodplain and channel to a quasi bed-rock channel, cut off from its former floodplain and partially with consolidated clay at the bottom. The transition is found to be approximately 50 km upstream of this model. Hence the upper part of the model is considered as quasi bed-rock. Especially in the deep pits of the bends between Reserve and Venice, Parker/ Nittrouer showed that the bed is composed

of hardly erodible cohesive sediment.
Another transition can be found when approaching Venice. The river turns shallow as water is diverted and the main stream looses a part of its sediment transport capacity. Also salt intrusion affects deposition. As a consequence, this area contains a relatively high amount of sediment leading to the already mentioned dredging activities.

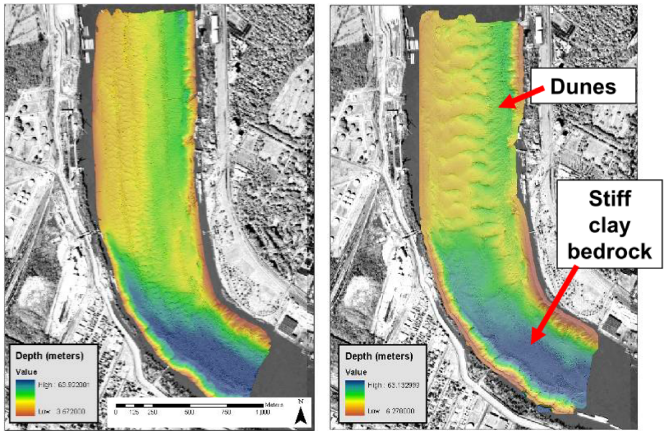

Figure 2.10: Bathymetry from Landsat Records in Audobon Bend, New Orleans. Left: April 2004, Discharge $Q = 13,564\ m^3/s$. Right: January 2005, Discharge $Q = 34,292\ m^3/s$. The figure shows the generation of bed forms in shallower sections and a layer of consolidated clay in the deeper sections. Courtesy Nittrouer, J., Mohring, D. and Allison, M.. Adapted from Parker (2009) [53].

The bed composition in the model domain is described by Mossa [47]. As expected the median grain diameter (D_{50}) decreases towards the mouth as sand fractions get less compared to finer silt and clay particles. This is a natural sorting process caused by decreasing transport capacity of the river (bed slope reduction, discharge diversion). Mossa, as well as Allison make a distinction between sand with a median grain diameter $D_{50} > 0.63\ \mu m$ and mud with a median diameter $D_{50} < 0.63\ \mu m$.
In this work, we split sand and mud into two fractions each. The mud is simulated as a silt fraction and a clay fraction to have more flexibility when it comes to the simulation and calibration of the salt wedge effects (increased settling in Southwest Pass and at Head of Passes due to flocculation).
According to Galler and Allison (2008) [31] the clay/silt distribution is 65% and 35%, respectively .

With these information and assumptions the bed composition and availability is generated. The total bed thickness is created from depth information. The consolidated clay layer in the deep pits is considered by setting the sediment availability to zero for river depths below 30 m NAVD88 [1]. By subtracting this threshold from the inversed depth and excluding all remaining negative values (areas deeper than 30 m), a gradually varying thickness is generated. Afterwards, the bed thickness is scaled to around 20m maximum depth which should cover all bed level variation over the anticipated simulation period (10 to 20 years). To account for bank revetments present along almost the entire river, the values of the outer gird cells were set to zero.

Next, three files were created containing the relative thickness of sand, silt and clay in every grid cell: The composition linearly changes from 80% sand at Reserve to 0% at the Gulf. Vice versa, the proportions of Clay and Silt increase [47].

Multiplied with the total thickness defined before, the availability along the Mississippi River of each fraction is defined and implemented.

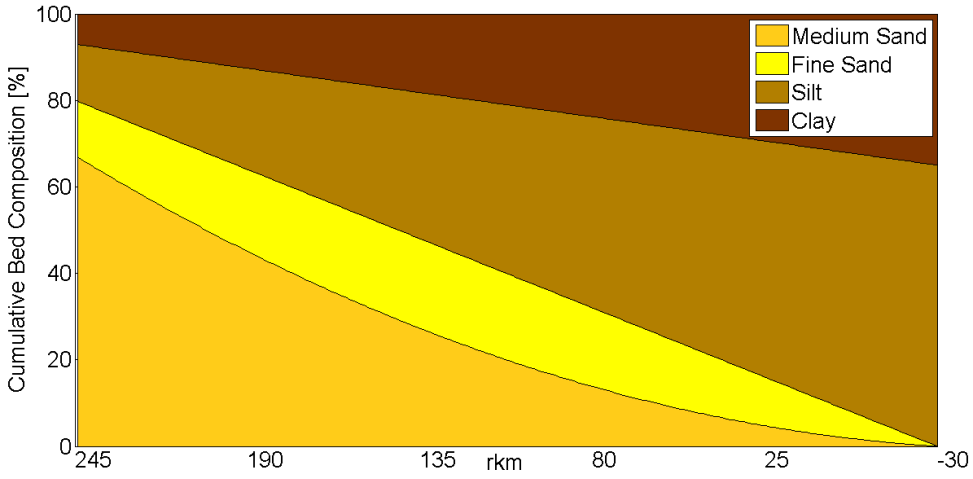

Figure 2.11: Bed Composition Along Model Domain. The bed composition is based on Mossa [47].

[1] Delft3D manual (section 11.4.4): "Areas may be initially specified as containing zero bottom sediment if non-erodible areas are required. It is likely that these areas will accrete a little sediment in order to allow an equilibrium bed load transport pattern to develop."

2.3.9 Sediment Boundary Conditions

The sediment input and distribution over the downstream tributaries are - as the flow distribution - derived from the supplementary file from Allison (2012) [5] for the chosen periods of constant discharge. It was decided to use the sediment discharge at Baton Rouge (rkm 365) as the closest to the upstream boundary and adapt the concentrations to the effective discharge.

Table 2.8: Concentrations of Sediment Fractions Imposed at Upstream Boundary for Periods of Constant Discharge, Accumulated Flow and Sediment Discharges

			Concentration			**Effective Discharge**	
Q_{nom} $[m^3/s]$	Q_{eff} $[m^3/s]$	$MorFac$ $[-]$	$Sand$ $[kg/m^3]$	$Silt$ $[kg/m^3]$	$Clay$ $[kg/m^3]$	$Q_{w,eff}$ $[km^3/year]$	$Q_{s,eff}$ $[10^6 t/year]$
7000	5516	100	0.00	0.14	0.08	47.7	10.5
10000	8781	55	0.01	0.12	0.07	41.7	8.4
13000	11591	40	0.03	0.11	0.06	40.1	7.9
16000	14268	40	0.04	0.10	0.05	49.3	9.6
20000	18283	60	0.06	0.09	0.05	94.8	17.7
24000	21738	30	0.07	0.07	0.04	56.3	10.4
28000	26373	20	0.09	0.06	0.03	45.6	8.1
33000	31839	20	0.10	0.05	0.02	55.0	9.4
						430.5	**82.1**

From literature, various transport rates can be derived. For example, Meade and Moody (2010) came to a 20-year average (1987 - 2006) of annual total suspended sediment transport at Tarbert Landing of $115 * 10^6$ $tons/year$. According to Horowitz (2010) the 1993 - 2007 average at St. Francisville was around $84 * 10^6$ $tons/year$. The analysis of Allison (2012) for the three flood years 2008, 2009 and 2010 comes to the conclusion that the flood year 2009 is close to this average value. The annual sediment input obtained as the sum of all discharge periods is around $82 * 10^6$ tons in case the nominal discharge is applied. This, as well as the total water discharge of 479.5 $km^3/year$, nicely agrees with the amounts including all available, daily data of the flood year 2009 (479 $km^3/year$ and $81 * 10^6$ $tons/year$).

Hence, by applying the above sediment boundary conditions, we have created a representative model in terms of average quantities of flow and sediment.

2.4 Hydraulic Model (2D)

2.4.1 Calibration Procedure

The grid was divided into six different sections. Within those sections, uniform Manning values were applied. Furthermore, each discharge period was calibrated individually. The calibration started downstream. Manning coefficients were subsequently adjusted in upstream direction until each discharge period showed an acceptable correlation with the water level data obtained from USACE [80].

The different roughness values corresponding to the above presented water levels are shown below:

Table 2.9: Manning Roughness Coefficients Applied on Different River Sections and Periods of Constant Discharge. All discharges given in m^3/s.

	7000	10000	13000	16000	20000	24000	28000	33000
Reserve - New Orleans	0.032	0.032	0.032	0.032	0.032	0.030	0.027	0.024
New Orleans - W. Pt. a la Hache	0.032	0.032	0.032	0.033	0.033	0.032	0.030	0.027
W. Pt. a la Hache - Empire	0.026	0.026	0.026	0.026	0.026	0.023	0.020	0.018
Empire - Venice	0.026	0.026	0.026	0.026	0.026	0.023	0.020	0.018
Venice - Head of Passes	0.018	0.018	0.018	0.018	0.018	0.018	0.015	0.014
Downstream Head of Passes	0.016	0.016	0.016	0.016	0.016	0.016	0.014	0.014

2.4.2 Results

Table 2.10: Water Levels of Hydraulic Calibration in m w.r.t. NAVD88. All discharges given in m^3/s.

	7000	10000	13000	16000	20000	24000	28000	33000
Reserve	0.88	1.51	2.29	3.03	4.24	4.91	5.67	6.25
New Orleans	0.88	1.51	2.29	3.03	4.24	4.91	5.67	6.25
W. Pt. a la Hache	0.52	0.70	1.00	1.24	1.67	1.90	2.10	2.40
Empire	0.47	0.57	0.80	0.94	1.21	1.39	1.50	1.69
Venice	0.42	0.46	0.61	0.67	0.79	0.95	1.07	1.24
Head of Passes	0.41	0.44	0.57	0.61	0.69	0.82	0.95	1.11
East Jetty	0.40	0.40	0.51	0.51	0.51	0.59	0.68	0.71

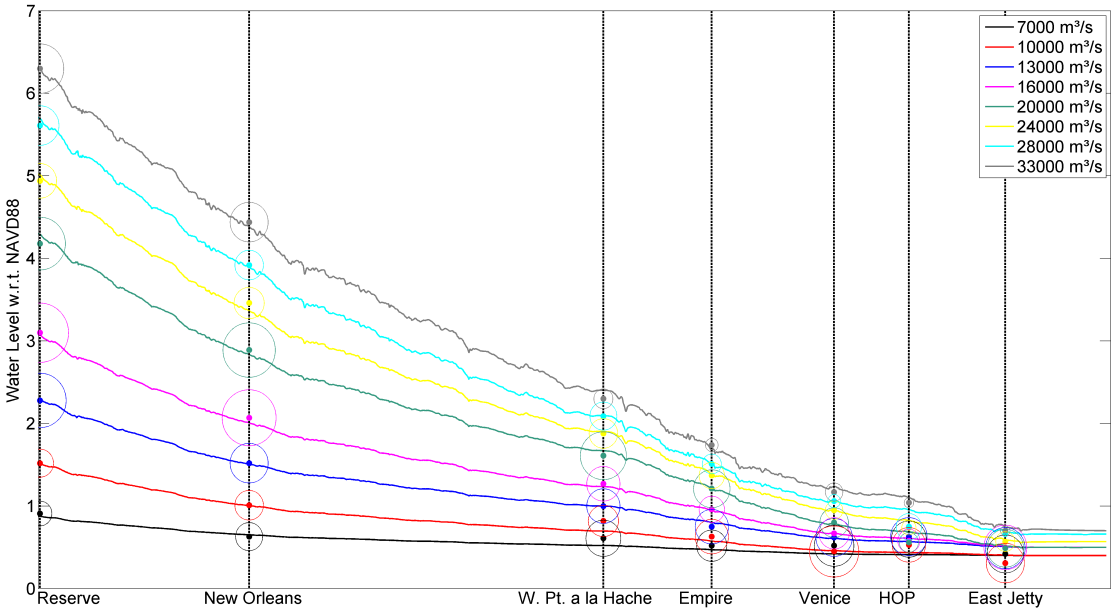

Figure 2.12: Results of Hydraulic Calibration. Results for periods of constant discharge.

As already mentioned, statistically obtained water levels at the downstream stages showed unphysical behavior, e.g. lower water levels upstream or lower water levels for higher discharges. However, the water levels obtained from the observation point in the Delft3D model for the different periods of constant discharge were predominantly close to the mean values or at least within the range of one standard deviation. In the following, we want to check, if the roughness coefficients are comprehensible from a physical point of view.

Remark:

An analytical model of the Manning roughness values can be found in the Annex (B.2.3, p. 119). Its outcome is comparable to the Manning values obtained during the calibration procedure.

The hydraulic validation based on ADCP velocity measurements near the upstream boundary showed reasonable results and can be found in the Annex (C.2.1 on p. 147.

2.5 Salinity Model (3D)

In order to correctly model three-dimensional effects in an estuarine environment, the model had to be extended in the vertical direction. In addition, salinity and tide were imposed at the Gulf of Mexico. In Section 2.2, the corresponding grids were already introduced. In short, the new properties can be found below:

- Extension towards the Gulf of Mexico with two additional grids (GOM1 and GOM2) connected to the main grid (MR)
- Connection of Southwest Pass, South Pass and Pass a Loutre to the Gulf of Mexico via domain-decomposition boundaries
- Sinusoidal water level applied along the downstream boundaries representing the diurnal tide
- Neumann boundaries imposed laterally
- Artificial upstream extension to prevent resonance phenomena

Although the three-dimensional model allows for more insight into estuarine effects, one has to be aware of certain limitations and simplifications:

- No wind, currents or thermal variations
- No consideration of extreme events like hurricanes and floodings
- Only the three main branches are affected by the water level boundary (other branches: constant discharge extraction)
- Quasi-steady discharge discretization (eight distinct discharge periods, no continuous time series)

Calibration with water levels can lead to an unrealistic behavior of the stratified flow. The intrusion length is a good indication but a calibration based on measurements of vertical flow profiles would generate a more reliable model (pers. comm. Pietrzak, 31.05.2013).
Even though the three-dimensional model may still not be a representative reflection of nature due to the above mentioned limitations and simplifications, it does consider a number of physical processes that could only be parametrized in a depth-averaged model. This allows for a better understanding of the interactions of river discharge, sediment transport and salinity in the Lower Mississippi River.

2.5.1 Result of Salinity Model

Table 2.11: Intrusion length of salt wedge for different discharge periods from model results

Q_{nom} $[m^3/s]$	Q_{eff} $[m^3/s]$	Intrusion Length [rkm]
7000	5516	60
10000	8781	40
13000	11691	10
16000	14268	0
20000	18283	-15
24000	21738	-20
28000	26373	-23
33000	31839	-25

The simulation outcome for $Q_{nom} = 7000\ m^3/s$ with $Q_{eff} = 5516\ m^3/s$ agrees with the value derived from Soileau (1989) [65]. The necessary discharge to push the salt back to Head of Passes is about $11,700\ m^3/s$ and hence found to be somewhat higher than the given value. However, the figure of Soileau focuses on progression and regression rather than on equilibrium situations for constant discharges.

Conlusion:
The three-dimensional model with salinity led to reasonable results for the salt intrusion length considering the sensitivity of the salt wedge.

Remark:
More information about the physical processes can be found in literature, e.g. Lely (2007) [42], Burchard (1998,2010) [15, 17], Geyer (1993) [16] or de Nijs (2011) [52].
In the Annex (B.3, p. 121), supplementary information is provided about parameters, numerical behavior and procedure of modeling salinity.

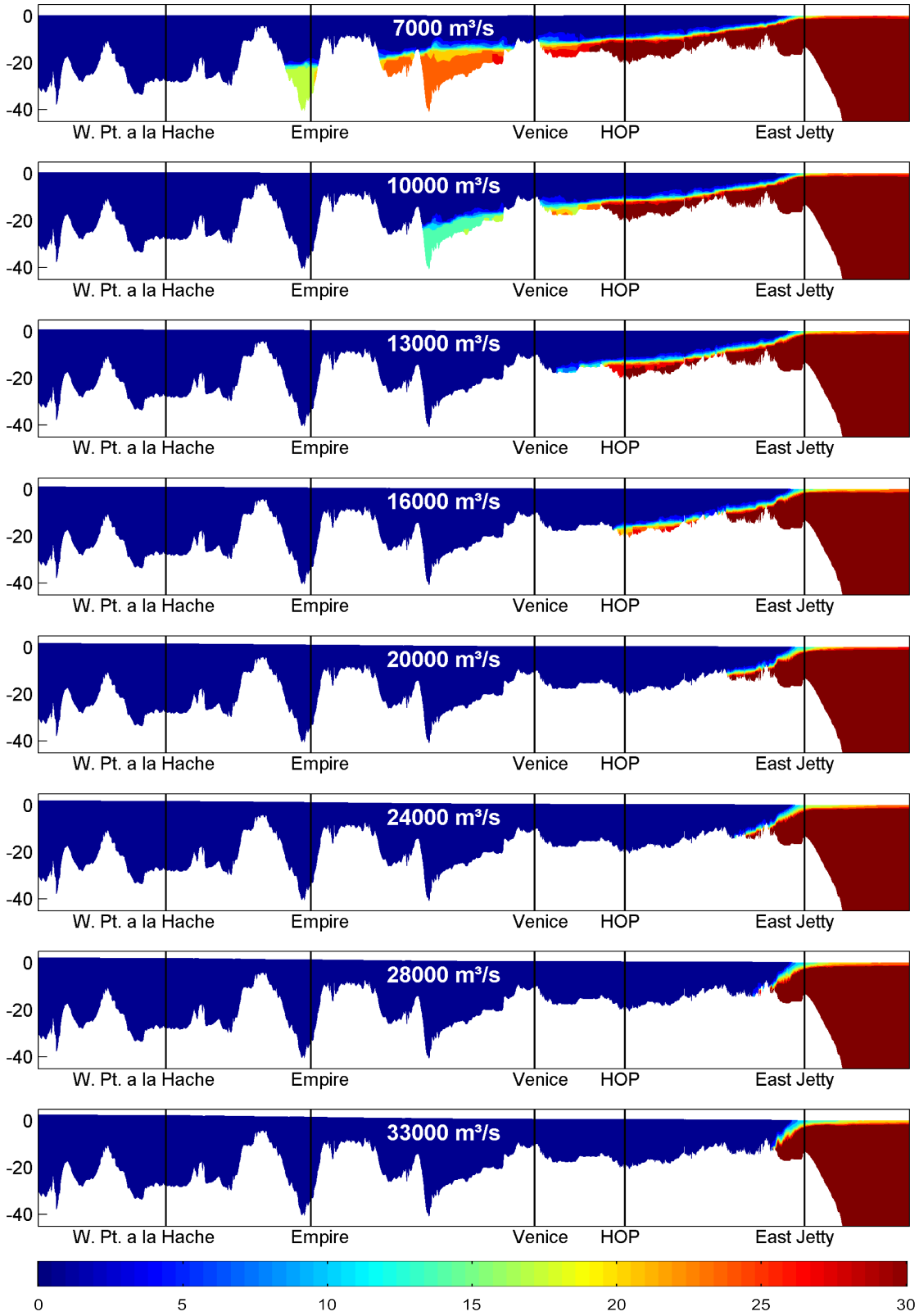

Figure 2.13: Result of Z-layer Model for Different Discharge Periods. With 30 layers.

2.6 Morphological Model (2D)

2.6.1 Settling Velocities for Sand and Mud Fractions

In the beginning the settling velocities for the sand fractions were obtained based on the median diameter and applying the formulae of van Rijn (1993) [22] with a kinematic viscosity of $\nu = 10^{-6}\ m^2/s$, a gravitational acceleration of $g = 9.81\ m/s^2$ and a sediment/water density ratio of $s = 2.65$.

Table 2.12: Settling Velocities for Sand Fractions Following van Rijn (1993) [22]

$D_{50}\ [mm]$	$w_s\ [cm/s]$
0.125	**1.18**
0.200	**2.57**
0.345	**5.12**

2.6.2 Settings for the River Bed

For the simulation of the river bed, graded sediment underlayers were chosen. A sensitivity analysis was carried out to define the parameters for the number and the thickness of the bed layer model.
Based on the outcome, it was decided to use four underlayers and one transport layer with 0.2 m thickness each to ensure a reasonable behavior of local bed levels.
More details on the concept of the Delft3D bed layer model and the analysis can be found in the Annex (see B.4.3, p. 131 and C.3.9, p. 154, respectively).
Bed layer composition, fixed layers and sediment properties strongly contribute to bed level changes and have already been set based on observations and measurements as well as modeling experience (see 2.3.7, p. 19).

2.6.3 Calibration Procedure

Using the available data, the morphodynamic model is calibrated based on three aspects.

- Suspended Sand Transport at Belle Chasse (rkm 123) - Comparison with Rating Curve 2004-2013, Allison (2013) [6]

- Bed Level Changes from 2003/4 to 2012/13 (approximately 10 years) from Reserve (rkm 223) to Venice (rkm 16)

- 20-year Average Dredging Volumes (focus on Southwest Pass - Head of Passes (rkm 16 to -35)

2.6.4 Calibration of Sand Transport

In order to calibrate the sand transport, sediment transport rates from Allison (2013) were used at Belle Chasse, between New Orleans and West Point a la Hache at rkm 123. In this region, sand transport is still relatively high as there a no significant diversions and hence the river still has enough energy.

After the transport of total suspended loads and sand in suspension in the 2009 floodyear was determined, calibration of the suspended sand transport was carried out based on two parameters: reference level and calibration parameter alpha.

Both parameters are part of the van Rijn 1984 approach. The reference height can be physically interpreted as the height of the bed load transport layer, whereas the calibration parameter alpha as no such meaning. Decreasing the reference height or increasing the calibration parameter alpha both lead to higher transport of suspended sand. During calibration the transport showed a similar sensitivity to both parameters. Below, different values and their impact on the transport of suspended sand and the total suspended load are presented. The final simulation with reference level equal to 0.5 meters and a calibration parameter alpha equal to 3 led to the best result regarding suspended sand transport compared to the reference transport at Belle Chasse. During calibration it was also decided to keep the reference height at minimum at 0.5 m which, from a physical point of view, better represents bed form elevations that usually develop during medium to high discharge periods (see also figure 2.10 on page 21).

Table 2.13: Results for Morphological Calibration of Suspended Sand with Reference Height and Calibration Parameter α. Reference: Rating curve 2008-2012, floodyear 2009, Allison (2013).

Sim no.	Ref. Level $[m]$	Alpha $[-]$	Susp. Sand Load $[10^6 tons/year]$	Total Susp. Load $[10^6 tons/year]$
132	0.2	1.5	8.9	69.9
133	0.2	2	10.8	72.6
134	0.5	2	9.1	69.4
135	0.5	2.5	10.6	71.6
138	0.5	3	**11.6**	73.1
Reference Allison (2013)			**11.6**	70.7

Remark: From the total suspended load, it becomes clear that the mud fractions are still slightly higher than one should expect from the rating curves. In the following, the mud fractions are further calibrated.

2.6.5 Calibration of Mud Fractions and Bed Level Changes

The USACE singlebeam bathymetry from 2004 used for hydraulic calibration is not the only data set available but the only consistent one and therefore used for hydraulic calibration.

In 2012/13, USACE carried out new multibeam measurements covering the Lower Mississippi River from Old River Control Structure to Venice (rkm 16). These data became recently available and were used to calibrate the bed level changes.

Below, a comparison between the two data sets is presented. It clearly shows, which reach experienced deposition or erosion or remained in a dynamic equilibrium.

For example, we can find such an equilibrium for the upper reach between Reserve (rkm 223) and New Orleans (rkm 165) followed by deposition down to Empire (rkm 47).

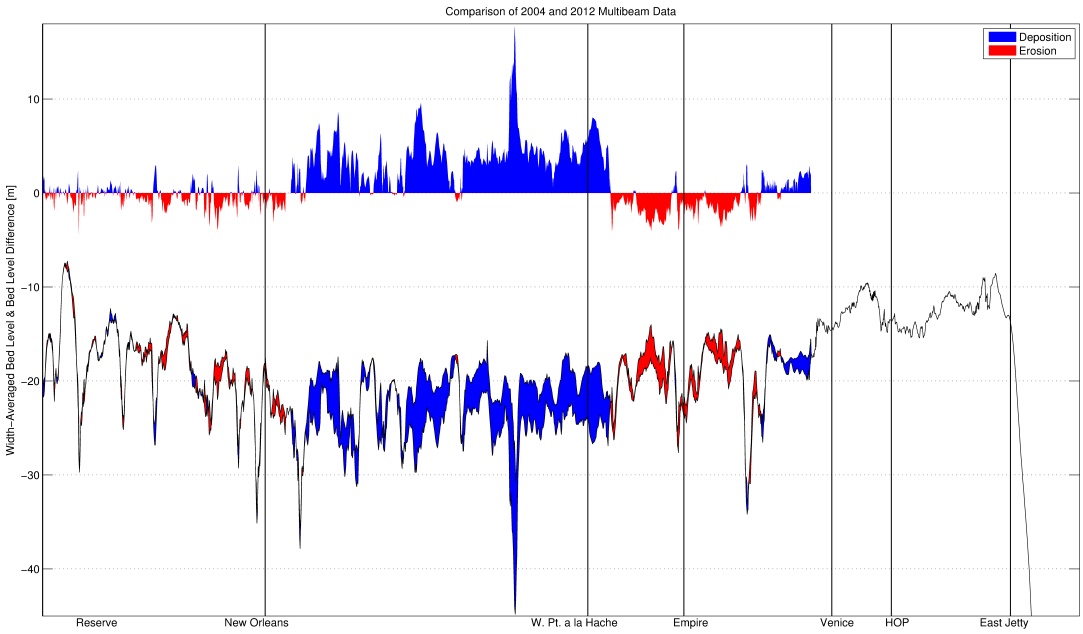

Figure 2.14: Comparison of 2004 and 2012 Multibeam Data. Source: USACE. Width-Averaged Bed Level and Bed Level Difference.

The calibration of the mud fractions involves three parameters, settling velocity, critical shear stress for deposition and critical shear stress for erosion. In general, high settling velocities, high critical shear stresses for erosion and low critical shear stresses for deposition lead to high deposition rates of mud fractions and vice versa.
Additional theoretical information can be found in the Annex B.4.9 on page 137. More detailed considerations about the application of critical shear stresses and settling velocities in the model can be found in the Annex C.1 on p. 145.

Remark:
The simulations were sped up by reducing the hydraulic simulation time and increasing the morphological factor instead. A comparison to a simulation with old settings revealed only minor changes in the order of centimeters in most parts of the domain. Only in one bend, larger initial changes occurred. However, the outcome is very well acceptable when taking into account the uncertainty for such long-term simulations (pers. comm. Kees Sloff, 12.09.2013). In order to avoid confusion and to allow for comparability, all other tables, included in following simulations and scenarios, are given with the normal hy-

draulic simulation period of 1440 minutes and their corresponding morphological factors as defined initially.

In the below table, different settings are presented. The values for critical shear stress for deposition refer to Reserve, the fresh water side at the tip of the salt wedge, the salt water side at the tip of the salt wedge and to East Jetty, respectively.

Table 2.14: Calibration of Mud and Bed Level Changes

sim no.	$\tau_{crit,dep}$ $[N/m^2]$	$\tau_{crit,ero}$ $[N/m^2]$	$w_{s,silt}$ $[m/s]$	$w_{s,clay}$ $[m/s]$	Correlation $[-]$	Deposition Rate $10^6 m^3/year$	Remarks
138	.01-.01-.05-20	1-1000	2.30E-05	3.60E-07	0.41	-14.3	Sand Calibration
157	1-3-3-10	1-1000	1.00E-03	1.00E-04	0.66	14.2	
158	1-2-2-10	1-1000	1.00E-03	1.00E-04	0.38	-5.2	
166	1-5-10-20	1-1000	1.00E-03	1.00E-04	0.68	23.6	
173	1-3-3-10	1-1000	1.00E-03	1.00E-04	0.65	16.4	as 157, 3 floodyears [1]
176	1-5-10-20	1-1000	1.00E-03	1.00E-04	0.69	23.6	as 166, dunes [2]
180	0.5-1-10-20	1-1000	1.00E-03	1.00E-03	0.59	7.4	dunes
181	0.5-3-10-20	1-1000	1.00E-03	1.00E-03	0.68	22.4	dunes
182	0.5-1-10-20	1-1000	1.00E-03	1.00E-03	0.67	19.8	dunes
188	0.1-3-10-20	1-1000	1.00E-03	1.00E-03	0.67	18.8	dunes

2.6.6 Calibration of Dredging Volumes

The model comprises three dredging areas whose annual dredging volumes were obtained from literature ([67, 68, 69, 70]).

- Head of Passes - Southwest Pass (from rkm -30 to 16)
- New Orleans Harbor (from rkm 165 to 150)
- Reserve - New Orleans (from rkm 223 to 165)

The dredging reaches Reserve - New Orleans and New Orleans Harbor show rather small average annual dredging volumes in the order of 0.6 *to about* $1.0 * 10^6$ m^3. The 20-

[1] The measured bed level changes were created during floodyears with varying discharges and amounts and composition of sediment. In order to test the response of the model to a wider range of floodyears, a year with a pronounced flood peak and a year with relatively low discharge were added to the "average" floodyear 2009. Results of this analysis can be found in the Annex, C.3.11, p. 158.

[2] see 2.6.6, p. 33.

year average of the dredging reach Southwest Pass - Head of Passes is around $13 * 10^6\ m^3$. This already indicates the importance of implementing dredging operations in the model. The dredging is also used for calibration because downstream of Venice (rkm 16) no multibeam data is available. Instead, it is decided to tune the deposition of mud fraction in such a way, that the annual dredging volumes fairly well agree with the 20-year average dredging volume in the Southwest Pass - Head of Passes reach.
As a consequence, the dredging volumes are closely related to the foregoing calibration of the bed level changes and are based on the same parameters.
High values for critical shear stresses for erosion and deposition, especially in the dredging reach from Venice (rkm 16) to East Jetty (rkm -30) lead to enhanced deposition and thus high dredging volumes.
Based in the above presented results, the final choice was made based on the annual dredging volume of Southwest Pass - Head of Passes.

Table 2.15: Calibration of Dredging Volumes

sim no.	Correlation [−]	Deposition Rate $10^6 m^3/year$	Dredging Volume SWP-HoP $10^6 t/year$	Remarks
138	0.41	-14.3		
157	0.66	14.2	3.5	
166	0.68	23.6	5.0	
176	0.69	23.6	9.5	dunes
181	0.68	22.4	11.5	dunes
182	0.67	19.8	11.0	dunes
188	0.67	18.8	12.0	dunes

Remark:
The simulation of dunes led to a satisfying result of dredging volumes. For more information about the simulation of dunes see Sensitivity Analysis, C.3.5, p. 152.

2.6.7 Calibration Result

The simulation that led to the best results in terms of suspended sand transport, bed level changes and dredging volumes was found to be simulation 188 with the following settings:

Table 2.16: Settings of Calibrated Model

Parameter / Property	Unit	Value / Range
Time Step	$[min]$	**0.50**
MorFac	$[-]$	**20-100 (80-400)**
Thickness of Bed Transport Layer	$[m]$	**0.20**
Thickness of Bed Underlayer	$[m]$	**0.20**
Number of Bed Underlayers	$[-]$	**4.00**
Fall velocity Medium Sand	$[m/s]$	**0.051**
Fall velocity Fine Sand	$[m/s]$	**0.012**
Fall velocity Mud	$[m/s]$	**0.001**
Alpha Calibration Parameter	$[-]$	**3.00**
Reference Level	$[m]$	**0.50**
Temperature	$[°C]$	**20**
Kinematic Viscosity	$[m^2/s]$	**1.00E-06**
Annual Water Input	$[km^3/year]$	**430**
Annual Sediment Input	$[10^6 t/year]$	**82**
Critical shear stress for deposition	$[N/m^2]$	**0,1-20**
Critical shear stress for erosion	$[N/m^2]$	**1-1000**

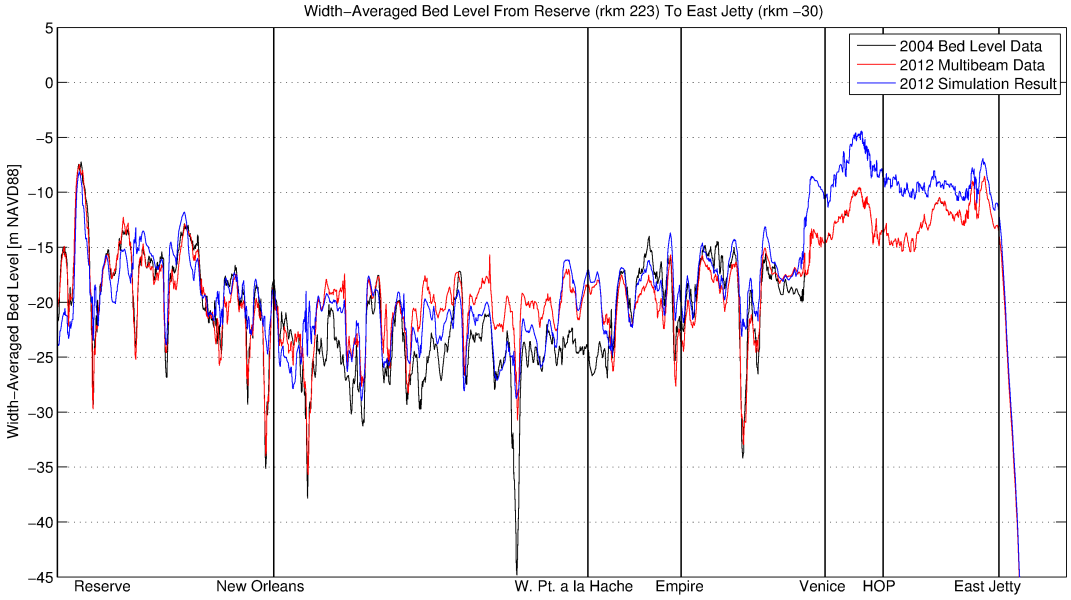

Figure 2.15: Sim 188 Bed Level Changes. The figure shows the width-averaged bed level of the main channel for the initial situation, the new multibeam data and the simulation result.

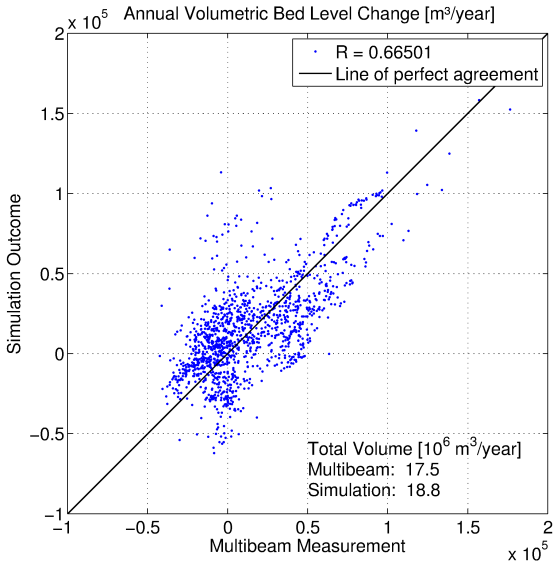

Figure 2.16: Sim 188 Correlation of Bed Level Changes. The figure shows the width-averaged annual volumetric bed level changes for the multibeam data and the simulation outcome with the corresponding correlation and total annual deposition rate.

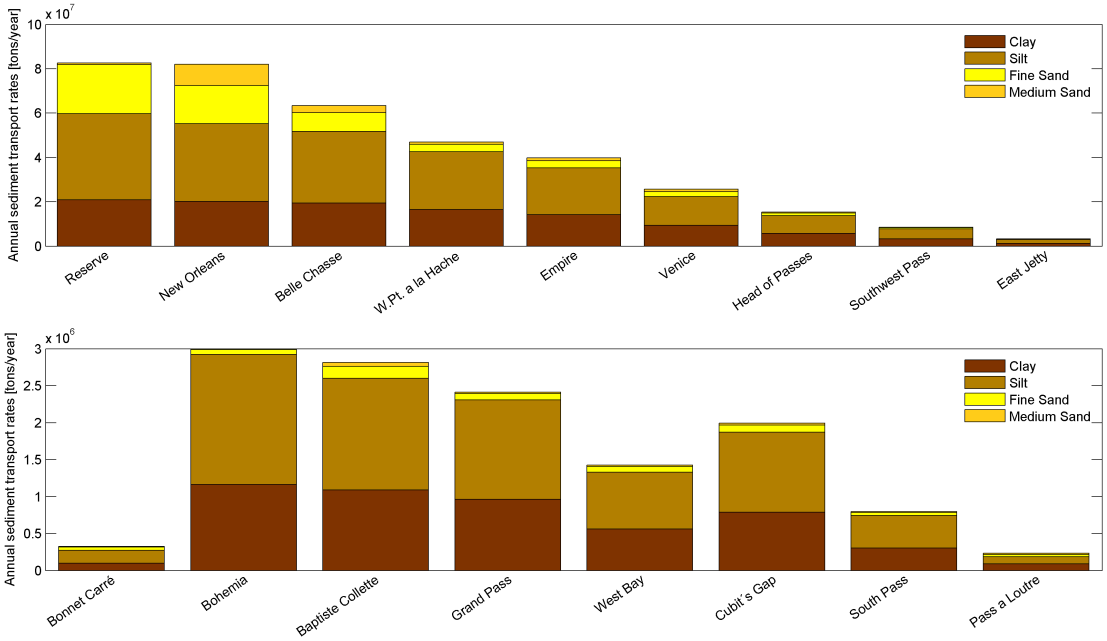

Figure 2.17: Sim 188 Sediment Transport. The figure shows the 10-year average sediment transport through cross-sections along the main channel and through side channels.

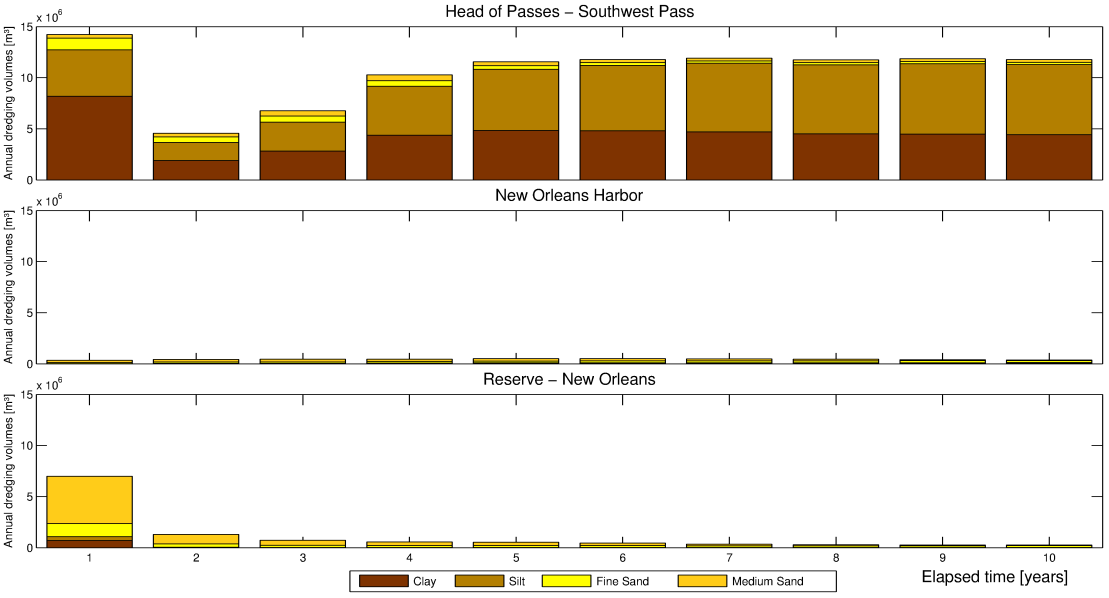

Figure 2.18: Sim 188 Dredging Volumes. The figure shows the annual dredging volumes for three different dredging reaches.

Remark:
Although other simulation produced slightly better dredging volumes in the Southwest Pass - Head of Passes dredging reach, it was decided to choose for the simulation that showed an annual deposition rate comparable to that from the field measurements as this affects more than 200 km of the model, whereas the corresponding dredging volumes are only generated in the last 45 km and, moreover, also varying due to annual budgets. Therefore, and taking into account the complexity of the estuarine processes, the calibration results of the dredging volumes were also considered to be satisfying.
The sand transport through a cross-sectional area at Myrtle Grove (rkm 95) was compared to measurements carried out in April and May 2011 by Allison [1] for validation purposes and led to satisfying results, see Annex C.2.2 on p. 149.

2.7 Conclusions from Calibration

Dredging Volumes
The calibration of the two-dimensional morphological model led to satisfying results for dredging volumes, especially around Head of Passes and Southwest Pass. Also the upper dredging reaches from Reserve to New Orleans and New Orleans Harbor gave realistic results.

Sediment Transport
The two-dimensional results are reasonable, also in the downstream region, as the diversion upstream of Head of Passes convey water with higher suspended sediment concentration. The water to sediment ratios of Baptiste Collette and Grand Pass as well as those of West Bay Diversion and Cubits Gap are comparable.
Flocculation and enhanced settling around Head of Passes leads to a decrease of sediment/water ratios.
An analysis of the sediment transport shows that sediment diversions constructed upstream of Venice will benefit from larger sand concentrations and hence be more effective for land building.

Bed Level Changes
The total annual deposition rate of the reach from Reserve (rkm 223) to Venice (rkm 16) was met by the morphological model. Despite local deviations, e.g. in originally deep bends, the local bed level changes followed the multibeam measurements reasonably well.

3 | Wetland Restoration with River Diversions

3.1 Definition, Importance and Restoration Policy

The wetlands in the Mississippi Delta are of great importance with respect to a broad range of aspects. But before assessing its value, we first want to find a definition for wetlands.

The United States Environmental Protection Agency (EPA) uses the definition of Cowardin (1979) among others which states that

"wetlands are lands where saturation with water is the dominant factor determining the nature of soil development and the types of plant and animal communities living in the soil and on its surface"

and are determined by

"[...] regional and local differences in soils, topography, climate, hydrology, water chemistry, vegetation, and other factors, including human disturbance" [26].

From an ecological point of view, wetlands provide a unique environment which serves as a habitat and breeding ground for aquatic life as well as land animals and birds.

The wetlands also serve the communities at the coast. Filtration of water and recreation are only some of the many provided advantages. Another important aspect is the safety against flooding caused by hurricanes and storm surges.

From an economic point of view, fishery, oyster farming and especially extraction of oil and gas are of importance [19].

Figure 3.1: Economic, ecological and social functions of the Mississippi Delta (Fishery , Gas Extraction, Oyster Farming, Habitat and Breeding Ground, Recreation, Protection Against Hurricanes and Storm Floods and Navigation

Consequently, in 1990, the "Coastal Wetlands Planning, Protection and Restoration Act", CWPPRA set the legislative framework for a variety of projects. The official website with information provided by the USGS National Wetlands Research Center states that 151 projects have been authorized with an affected area of approximately $44,500\ km^2$ [19]. The project types comprise coastal protection as well as marsh creation and restoration where several restoration techniques like the beneficial use of dredged material, sediment trapping mechanisms, bank stability and vegetation are considered. A new coastal restoration Masterplan by the State of Louisiana, CPRA (Coastal Protection and Restoration Authority of Louisiana) from 2012 is the most recent concept which also specifies new sediment diversion sites [58, 71].

Figure 3.2: CWPPRA & CPRA Logo. Source: Office of the Governor & [58]

3.2 Functions, Guidelines and Examples of Diversions

In this chapter, a short overview is given on types of diversions. Moreover, we elaborate on various aspects that influence the diversion of water and sediment. Finally, diversions along the Lower Mississippi River are presented together with information about purpose, capacity and operation.

3.2.1 Concept of Sediment Diversions

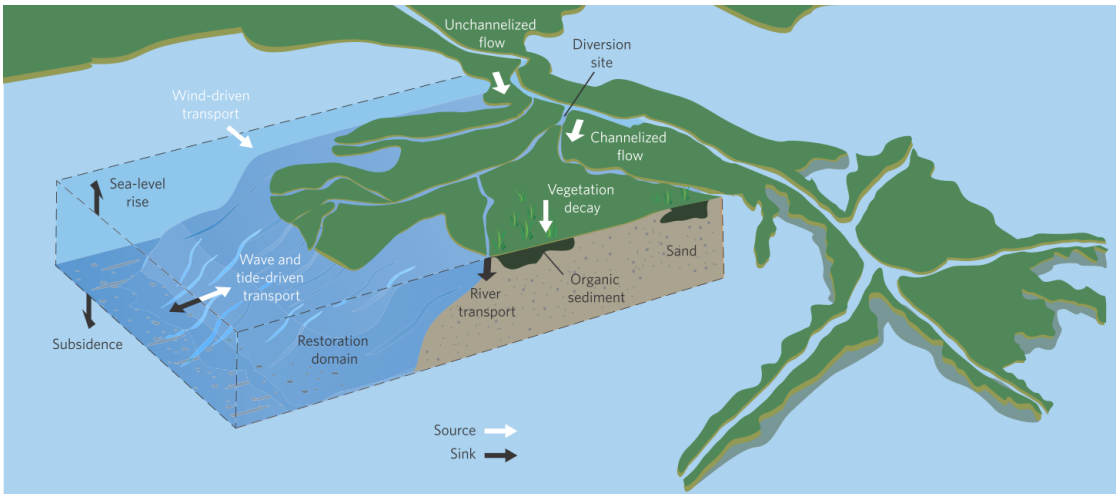

Figure 3.3: Schematization of Diversion and Accompanying Delta Processes. The figure shows an artificial diversion that induces the building up of new marsh land. Courtesy of Edmonds 2012 [25].

In the above figure, Edmonds (2012) included all important aspects at a diversion site that contribute to the development of the restoration domain. Flow can enter the wetland in a channelized and an unchannelized way, e.g. through smaller crevasses. The water also transports sediment that is settling or trapped by vegetation. Together with organic sediment from decaying vegetation, the sediment forms the basis of the marsh area. In addition, wind, wave and tide-driven transport might be of importance, especially during storm events. Another important aspect already described in the introduction are the sink terms sea-level rise and land subsidence that, in most ares of the Mississippi Delta, dominate and lead to high land losses.

3.2.2 Diversion Types

Following Heer & Mosselman (2004) [34], a diversion is a special case of a bifurcation where only the diversion has a bifurcation angle.
River diversions can be applied to deal with various problems. For example, the focus may be diversion of river discharge in order to relieve the river system and to prevent flooding. These diversions are flood water diversions.
Another type of diversion is the fresh water diversion that is used to decrease salt concentrations in marsh areas which ensures favorable conditions for vegetation and hence stability of wetlands.
At last, diversions can be used to convey sediment-laden water for wetland restoration purposes. These sediment diversions are what we are interested in.
We can further distinguish two forms of sediment diversions that will play an important role in this work.

Controlled Sediment Diversion

The operation of a diversion is important. An uncontrolled diversion can, depending on the design, constantly divert water and sediment. From an economic point of view, this option is favorable due to lower construction and maintenance costs. However, also controlled diversion can be a feasible option. Allison and Meselhe (2010) [3] already showed that large river diversions can be operated only during high sediment loads.
Because of the highly non-linear relation between water and sediment discharge, short periods suffice to convey large amounts of sediment to the marsh areas. The sediment load varies enormously with approximately a factor 50 throughout the year.
The sediment transport depends on the grain size distribution and the type of sediment. There is a hysteresis effect in the Mississippi meaning that the sediment load varies for the same discharge depending on whether it is falling or rising.

Large-Scale Sediment Diversion

Large-scale sediment diversion are a promising solution to effectively convey sediment-laden water.
However, the large amounts of fresh water will decrease the local salinity and thus endanger speckled trout or shrimp farms.

3.2.3 Guidelines for Sediment Diversions

In general, the efficiency of a sediment diversion depends on a number of hydraulic, economic and operational aspects (see Melman (2012) [45], Heer & Mosselman (2004) [34] and Dean (2012) [21]). Those are:

- Water and sediment discharge in the river
- Local flow patterns (bends, bathymetry, interactions with adjacent hydraulic structures or bed forms)
- Sediment concentration (including spatial and temporal variations)
- Sediment characteristics (diameter, bed load, wash load)
- Sediment trapping efficiency of developing wetland
- Dimension of diversion (small-scale, large-scale)
- Geometry of diversion (diversion angle and cross-sectional shape)
- Operation type (uncontrolled, controlled)
- Operation mode (constant, "pulsed" operation)
- Maintenance and construction costs
- Indirect costs (ecological and economic footprint/ consequences)

3.2.4 Diversions at the Lower Mississippi River

Although constructed for a different purpose, the effect of many diversions in the Lower Mississippi Delta on the adjacent wetlands generated a basic knowledge. The following table gives an overview about the diversions and their contributions [21].

Figure 3.4: Examples of Diversions at the Lower Mississippi River, Top Left: Caernarvon Fresh Water Diversion, Top Middle: Davis Pond Fresh Water Diversion, Top Right: Bayou Lamoque Fresh Water Diversion, Down Left: West Bay Diversion with view on Mississippi downstream, Down Right: Bonnet Carre Spillway.

Table 3.1: Diversions at the Lower Mississippi River

Name	Diversion Type	Capacity $[m^3/s]$	Comments
Bonnet Carré	flood water	7075	Not optimized for sediment conveyance, 2011: 42 days opening leads to 3 million tons of accretion (Nittrouer 2012).
Caernarvon	fresh water	100 (gated), 285 (max)	Expected to reduce land loss by $335km^2$ in 50 years. Inversed annual land loss into land growth ($-4km^2 to +1.6km^2$) in 1992 - 1994 but was heavily affected by Hurricane Katrina.
Davis Pond	fresh water	225 - 300	Expected to preserve $134km^2$ in 50 years. Ongoing land loss and water quality issues
Bayou Lamoque	fresh water	225, Plan: 365 without gates	small amount of data, Plan: creation of $2,5km^2$ in 20 years, neglected in model
West Bay	sediment	570 (planned extension to 1415)	Expected to create $40km^2$ in 20 years. Achieved reduction of land loss during 2001 - 2009 (Barras et al. 2009). Creation of land by means of pumped sediment. In addition, contributed to downstream shoaling of anchorage area.
Myrtle Grove	sediment	425 (gated)	Expected to preserve $137km^2$ in 50 years. Pulsed operation showed to be beneficial, coupled with pipeline conveyance, only used for engineering and design studies so far.

3.3 Scenario Overview

Different approaches were developed to tackle the loss of wetlands at the Louisiana coast. In short, they will be presented in the following sections of this chapter.

3.3.1 Scenario 1: Do-Nothing

Blum and Roberts (2009) pointed out that there is not enough sediment supply coming from upstream to effectively counteract land losses. Based on their quantitative analysis including land subsidence and sea-level rise they developed the following figure:

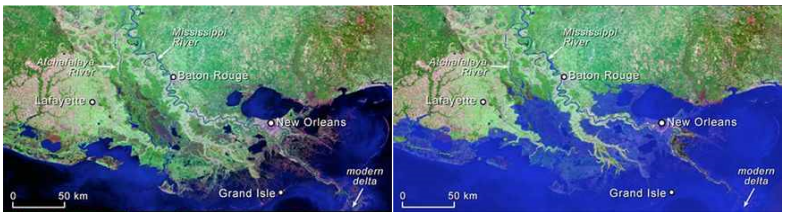

Figure 3.5: Land loss for Do-Nothing Scenario, Blum and Roberts (2009). Adapted from National Geographic.

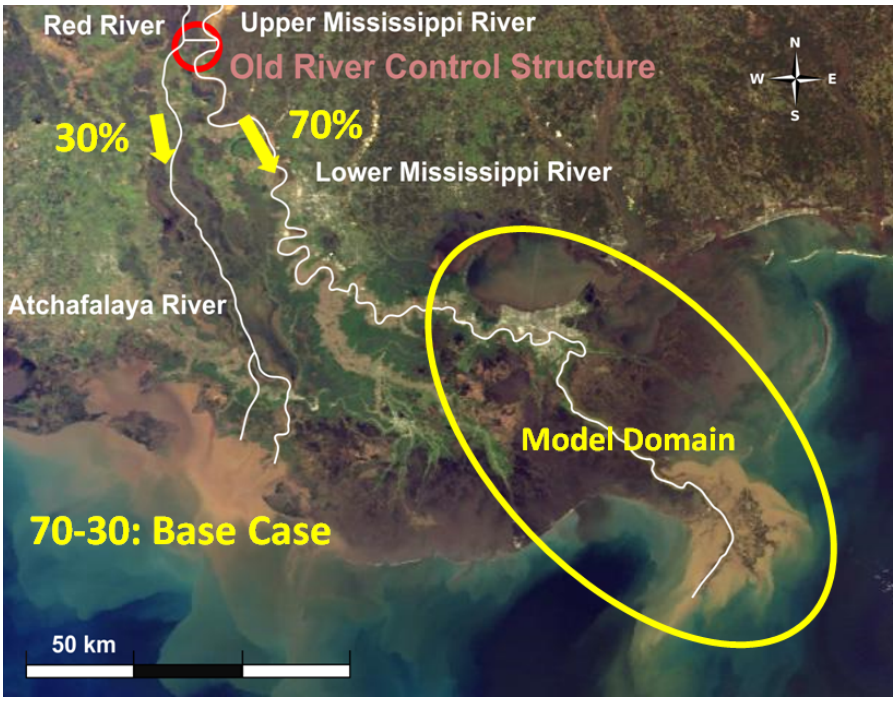

Figure 3.6: Overview Do-Nothing Scenario/ Base Case. . Adapted from NASA.

3.3.2 Scenario 2: Multiple Diversions

CPRA is planning sediment diversions at multiple locations and with different discharges. In general, it is intended to construct operated diversions as they are more efficient and also more unlikely to drastically increase like West Bay Diversion or Cubit's Gap. However, options for the exact location, design and configuration still have to be evaluated [71].

The main idea behind multiple diversions is to increase the amount of sediment-laden water into the adjacent wetlands at favorable or strategically important areas. There has already been gathered plenty of theoretical and practical knowledge about building and operating diversions along the main channel. Although some diversions showed promising results in terms of land building (see e.g. CWPPRA), most of the projects were not convincing or interfered with navigability, e.g. West Bay Diversion. Others did not go beyond their research status, e.g. Davis Pond [83].

In general, significantly more and also larger diversions have to be operated to achieve the necessary land-building capacities. Therefore, the implementation of 5 additional diversions with design discharges from $1,000\ m^3/s$ to $7,000\ m^3/s$ based on the CPRA Coastal Masterplan in the present model represents the next step [4, 46, 71]. The relevant sediment diversions downstream of New Orleans are Upper, Mid and Lower Breton as well as Mid and Lower Barataria.

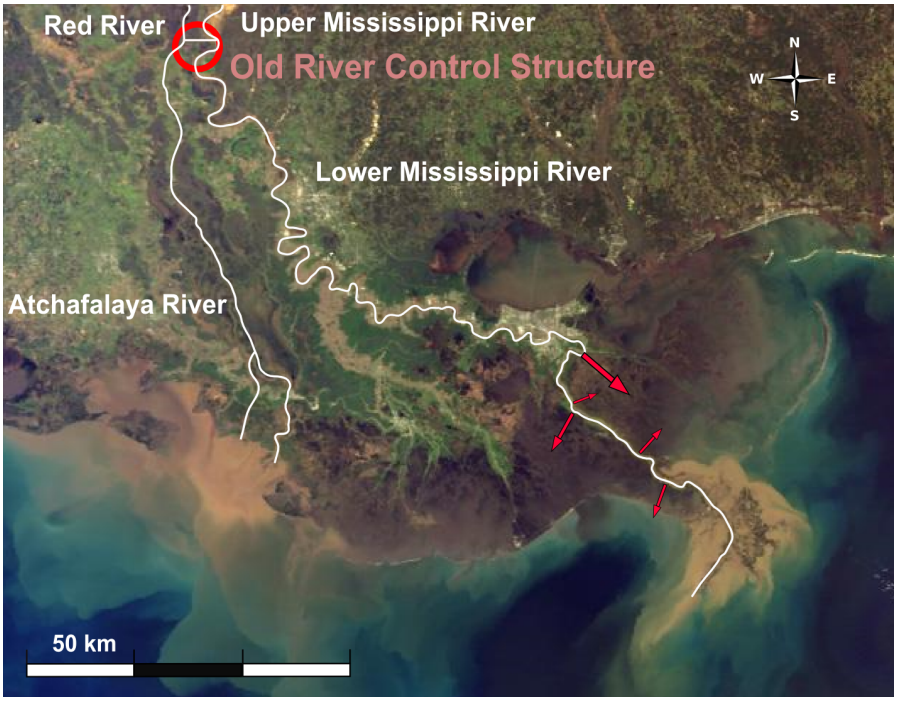

Figure 3.7: Multiple Sediment Diversions. Adapted from NASA.

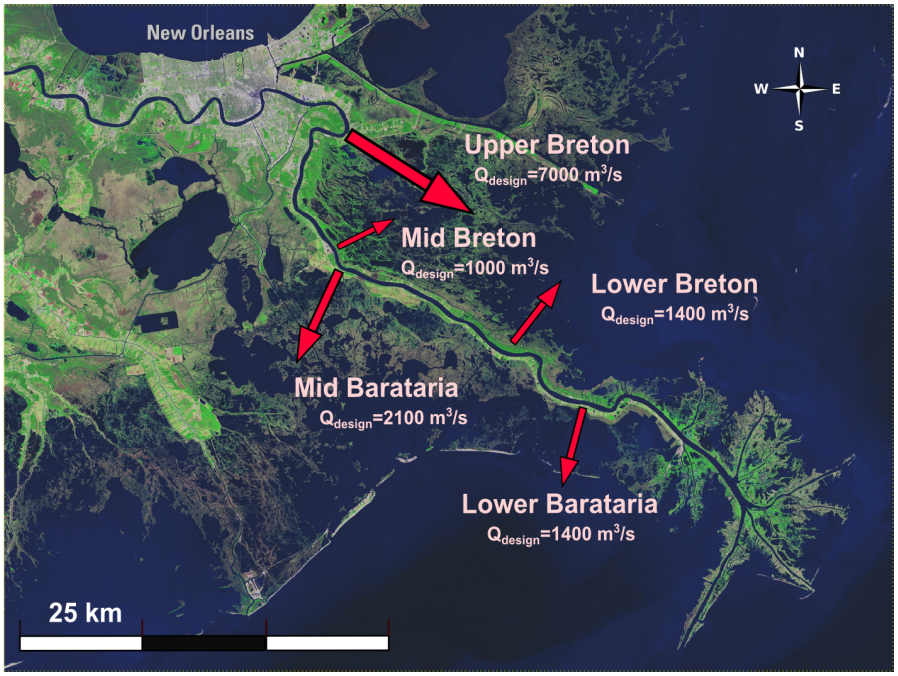

Figure 3.8: Multiple Sediment Diversions. Adapted from USGS.

3.3.3 Scenario 3: Large-Scale Sediment Diversions

Parker, Kim et al. (2008) [40] showed an example for large-scale sediment diversions around rkm 65 to 70 that could build 1000 km^2 of new wetlands until 2100.
To avoid negative impacts on navigation, controlled diversions should only convey water in times of sufficiently high discharge.
This approach already includes the idea of a pulsed diversion that conveys water with high sediment concentrations. We can test these pulsed large-scale sediment diversions in our model.

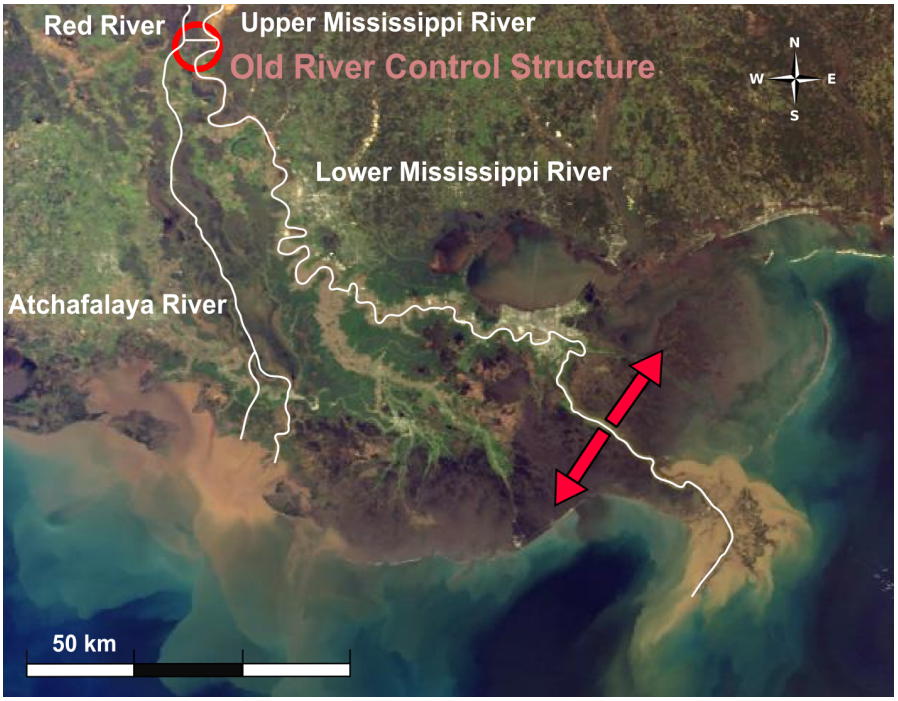

Figure 3.9: Large-Scale Sediment Diversions. Adapted from NASA.

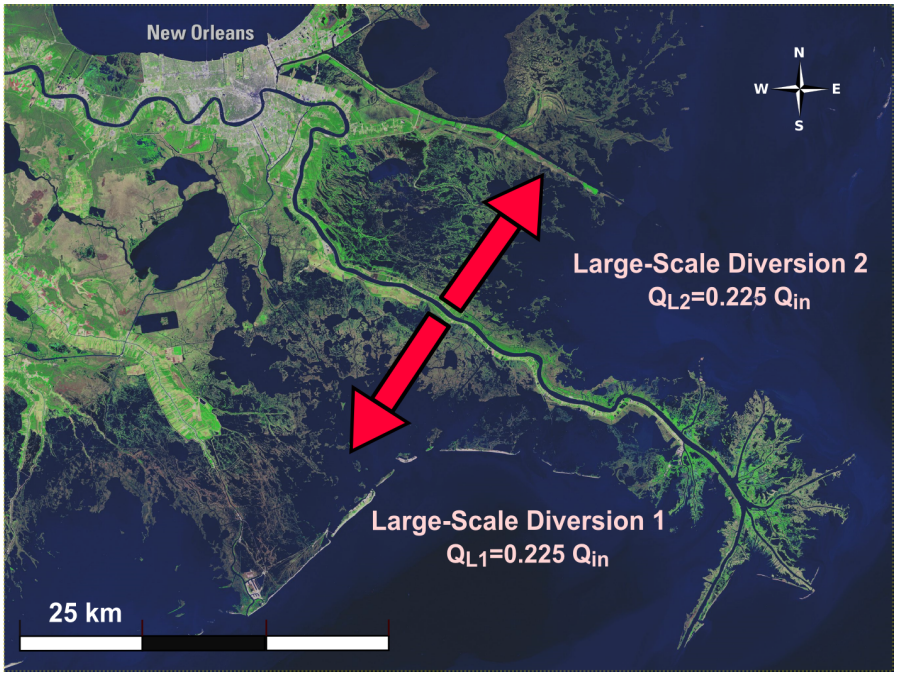

Figure 3.10: Large-Scale Sediment Diversions. Adapted from USGS.

3.3.4 Scenario 4: Abandon Birdfoot

In this scenario, a new navigation channel is constructed somewhat downstream of New Orleans. There are two options for the orientation of the new channel, to the east or to the west ("hang a right" / "hang a left)". At the same time, the downstream navigation channel is closed by locks. The operation of sail-through locks could ensure a continuous vessel speed when entering and leaving the channel [83].
Winer (2011) discarded this approach referring to the negative experience made with navigation channels crossing an estuary, e.g. the Mississippi River Gulf Outlet (MRGO) which was very vulnerable to extreme events like Hurricanes and subsequent filling.

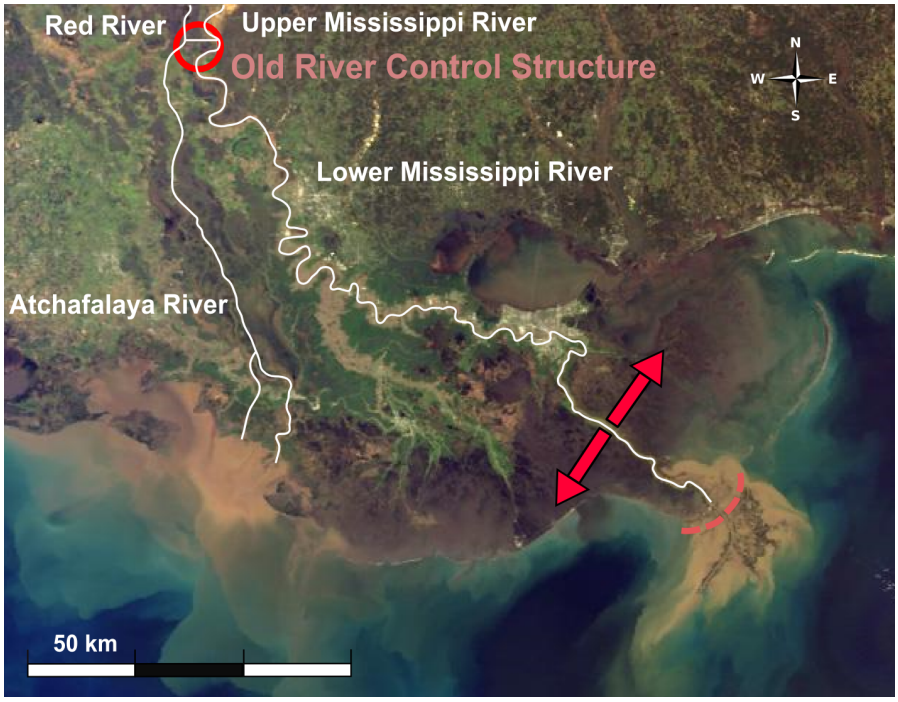

Figure 3.11: Abandonment of Birdfoot Delta. Adapted from NASA and New York Times .

3.3.5 Scenario 5: Discharge Reduction at ORCS

The idea of Winer (2011) [83] is to divert more water and sediment to the Atchafalaya River via Old River Control Structure. Only the necessary amount of water should be diverted to the Lower Mississippi to ensure navigation and to keep the salt wedge away from fresh water intakes. Winer argues that
"[...] a dredged navigation channel is incompatible with natural delta building"
and strives for a sustainable solution in the Atchafalaya which comes close to a closure of this river for deep-draft navigation.

Figure 3.12: Discharge Reduction at ORCS. Adapted from NASA and 3 BP Blogspot.

We can run a simulation with only low discharges from $7,000$ to $13,000$ m^3/s to check, how the system would respond to the measure proposed by Winer (2011).
In addition to this rather extreme reduction, another simulation will run with a 60-40 instead of a 70-30 flow distribution.

3.3.6 Scenario 6: Create a Third Delta

In 1904, a natural tributary was closed by a dam between the subdeltas of the Atchafalaya River and the Lower Mississippi River at Donaldsonville (below Old River Control Structure and still upstream of the model area). Since this intervention, land loss rates dramatically increased in the coastal area around Terrebonne and Barataria Bay as sediment supply stopped [57]. The approach of creating a third delta includes the concept of replacing the dam with a control structure, reopening the old channel by means of initial dredging and to establish a bifurcation further downstream that diverts the water and sediment loads to each of the bays [83].

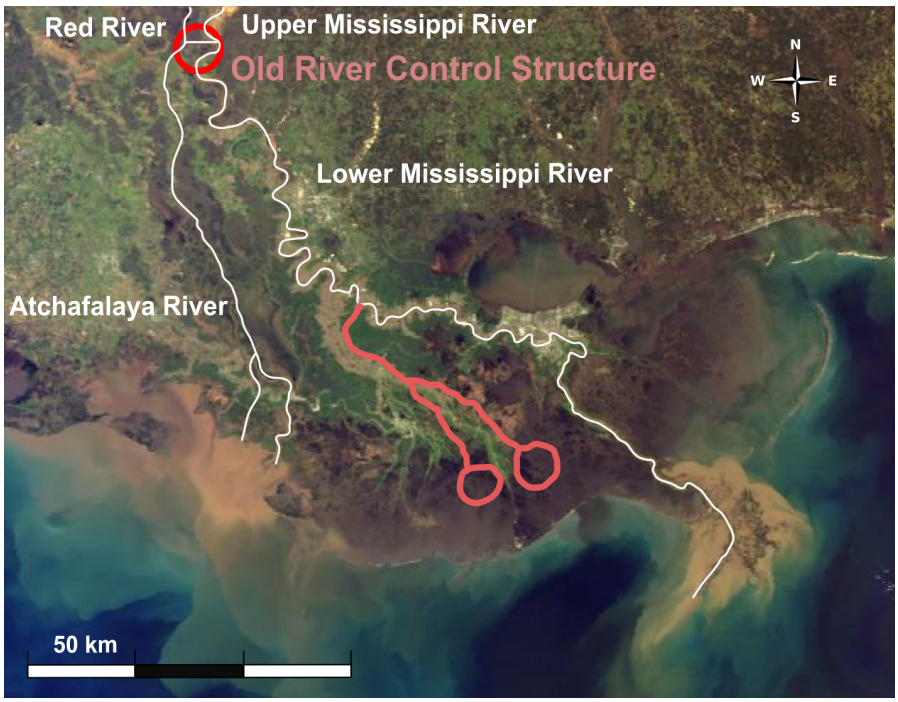

Figure 3.13: Third Delta Conveyance Channel. Adapted from NASA and Restore or Retreat.

The project was planned with a discharge around $5,600\ m^3/s$ to build two subdeltas. A number of advantages, such as better flood protection and decreasing dredging quantities for the Lower Mississippi River were given [60].
However, high construction costs are expected as a channel of more than 100 km length has to be built implying several pipeline crossings and large dredging volumes [83].

3.3.7 Scenario 7: Pulsed Operation of ORCS

Various authors made estimates about the sediment discharge at Old River Control Structure for the pre-dam situation in the 19th century. As stated by Blum (2009) [10] there has been a decrease from $450 * 10^6$ to $205 * 10^6$ tons/year.
It is argued that even with a sediment trapping efficiency of 100% (realistic value given with 40%) the actual sediment discharge does not suffice to maintain the Mississippi delta. Although sediment diversions might work temporarily they are only limited to a small region. On the long term, the birdfoot cannot be sustained without increased sediment supply.
According to Parker, Kim et al. (2008) [39], the sediment distribution at Old River Control structure deviates from the flow distribution with relations of 40-60 and 30-70, respectively. Hence, the Old River Control Structure further reduces the sediment supply for the Lower Mississippi River. Originally, this was also intended to slow down sedimentation in the main channel and the natural process of increasing diversion towards the Atchafalaya River [72].
A way to increase sediment loads and mitigate accretion could be a pulsed operation of this structure in combination with controlled sediment diversions in the Lower Mississippi River: During times with sediment loads, more water could be conveyed through these downriver diversions. This would not only go a step further than making use of the normally available sediment in the Lower Mississippi River but also convey water when the sediment concentration is favorable and navigational depth is ensured.
During low discharge the water could be predominantly conveyed through the main channel. This would provide sufficient draft and help to decrease dredging quantities.

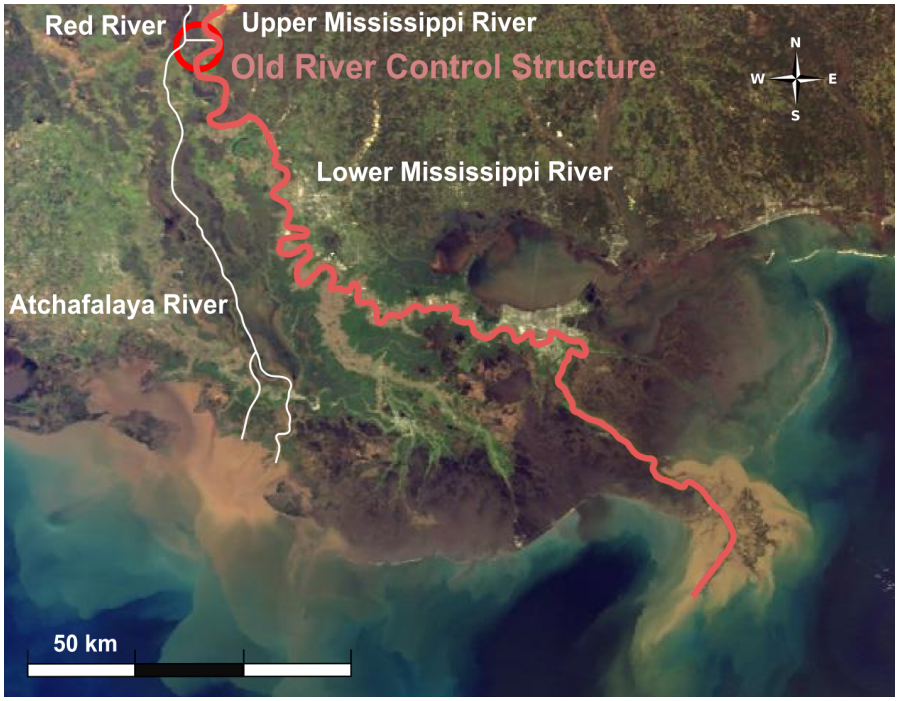

Figure 3.14: Changing Discharge Distribution at ORCS. Adapted from NASA.

4 | Numerical Implementation

4.1 Concept of Implementation

A number of scenarios was presented in the forgoing chapter. Now, the relevant scenarios have to be implemented in the numerical model.

The basic idea for the discharge input is to stick to the calibrated periods of constant discharge while changing the morphological factor, i.e. the duration of the discharge periods, as well as the number of occurrence, e.g. in some scenarios, all discharges might be above $Q = 10,000\ m^3/s$ so that $Q = 7,000\ m^3/s$ is excluded. This way, a large variety of discretized annual hydrographs and annual average discharges can be achieved.

The application of new sediment diversions, on the other hand, will lead to local extractions of water (and sediment), which can be regulated by setting up new hydrodynamic boundary conditions. However, as the flow diversion will also affect the flow distribution, adaptations have to be made at all downstream offtakes, as well.

As we are dealing with a fixed number of discharge periods, whose hydrodynamic boundary conditions are changed for the implementation of diversions, we can easily combine different scenarios and a series of simulations that allow for a detailed analysis of the impact of sediment diversions on the morphology of the main channel for changes in upstream water and sediment supply.

4.2 Implementation of Scenarios

4.2.1 Operation Mode Large-scale Diversions

The sediment diversions were proposed to be operated with controlled structures. In order to achieve a diversion of 45% of the flow, three different scenarios were set up.

- Large 01
  The first scenario (Large 01) assumes limiting the downstream discharge in the Mississippi to $10,000\ m^3/s$. Everything above this limit is conveyed via the diversions. This way, we achieve an average diversion rate of 43% for the 2009 floodyear.

- Large 02
  In this case, we assume a fixed diversion rate of 45% for all discharge periods. Of course, this might lead to problems with navigation and enhanced salt intrusion during low river stages and surely is not the case to be recommended. However, it also provides insight into how the diversions would work without a control structure and serves as reference for sediment diversion efficiency.

- Large 03
  The third case uses a progressive diversion rate. The distribution is no longer proportional but the structure conveys an extra amount of flow in case of high discharge and reduces the diverted flow in case of low discharge. This way, ecological as well as navigational aspects are considered.
  In order to achieve around 45% diversion of the annual flow 75% has to be diverted during high discharges and only 16% during low discharges.
  Still, problems with navigation and salt intrusion may arise during extreme low river stages. Therefore, it would be a wise to set a lower bound for operation, e.g. for discharges of $3 - 4,000\ m^3/s$.

The different discharge extractions of the large-scale diversions for the above presented operation modes are summarized in table 4.1.
In all scenarios of the large-scale diversions, we have to assume changes in downstream discharge distribution, as a large part of the water gets diverted. It was decided to reduce the amount of water extracted through the downstream branches proportionally to the reduction of flow just downstream of the large-scale diversions. In table 4.2, the new

flow distributions are presented. The abbreviations of the diversions and side channels correspond to those used in figure 2.1 on p. 7. The large-scale diversions are L1 on the right bank and L2 on the left bank, respectively.

Table 4.1: Discharges for Different Operation Modes of Large-Scale Diversions

2009			Large 01	Large 02	Large 03
Q_{nom} $[m^3/s]$	MorFac $[-]$	No. Period	$Q_{L\ 01}$ $[m^3/s]$	$Q_{L\ 02}$ $[m^3/s]$	$Q_{L\ 03}$ $[m^3/s]$
7000	100	1	0	3150	1114
10000	55	1	0	4500	2273
13000	40	1	3000	5850	3841
16000	40	1	6000	7200	5818
20000	60	1	10000	9000	9091
24000	30	1	14000	10800	13091
28000	20	1	18000	12600	17818
33000	20	1	23000	14850	24750
	365	8	6014	6842	6609

Table 4.2: Relative Flow Distribution for Large-Scale Diversions

Large 01	**BON**	**DP**	**CAE**	**L1**	**L2**	**BOH**	**OST**	**FSP**	**BC**	**GP**	**WB**	**SC**	**CG**	**GOM**	**SP**	**PAL**	**TOTAL**
7000	0.0	0.6	0.4	0.0	0.0	0.0	0.0	0.5	11.1	14.6	7.8	5.5	7.7	23.6	12.8	15.4	**100**
10000	0.0	0.8	0.6	0.0	0.0	0.0	0.0	3.6	10.5	12.4	7.2	3.6	9.4	29.3	11.0	11.6	**100**
13000	0.0	0.5	0.4	11.5	11.5	0.0	0.0	2.8	8.1	9.6	5.6	2.8	7.2	22.6	8.5	8.9	**100**
16000	0.0	0.7	0.3	18.8	18.8	0.0	0.0	2.2	6.5	7.7	4.5	2.2	5.9	18.3	6.9	7.2	**100**
20000	0.0	0.5	0.2	25.0	25.0	0.0	0.0	1.8	5.3	6.2	3.6	1.8	4.7	14.7	5.5	5.8	**100**
24000	0.0	0.7	0.2	29.2	29.2	0.0	0.0	1.5	4.3	5.1	3.0	1.5	3.9	12.1	4.5	4.8	**100**
28000	0.1	0.6	0.1	32.1	32.1	0.0	0.0	1.3	3.7	4.4	2.5	1.3	3.3	10.4	3.9	4.1	**100**
33000	0.4	0.5	0.2	34.8	34.8	0.0	0.0	1.1	3.1	3.7	2.1	1.1	2.8	8.7	3.3	3.4	**100**

Large 02	**BON**	**DP**	**CAE**	**L1**	**L2**	**BOH**	**OST**	**FSP**	**BC**	**GP**	**WB**	**SC**	**CG**	**GOM**	**SP**	**PAL**	**TOTAL**
7000	0.0	0.6	0.4	22.5	22.5	0.0	0.0	0.3	6.1	8.0	4.3	3.0	4.2	12.9	7.0	8.4	**100**
10000	0.0	0.8	0.6	22.5	22.5	0.0	0.0	2.0	5.7	6.7	3.9	2.0	5.1	15.9	6.0	6.3	**100**
13000	0.0	0.5	0.4	22.5	22.5	0.0	0.0	2.9	5.6	6.2	3.8	1.5	5.5	17.4	5.6	5.5	**100**
16000	0.0	0.7	0.3	22.5	22.5	0.0	0.0	3.4	5.6	5.9	3.7	1.3	5.7	18.1	5.4	5.0	**100**
20000	0.0	0.5	0.2	22.5	22.5	0.0	0.0	4.0	5.5	5.7	3.6	1.0	6.0	18.9	5.2	4.5	**100**
24000	0.0	0.7	0.2	22.5	22.5	0.0	1.2	4.0	5.3	5.4	3.5	0.9	6.0	18.7	5.0	4.1	**100**
28000	0.1	0.6	0.1	22.5	22.5	0.2	2.8	3.8	5.2	5.1	3.4	0.7	5.8	18.5	4.7	3.8	**100**
33000	0.4	0.5	0.2	22.5	22.5	0.7	2.7	3.8	5.1	5.0	3.3	0.7	5.9	18.6	4.6	3.6	**100**

Large 03	**BON**	**DP**	**CAE**	**L1**	**L2**	**BOH**	**OST**	**FSP**	**BC**	**GP**	**WB**	**SC**	**CG**	**GOM**	**SP**	**PAL**	**TOTAL**
7000	0.0	0.6	0.4	8.0	8.0	0.0	0.0	0.4	9.3	12.3	6.5	4.6	6.5	19.8	10.7	12.9	**100**
10000	0.0	0.8	0.6	11.4	11.4	0.0	0.0	2.8	8.1	9.5	5.5	2.8	7.2	22.5	8.5	8.9	**100**
13000	0.0	0.5	0.4	14.8	14.8	0.0	0.0	3.7	7.2	8.0	4.8	2.0	7.1	22.3	7.2	7.0	**100**
16000	0.0	0.7	0.3	18.2	18.2	0.0	0.0	4.0	6.5	6.9	4.3	1.5	6.6	20.9	6.3	5.8	**100**
20000	0.0	0.5	0.2	22.7	22.7	0.0	0.0	4.0	5.5	5.6	3.6	1.0	5.9	18.7	5.2	4.4	**100**
24000	0.0	0.7	0.2	27.3	27.3	0.0	1.0	3.3	4.4	4.5	2.9	0.7	4.9	15.4	4.1	3.4	**100**
28000	0.1	0.6	0.1	31.8	31.8	0.1	1.8	2.5	3.4	3.4	2.2	0.5	3.8	12.2	3.1	2.5	**100**
33000	0.4	0.5	0.2	37.5	37.5	0.3	1.2	1.7	2.2	2.2	1.4	0.3	2.6	8.3	2.0	1.6	**100**

4.2.2 Operation Mode Multiple Diversions

Contrary to the proposal by Parker, Kim et al. (2008), CPRA is planning sediment diversions at multiple locations and with different discharges. In general, it is intended to construct operated diversions as they are more efficient and also more unlikely to drastically increase like West Bay Diversion or Cubit's Gap.
However, options for the exact location, design and configuration still have to be evaluated (pers. comm. Meselhe, 09.09.2013).
For the simulations, fixed locations with three different overall settings for diversion rates were established.

- Multi 01
  The first setting imposes the design discharges for the discharge period of $Q = 33,000\ m^3/s$ at all five diversions and keeps the obtained discharge ratio constant for all lower discharge periods. This setting could also represent an uncontrolled scenario.

- Multi 02
  The second setting only differs for the lower discharge periods below $Q = 13,000\ m^3/s$ where the sediment diversions are closed. In reality, this might be achieved by a sill (non-operating structure) or, for example, by a gated structure.

- Multi 03
  The third setting combines the second setting with a pulsed operation. This means that the diversions are closed for $Q < 13,000\ m^3/s$ and that the diversion ratio is increasing until the design discharge is reached for the highest discharge period.

The different discharge extractions of the multiple sediment diversions for the above presented operation modes are summarized in table 4.3. In all scenarios of the multiple sediment diversions, we have to assume changes in downstream discharge distribution, as a large part of the water gets diverted. It was decided to reduce the amount of water extracted through the downstream branches proportionally to the reduction of flow just downstream of the implemented sediment diversions. In table 4.4, the new flow distributions are presented together with the additional diversions Upper Breton (UBR), Mid Breton (MBR), Lower Breton (LBR), Mid Barataria (MBA) and Lower Barataria (LBA).

Table 4.3: Discharges for Different Operation Modes of Multiple Diversions

2009			Multi 01	Multi 02	Multi 03
Q_{nom} $[m^3/s]$	MorFac $[-]$	No. Period	$Q_{Multi\ 01}$ $[m^3/s]$	$Q_{Multi\ 02}$ $[m^3/s]$	$Q_{Multi\ 03}$ $[m^3/s]$
7000	100	1	2736	0	0
10000	55	1	3909	0	0
13000	40	1	5082	5082	1677
16000	40	1	6255	6255	3353
20000	60	1	7818	7818	5589
24000	30	1	9382	9382	7825
28000	20	1	10945	10945	10060
33000	20	1	12900	12900	12900
	365	8	5944	4605	3371

Table 4.4: Relative Flow Distribution for Multiple Diversion Scenarios

Multi 01	**BON**	**DP**	**CAE**	**UBR**	**MBR**	**MBA**	**BOH**	**LBR**	**LBA**	**OST**	**FSP**	**BC**	**GP**	**WB**	**SC**	**CG**	**GOM**	**SP**	**PAL**	**TOTAL**
7000	0.0	0.6	0.0	21.2	3.0	6.4	0.0	4.2	4.2	0.0	0.3	6.7	8.9	4.7	3.3	4.7	14.3	7.8	9.3	**100**
10000	0.0	0.8	0.0	21.2	3.0	6.4	0.0	4.2	4.2	0.0	2.2	6.4	7.5	4.4	2.2	5.7	17.8	6.7	7.0	**100**
13000	0.0	0.5	0.0	21.2	3.0	6.4	0.0	4.2	4.2	0.0	3.2	6.3	6.9	4.2	1.7	6.1	19.3	6.3	6.1	**100**
16000	0.0	0.7	0.0	21.2	3.0	6.4	0.0	4.2	4.2	0.0	3.8	6.2	6.6	4.1	1.4	6.4	20.1	6.0	5.5	**100**
20000	0.0	0.5	0.0	21.2	3.0	6.4	0.0	4.2	4.2	0.0	4.4	6.1	6.3	4.0	1.1	6.6	20.9	5.8	5.0	**100**
24000	0.0	0.7	0.0	21.2	3.0	6.4	0.0	4.2	4.2	1.3	4.5	5.9	6.0	3.9	1.0	6.6	20.8	5.5	4.6	**100**
28000	0.1	0.6	0.0	21.2	3.0	6.4	0.3	4.2	4.2	3.1	4.3	5.8	5.7	3.8	0.8	6.5	20.6	5.2	4.3	**100**
33000	0.4	0.5	0.0	21.2	3.0	6.4	0.9	4.2	4.2	3.0	4.3	5.7	5.6	3.7	0.7	6.6	20.9	5.1	4.0	**100**

Multi 02	**BON**	**DP**	**CAE**	**UBR**	**MBR**	**MBA**	**BOH**	**LBR**	**LBA**	**OST**	**FSP**	**BC**	**GP**	**WB**	**SC**	**CG**	**GOM**	**SP**	**PAL**	**TOTAL**
7000	0.0	0.6	0.0	0.0	0.0	0.0	0.0	0.0	0.0	0.0	0.5	11.1	14.6	7.8	5.5	7.7	23.6	12.8	15.4	**100**
10000	0.0	0.8	0.0	0.0	0.0	0.0	0.0	0.0	0.0	0.0	3.6	10.5	12.4	7.2	3.6	9.4	29.3	11.0	11.6	**100**
13000	0.0	0.5	0.0	21.2	3.0	6.4	0.0	4.2	4.2	0.0	3.2	6.3	6.9	4.2	1.7	6.1	19.3	6.3	6.1	**100**
16000	0.0	0.7	0.0	21.2	3.0	6.4	0.0	4.2	4.2	0.0	3.8	6.2	6.6	4.1	1.4	6.4	20.1	6.0	5.5	**100**
20000	0.0	0.5	0.0	21.2	3.0	6.4	0.0	4.2	4.2	0.0	4.4	6.1	6.3	4.0	1.1	6.6	20.9	5.8	5.0	**100**
24000	0.0	0.7	0.0	21.2	3.0	6.4	0.0	4.2	4.2	1.3	4.5	5.9	6.0	3.9	1.0	6.6	20.8	5.5	4.6	**100**
28000	0.1	0.6	0.0	21.2	3.0	6.4	0.3	4.2	4.2	3.1	4.3	5.8	5.7	3.8	0.8	6.5	20.6	5.2	4.3	**100**
33000	0.4	0.5	0.0	21.2	3.0	6.4	0.9	4.2	4.2	3.0	4.3	5.7	5.6	3.7	0.7	6.6	20.9	5.1	4.0	**100**

Multi 03	**BON**	**DP**	**CAE**	**UBR**	**MBR**	**MBA**	**BOH**	**LBR**	**LBA**	**OST**	**FSP**	**BC**	**GP**	**WB**	**SC**	**CG**	**GOM**	**SP**	**PAL**	**TOTAL**
7000	0.0	0.6	0.0	0.0	0.0	0.0	0.0	0.0	0.0	0.0	0.5	11.1	14.6	7.8	5.5	7.7	23.6	12.8	15.4	**100**
10000	0.0	0.8	0.0	0.0	0.0	0.0	0.0	0.0	0.0	0.0	3.6	10.5	12.4	7.2	3.6	9.4	29.3	11.0	11.6	**100**
13000	0.0	0.5	0.0	7.0	1.0	2.1	0.0	1.4	1.4	0.0	4.6	9.0	9.9	6.0	2.4	8.8	27.7	9.0	8.7	**100**
16000	0.0	0.7	0.0	11.4	1.6	3.4	0.0	2.3	2.3	0.0	5.0	8.0	8.6	5.4	1.8	8.3	26.1	7.8	7.2	**100**
20000	0.0	0.5	0.0	15.2	2.2	4.6	0.0	3.0	3.0	0.0	5.2	7.3	7.5	4.7	1.3	7.8	24.8	6.8	5.9	**100**
24000	0.0	0.7	0.0	17.7	2.5	5.3	0.0	3.5	3.5	1.5	5.0	6.6	6.6	4.3	1.1	7.3	23.0	6.1	5.1	**100**
28000	0.1	0.6	0.0	19.6	2.8	5.9	0.3	3.9	3.9	3.3	4.5	6.1	6.0	4.0	0.8	6.8	21.7	5.5	4.5	**100**
33000	0.4	0.5	0.0	21.2	3.0	6.4	0.9	4.2	4.2	3.0	4.3	5.7	5.6	3.7	0.7	6.6	20.9	5.1	4.0	**100**

4.2.3 Operation Mode Changing Discharge Distribution at ORCS

Discharge Reduction at ORCS: Change Distribution to 35-65

Winers proposal of diverting most of the flow to the Atchafalaya River implies a minimum conveyance through the Lower Mississippi River to ensure navigability and limit salt wedge intrusion.

With three discharge levels ($7,000\ m^3/s, 10,000\ m^3/s, 13,000\ m^3/s$) and an annual average discharge of $8,890\ m^3/s$ this situation is simulated.

In this simulation, we cannot assess location or design as the diversion takes place upstream of the model domain. However, we can compare the outcome of this simulation with the results from the first case for large-scale sediment diversions (L 01) as the discharges downstream of rkm 60 are similar.

Discharge Reduction at ORCS: Change Distribution to 60-40

The above shown scenario of Winer represents a very strong change in discharge distribution. In long term simulations, the scenario turned out to cause to much deposition and dredging volumes so that navigation will be at stake after one decade.

Another scenario that is frequently discussed and based on the same approach from Winer is to change the flow distribution at ORCS from 70-30 to 60-40. This means that only 60% of the flow coming from Red River and Upper Mississippi River gets diverted to the Lower Mississippi River. A comparison is given in figure 4.1.

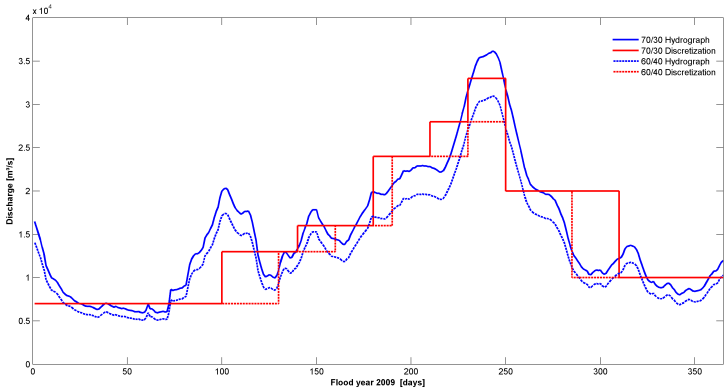

Figure 4.1: Comparison of 70-30 and 60-40 ORCS Flow Distribution. The figure shows the hydrographs and discretization for a 70-30 and a 60-40 discharge distribution at Old River Control Structure.

Pulsed Operation of ORCS

Another way to increase the sediment load in the Lower Mississippi River is a pulsed operation of the Old River Control Structure.
Based on the supplementary file of Allison (2012) [5] and the difference between sediment loads during pulsed and controlled operation of the large-scale river diversions we can estimate how much water and sediment can be conveyed.

Upstream of ORCS, at Natchez, we find an annual average of $19,272\ m^3/s$ for the flood year 2009 which is about 29% more than in the Lower Mississippi. Even during dry periods the river discharge upstream of ORCS hardly drops below $9,000\ m^3/s$.

Remark:

According to Allison (2012) [5] the annual sediment transport is even smaller than at Baton Rouge with 77.2 instead of 82.1 million tons per year.
This would imply lower sediment concentrations and hence counteract any pulsed operation. However, as already mentioned, the Mississippi River carries varying sediment loads. A simplified case would be to adapt the present discharge discretization by replacing low discharge periods by higher ones.

In addition, the large-scale sediment diversions have to be operated simultaneously to convey the extra sediment to the wetlands.
Only the combination of both pulsed operation of ORCS and sediment diversions will have the desired effect.
in the following, four different scenarios are presented assuming different diversion strategies:

- ORCS 01 has an average discharge of $17,300\ m^3/s$ based on reducing the conveyance from the Upper Mississippi River towards the Atchafalaya River by 50%.
- ORCS 02 conveys everything coming from the Upper Mississippi River towards the Lower Mississippi River. No diversion towards the Atchafalaya takes place which is hence solely supplied by the Red River. In fact this could be interpreted as a separation of the river systems.

- ORCS 03 assumes that no additional water is diverted towards the Lower Mississippi River during dry periods (100 days per year). During all other discharge periods, $3 - 5000\ m^3/s$ are diverted additionally.
- ORCS 04 is comparable to ORCS 01 in terms of average discharge. The operation mode is similar to ORCS 03 where the difference is a more pronounced pulsed operation.

Table 4.5: Duration of Discharge Periods and Average Discharges for Different Scenarios

Q_{nom} $[m^3/s]$	35-65			60-40			ORCS 01		
	MorFac [–]	No. Period	Q_{35-65} $[m^3/s]$	MorFac [–]	No. Period	Q_{60-40} $[m^3/s]$	MorFac [–]	No. Period	Q_{ORCS} $[m^3/s]$
7000	100	2	3836	130	1	2493	100	0	0
10000	50	2	2740	80	1	2192	135	1	3699
13000	65	1	2315	30	1	1068	40	1	1425
16000	40	0	0	30	1	1315	40	1	1753
20000	60	0	0	35	1	1918	60	1	3288
24000	30	0	0	20	2	2630	30	1	1973
28000	20	0	0	20	1	1534	20	1	1534
33000	20	0	0	0	0	0	20	2	3616
	365	5	8890	365	8	13151	365	8	17288

Q_{nom} $[m^3/s]$	ORCS 02			ORCS 03			ORCS 04		
	MorFac [–]	No. Period	Q_{ORCS} $[m^3/s]$	MorFac [–]	No. Period	Q_{ORCS} $[m^3/s]$	MorFac [–]	No. Period	Q_{ORCS} $[m^3/s]$
7000	100	0	0	100	1	1918	100	1	1918
10000	55	0	0	55	0	0	55	0	0
13000	155	1	5521	65	1	2315	95	1	3384
16000	40	1	1753	50	1	2192	40	0	0
20000	60	1	3288	60	1	3288	60	1	3288
24000	30	1	1973	30	1	1973	30	1	1973
28000	20	1	1534	20	1	1534	20	1	1534
33000	20	3	5425	20	2	3616	20	3	5425
	365	8	19493	365	8	16836	365	8	17521

4.2.4 Operation Mode ORCS & Large-Scale Diversions

Now, we have to evaluate the combination of pulsed operation of ORCS and large-scale sediment diversions. Because of the experience already gained, the large-scale diversions with progressively increasing diversion rates are used.

Due to increased discharges from upstream, the average discharge conveyed through the large-scale diversions also changes from 6609 to values between 8045 and 9884 m^3/s as presented in table 4.6.

Table 4.6: Discharge Distributions for Changed Operation at ORCS and Large-Scale Diversions

		60-40 L 03				Base Case L 03			
Q_{nom} $[m^3/s]$	Diversion [%]	MorFac [–]	No. Period	Q_{Large} $[m^3/s]$	Q_{60-40} $[m^3/s]$	MorFac [–]	No. Period	Q_{Large} $[m^3/s]$	Q_{ORCS} $[m^3/s]$
7000	16	130	1	397	2493	100	1	305	1918
10000	23	80	1	498	2192	55	1	342	1507
13000	30	30	1	316	1068	40	1	421	1425
16000	36	30	1	478	1315	40	1	638	1753
20000	45	35	1	872	1918	60	1	1494	3288
24000	55	20	2	1435	2630	30	1	1076	1973
28000	64	20	1	976	1534	20	1	976	1534
33000	75	0	0	0	0	20	1	1356	1808
		365	8	4971	13151	365	8	6609	15205

		ORCS 01 L 03				ORCS 02 L 03			
Q_{nom} $[m^3/s]$	Diversion [%]	MorFac [–]	No. Period	Q_{Large} $[m^3/s]$	Q_{ORCS} $[m^3/s]$	MorFac [–]	No. Period	Q_{Large} $[m^3/s]$	Q_{ORCS} $[m^3/s]$
7000	16	100	0	0	0	100	0	0	0
10000	23	135	1	841	3699	55	0	0	0
13000	30	40	1	421	1425	155	1	1631	5521
16000	36	40	1	638	1753	40	1	638	1753
20000	45	60	1	1494	3288	60	1	1494	3288
24000	55	30	1	1076	1973	30	1	1076	1973
28000	64	20	1	976	1534	20	1	976	1534
33000	75	20	2	2712	3616	20	3	4068	5425
		365	8	8158	17288	365	8	9884	19493

		ORCS 03 L 03				ORCS 04 L 03			
Q_{nom} $[m^3/s]$	Diversion [%]	MorFac [–]	No. Period	Q_{Large} $[m^3/s]$	Q_{ORCS} $[m^3/s]$	MorFac [–]	No. Period	Q_{Large} $[m^3/s]$	Q_{ORCS} $[m^3/s]$
7000	16	100	1	305	1918	100	1	305	1918
10000	23	55	0	0	0	55	0	0	0
13000	30	65	1	684	2315	95	1	1000	3384
16000	36	50	1	797	2192	40	0	0	0
20000	45	60	1	1494	3288	60	1	1494	3288
24000	55	30	1	1076	1973	30	1	1076	1973
28000	64	20	1	976	1534	20	1	976	1534
33000	75	20	2	2712	3616	20	3	4068	5425
		365	8	8045	16836	365	8	8920	17521

4.2.5 Operation Mode ORCS & Multiple Diversions

A combination of pulsed operation of ORCS and multiple sediment diversions will also be part of the analysis. In this case, the set-up Multi 02 is chosen with a constant diversion rate of 39% and closure for $Q < 13,000 m^3/s$. Discharge distributions for the different cases are presented in table 4.7.

Table 4.7: Discharge Distributions for Pulsed Operation of ORCS and Multiple Diversions

60-40 Multi 02										
Q_{nom} $[m^3/s]$	MorFac $[-]$	No. Period	Diversion [%]	UBR $[m^3/s]$	MBR $[m^3/s]$	MBA $[m^3/s]$	LBR $[m^3/s]$	LBA $[m^3/s]$	Total $[m^3/s]$	Q_{ORCS} $[m^3/s]$
7000	130	1	0	284	40	85	56	56	523	2493
10000	80	1	0	333	47	100	66	66	612	2192
13000	30	1	39	190	27	57	38	38	348	1068
16000	30	1	39	257	36	77	51	51	472	1315
20000	35	1	39	407	58	122	81	81	750	1918
24000	20	2	39	0	0	0	0	0	0	2630
28000	20	1	39	0	0	0	0	0	0	1534
33000	0	0	39	0	0	0	0	0	0	0
	365	8		1471	209	441	292	292	2706	13151

Base Case Multi 02										
Q_{nom} $[m^3/s]$	MorFac $[-]$	No. Period	Diversion [%]	UBR $[m^3/s]$	MBR $[m^3/s]$	MBA $[m^3/s]$	LBR $[m^3/s]$	LBA $[m^3/s]$	Total $[m^3/s]$	Q_{ORCS} $[m^3/s]$
7000	100	1	0	0	0	0	0	0	0	1918
10000	55	1	0	0	0	0	0	0	0	1507
13000	40	1	39	302	43	91	60	60	557	1425
16000	40	1	39	372	53	112	74	74	685	1753
20000	60	1	39	697	100	209	139	139	1285	3288
24000	30	1	39	418	60	126	84	84	771	1973
28000	20	1	39	325	46	98	65	65	600	1534
33000	20	1	39	384	55	115	77	77	707	1808
	365	8		2499	357	750	500	500	4605	15205

ORCS 01 Multi 02										
Q_{nom} $[m^3/s]$	MorFac $[-]$	No. Period	Diversion [%]	UBR $[m^3/s]$	MBR $[m^3/s]$	MBA $[m^3/s]$	LBR $[m^3/s]$	LBA $[m^3/s]$	Total $[m^3/s]$	Q_{ORCS} $[m^3/s]$
7000	100	0	0	0	0	0	0	0	0	0
10000	135	1	0	0	0	0	0	0	0	3699
13000	40	1	39	302	43	91	60	60	557	1425
16000	40	1	39	372	53	112	74	74	685	1753
20000	60	1	39	697	100	209	139	139	1285	3288
24000	30	1	39	418	60	126	84	84	771	1973
28000	20	1	39	325	46	98	65	65	600	1534
33000	20	2	39	767	110	230	153	153	1414	3616
	365	8		2883	412	865	577	577	5312	17288

ORCS 02 Multi 02										
Q_{nom} $[m^3/s]$	MorFac [–]	No. Period	Diversion [%]	UBR $[m^3/s]$	MBR $[m^3/s]$	MBA $[m^3/s]$	LBR $[m^3/s]$	LBA $[m^3/s]$	Total $[m^3/s]$	Q_{ORCS} $[m^3/s]$
7000	100	0	0	0	0	0	0	0	0	0
10000	55	0	0	0	0	0	0	0	0	0
13000	155	1	39	1171	167	351	234	234	2158	5521
16000	40	1	39	372	53	112	74	74	685	1753
20000	60	1	39	697	100	209	139	139	1285	3288
24000	30	1	39	418	60	126	84	84	771	1973
28000	20	1	39	325	46	98	65	65	600	1534
33000	20	3	39	1151	164	345	230	230	2121	5425
	365	8		4135	591	1240	827	827	7620	19493

ORCS 03 Multi 02										
Q_{nom} $[m^3/s]$	MorFac [–]	No. Period	Diversion [%]	UBR $[m^3/s]$	MBR $[m^3/s]$	MBA $[m^3/s]$	LBR $[m^3/s]$	LBA $[m^3/s]$	Total $[m^3/s]$	Q_{ORCS} $[m^3/s]$
7000	100	1	0	0	0	0	0	0	0	1918
10000	55	0	0	0	0	0	0	0	0	0
13000	65	1	39	491	70	147	98	98	905	2315
16000	50	1	39	465	66	139	93	93	857	2192
20000	60	1	39	697	100	209	139	139	1285	3288
24000	30	1	39	418	60	126	84	84	771	1973
28000	20	1	39	325	46	98	65	65	600	1534
33000	20	2	39	767	110	230	153	153	1414	3616
	365	8		3164	452	949	633	633	5832	16836

ORCS 04 Multi 02										
Q_{nom} $[m^3/s]$	MorFac [–]	No. Period	Diversion [%]	UBR $[m^3/s]$	MBR $[m^3/s]$	MBA $[m^3/s]$	LBR $[m^3/s]$	LBA $[m^3/s]$	Total $[m^3/s]$	Q_{ORCS} $[m^3/s]$
7000	100	1	0	0	0	0	0	0	0	1918
10000	55	0	0	0	0	0	0	0	0	0
13000	95	1	39	718	103	215	144	144	1323	3384
16000	40	0	39	0	0	0	0	0	0	0
20000	60	1	39	697	100	209	139	139	1285	3288
24000	30	1	39	418	60	126	84	84	771	1973
28000	20	1	39	325	46	98	65	65	600	1534
33000	20	3	39	1151	164	345	230	230	2121	5425
	365	8		3310	473	993	662	662	6099	17521

4.2.6 Increased Sediment Loads

Thousands of dams have been built throughout the last two centuries. Together with improving land conservation, the sediment load decreased by 70% as described by Blum & Roberts (2009) [10]. Although there were processes that led to a high sediment input in the 19th century, the question remains, how the system would react, if sediment is reintroduced, e.g. by improving reservoir management and regularly flushing out deposits. Reservoirs and dams upriver have many functions, the most important are flood protection and storage of fresh water. Although it might be a taff challenge, removal of dams or continuous opening of structures (except for extreme events) would provide even more sediment. It is important to notice that the best and largest diversions alone do not suffice to restore the entire Mississippi Delta if there is not enough sediment supply.

Nourishments, as they also happen in the River Rhine, may be an option to increase the sediment concentrations and convey more sediment ot the wetlands.
Starting from 82 million tons per year of total sediment, we want to examine the effect of increased sediment loads. Therefore, four additional cases are set up.

- 82 million tons per year, derived from Allison (2012)
- 124 million tons per year, assumption from Parker (no settling to Reserve)
- 178 million tons per year, amount available at ORCS, Allison (2012)
- 208 million tons per year, sediment load 150 years ago (like Base Case)
- 268 million tons per year, sediment load 150 years ago (no settling to Reserve)

4.2.7 Design of Sediment Diversions

In order to get more information on what is a favorable design for a sediment diversion, the Parker Diversion at the right river bank is modified based on two aspects, cross-section and diversion angle. By keeping the other diversion unchanged, we will also be able to identify side effects of the applied changes.

Cross-Section
The original 90° offtaking large-scale diversion has a trapezoidal profile with up to 25 m depth and approximately 1350 m width. We want to see the effect of different width to depth ratios and cross-sectional areas and hence introduce the following cases:

- Parker 03 - original cross-section (1350 x 25 m)
- Parker 04 - twice as wide, half as deep (2700 x 12.5 m)
- Parker 05 - half as wide (675 x 25 m)
- Parker 06 - half as deep (1350 x 12.5 m)
- Parker 07 - twice as wide, 1/4 as deep (2700 x 6.25 m)

Diversion Angle
The operational cases comprised a relatively simple geometry with 90° offtaking diversions. Now, four additional cases were set up:

- Parker 03 01 - diversion angle 15°
- Parker 03 02 - diversion angle 20°
- Parker 03 03 - diversion angle 25°
- Parker 03 04 - diversion angle 30°

4.2.8 Sea-Level Rise and Land Subsidence

The Mississippi Delta is subject to sea-level rise and land subsidence which might have noticeable effects in long-term simulations of 50 years.
The 5th IPCC Report (2013) indicates that the global sea-level rise might be in the order of 82 cm until the end of the century.

Based on IPCC (2007) [9], sea-level rise can be up to 2-4 mm/year. In case of only little melting of the continental ice sheets, sea-level rise might even be neglected.
Compared to a medium scenario of sea-level rise, the land subsidence rate is relatively large, mainly due to extraction of gas and oil and because of the compactation processes of the deltaic plain.
According to Kim (2008) [39], the average historical subsidence rates over the last 80 years is 11 mm/year.

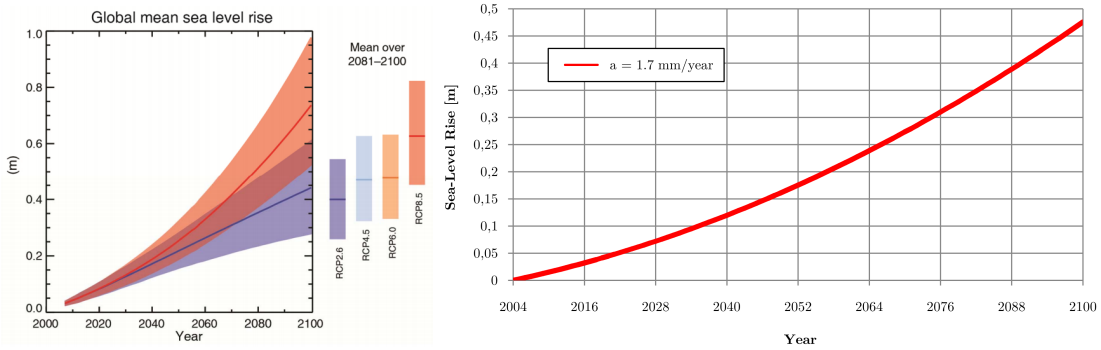

Figure 4.2: Global Sea-Level Rise Scenarios and Model Implementation. Source: 5th IPCC Report 2013 & IPCC Report 2007.

As the above figure demonstrates, different scenarios exist for sea-level rise. As there is a correlation with human interventions, there should also be different scenarios for land subsidence. Due to time constraints it is not possible to consider all of them. Hence, it was decided to make use of actual field data and to choose a medium annual subsidence rate based on this information. For more background information one is referred to IPCC [9], Ayres (2012) [8], Dokka (2012) [23], Shinkle (2004) [61], National Research Council (1987) [50] and USACE (2009 &2011) [75],[76].

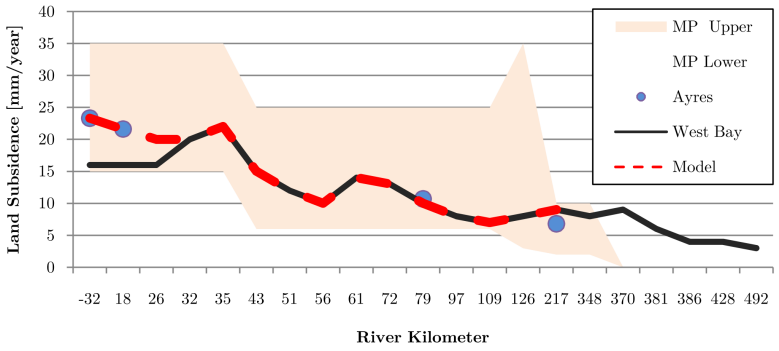

Figure 4.3: Annual Land Subsidence. The figure shows results from different field measurements together with an upper and lower bound and the scenario chosen for the model. Adapted from [8].

Implementation:

The land-subsidence was implemented by increasing the depth values after simulating a discharge period. This way, the new discharge period restarts based on the adapted bathymetry.

The rates for land subsidence are spatially varying: At the birdfoot, subsidence rates are highest, whereas they are decreasing towards New Orleans. In order to cope with this variability, a depth file with the annual subsidence rates was created. After completion of one simulation period, a Matlab function is started through the Python scripts. Its task is to read the bathymetric information from the output and to add the values for land subsidence before the output file is used to restart the next period.

The implementation of the sea-level rise is similar: Instead of the output file the boundary condition file with the water level at East Jetty is adapted accordingly after each simulation period of constant discharge.

5 | Analytical Model

5.1 Concept of Analytical Model

Based on the settings for the implementation in Delft3D, an analytical 1D model is set up to predict the behavior of different scenarios. The results of this model give a first insight into basic processes and, furthermore, can be used to validate the numerical outcome.

All eight discharge periods and their contributions to the annual sediment transport are considered. The focus lies on the determination of the final equilibrium situation. However, the analytical model inherits a number of simplifications. It is emphasized that only one sand fraction and no estuarine effects are considered. Moreover, bed level slope, water depths and roughness coefficients are average values along the domain.

5.2 Governing Equations

Once a river is brought out of its equilibrium it adapts to the new situation striving towards establishing a new equilibrium. The time scales involved in this process can be in the order of decades and even centuries. The final equilibrium can be obtained from the so called "forget-me-nots", a number of equations derived from the quasi-steady one-dimensional equations for water and sediment discharge.

However, the above equations do not consider the simultaneous extraction of both water and sediment as it occurs at sediment diversions. Moreover, we want to consider the impact of a quasi-steady discharge. This means, that we have to deal with a hydrograph containing eight different discharge periods with relative duration $p(Q)$ whose

Table 5.1: Forget-Me-Nots

Intervention	i_1/i_0	h_1/h_0
Water withdrawal	$\frac{Q_0}{Q_0-\Delta Q}$	$1-\frac{\Delta Q}{Q_0}$
Sediment withdrawal	$\left(1-\frac{\Delta Q_{s0}}{Q_{s0}}\right)^{\frac{3}{b}}$	$\left(1-\frac{\Delta Q_{s0}}{Q_{s0}}\right)^{-\frac{1}{b}}$
Long constriction	$\left(\frac{B-\Delta B}{B}\right)^{1-\frac{3}{b}}$	$\left(\frac{B-\Delta B}{B}\right)^{1-\frac{1}{b}}$

single effects accumulate to a dynamic equilibrium situation.
For this purpose and additional cross-sectional changes, Crosato [18] provides us with the corresponding equations for equilibrium slope and water level.

At the river mouth, the adapted equations read:

$$\frac{h_{M,\infty}}{h_{M,0}} = \left(\frac{B_0}{B_\infty}\right)^{1-1/b} * \left(\frac{Q_{S,0}}{Q_{S,\infty}}\right)^{1/b} * \left[\frac{\sum\left(p(Q) * Q_{W,\infty}^b\right)}{\sum\left(p(Q) * Q_{W,0}^b\right)}\right]^{1/b} \tag{5.1}$$

$$\frac{i_\infty}{i_0} = \left(\frac{Q_{S,\infty}}{Q_{S,0}}\right)^{3/b} * \left(\frac{B_\infty}{B_0}\right)^{1-3/b} * \left[\frac{\sum\left(p(Q) * Q_{W,0}^{3/b}\right)}{\sum\left(p(Q) * Q_{W,\infty}^{3/b}\right)}\right]^{3/b} \tag{5.2}$$

The analytical model is based on the sediment transport formula of Engelund-Hansen. The equations can be found in the Annex (see B.4.2, p. 131).

5.3 Analytical Solutions of Scenarios

5.3.1 Base Case

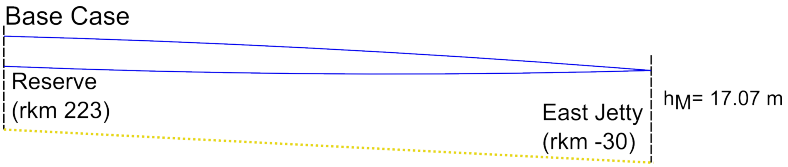

Figure 5.1: Analytical Model Base Case.

The Base Case with an average discharge of $15,205\ m^3/s$ has an the equilibrium transport of sand of approximately 10 millions tons/year. The constant depth at the mouth of the river was determined to be around $h_{M,0} = 17\ m$.
The equilibrium slope is approximately $i_{b,0} = 2.5 * 10^{-5}$.
The result in terms of bed and water levels is given in figure 5.1, where the water levels of the eight different discharge periods is represented by an envelope of two blue lines.
Remark:
The results from the Base Case serve as a reference for the following cases. The original bed and water levels are always displayed as dashed lines. Sedimentation of the bed is emphasized with light yellow, erosion with light blue.

5.3.2 Large-Scale Diversions

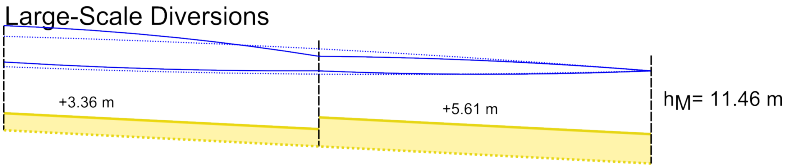

Figure 5.2: Analytical Model Large-Scale Diversions.

If we convey 45% of the water and sediment at a distance of 100 km from the mouth (East Jetty) the analytical model shows a bed level increase of 5.61 m at the mouth, $h_{M,1} = 11.46\ m$. Because water and sediment are diverted at the same time, the bed level slope stays constant. The actual water levels at the transition 100 kilometers upstream of East Jetty vary between 14.19 and 15.66 m which suffices for navigation.

At the location of the large-scale diversion, a bed step of $\Delta z = -2.25\ m$ develops as the hydraulic conditions return to the initial situation. This also leads to a 3.36 m higher bed level upstream.
The water levels at Reserve (rkm 223) were determined to vary between 11.87 to 17.10 m This means, that the maximum water levels at Reserve are almost 2 m (1.93) higher than before the intervention.

The above described equilibrium bed level can be made comprehensible by looking at the effects of the intervention on the flow velocities. In the initial situation there is a uniform equilibrium velocity for each discharge period. By extracting 45% of the water, the velocities and hence the transport capacity downstream decreases. Due to non-linearity of the sediment transport, 55% of the water can only transport 37% of the sediment. This means, that the remaining portion of the sediment starts to deposit near the mouth (lowest velocities in the reach) and proceeds upriver.
Upstream, the initial morphological response is gradually increasing erosion towards the intervention because the extraction leads to a drop in downstream water level and hence to steeper backwater curves and higher velocity gradients.

On a longer time-scale, when the downstream bed level is rising, the slope of the backwater curves reduce and so do the velocity gradients at the intervention until the acceleration turns into a deceleration, the sediment transport capacity drops and deposition also starts upstream.

Time Scales of Morphological Changes

The time scale of this process can be estimated with $T_{50\%}$ that represents the period in which half of the morphological changes have taken place. Because the morphological reaction diminishes in time, it usually takes a multiple of times until we are close to equilibrium. The equations can be found in the Annex (see B.4.6, p. 134).
For the entire reach we find

$$T_{50\%} = \frac{3 * (253000\ m)^2 * 850\ m * 2.5 * 10^{-5}\ m/m}{5 * 9.85 * 10^6\ m^3/year} \approx 83\ years \tag{5.3}$$

For this result, the normal sediment transport rate was assumed for the whole reach. Half of the morphological equilibrium downstream of the intervention might be reached

after

$$T_{50\%} = \frac{3 * (100000\ m)^2 * 850\ m * 2.5 * 10^{-5}\ m/m}{5 * 3.64 * 10^6\ m^3/year} \approx 35\ years \tag{5.4}$$

Once again, this estimate does only consider equilibrium sand concentrations and no mud fractions and estuarine effects. However, the example shows that we are talking about several decades to centuries of morphological adaptions.

5.3.3 Multiple Diversions

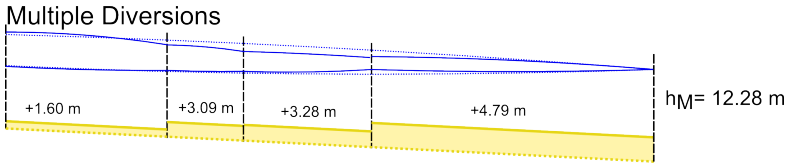

Figure 5.3: Analytical Model Multiple Diversions.

The case of multiple diversions is similar to the foregoing analysis of the large-scale diversions except for the number of diversion sites. Instead of considering all five diversions site, it was decided to combine the nearby diversions of Mid-Breton and Mid-Barataria as well as Lower Breton and Lower Barataria. As morphological responses are similar to the large-scale diversions, the processes will not be explained in more detail. However, it should be noted that the bed level and effective water level increase is somewhat smaller, mainly due to less extraction of water and sediment.

5.3.4 Changing Discharge Distribution at ORCS

Changing the discharge distribution of ORCS is composed of cases with discharge reduction and cases with higher discharges as presented in the following.

Discharge Reduction at ORCS: Change Distribution to 35-65

In case of changing the discharge distribution to 35-65, we consider a water and sediment extraction upstream of the model domain. We only use the three lowest discharge periods with adapted durations and an annual average discharge of 8890 m^3/s.
Similar to the large-scale diversions, the extraction of sand and sediment leads to an overall increase in bed level. The depth at the mouth (East Jetty) reduces from 17 to

under 10 m. The slope stays almost constant. This means, that the bed level rises more than 7 m. The water levels at Reserve (rkm 223) vary between 12.58 and 14.69 m and are further decreasing upriver.

From the analytical solution it becomes clear that for this scenario safe navigation might be at stake due to the morphological consequences of only diverting low discharges through the Lower Mississippi River. The result is presented in figure 5.4.

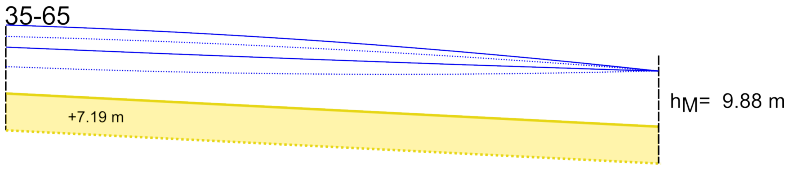

Figure 5.4: Analytical Model 35-65.

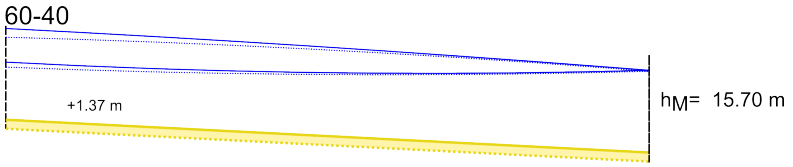

Figure 5.5: Analytical Model 60-40.

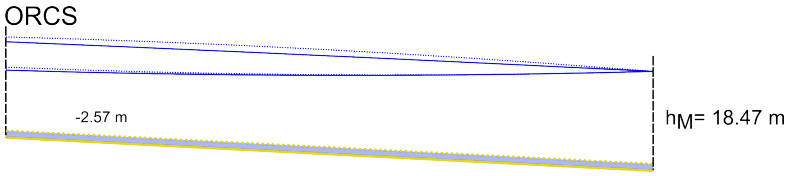

Figure 5.6: Analytical Model ORCS.

Discharge Reduction at ORCS: Change Distribution to 60-40

An average discharge reduction of 10% show the same morphological trends. However, the changes in bed and water level stay well below those of the 35-65 discharge reduction case. This can be expected, as the sediment transport is usually depending linearly on the 3rd to 5th power of the flow velocity. An overall decrease of flow velocities leads to smaller sediment transport capacities. The main channel adapts to the new condition by decreasing the cross-sectional area through deposition.

Pulsed Operation of ORCS

Vice-versa, increasing the upstream discharge leads to a decreasing bed level. As flow velocities increase, sediment transport capacities do and the cross-sectional area of the main channel adapts to the new situation by incision.

5.3.5 Groin Fields

The effect of groin fields in the Southwest Pass might counteract the bed level rise with a time scale of several decades to centuries. We can test the effect of the groin field as a stand-alone solution and in combination with new sediment diversions, e.g. Parker. The following figures show the analytical solution for different cases.

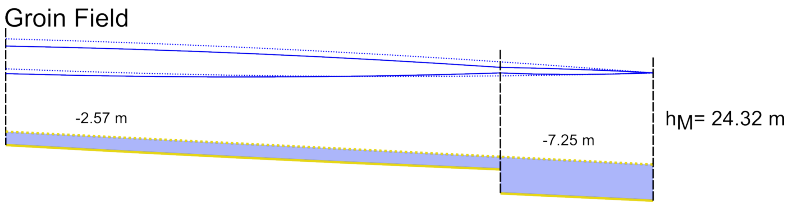

Figure 5.7: Analytical Model Groin Field.

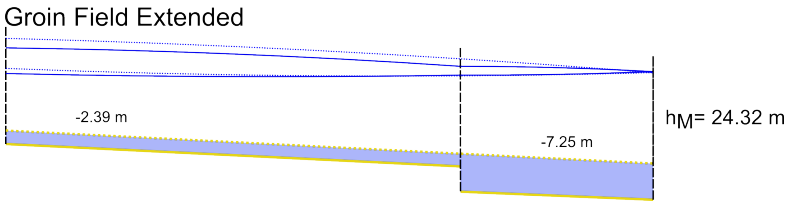

Figure 5.8: Analytical Model Extended Groin Field.

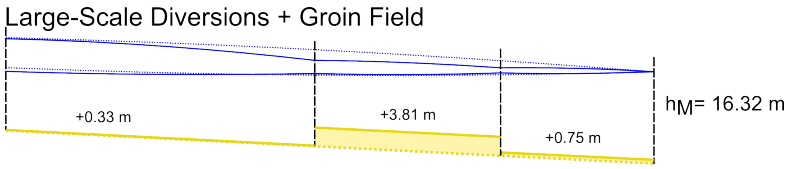

Figure 5.9: Analytical Model Large-Scale Diversions & Groin Field.

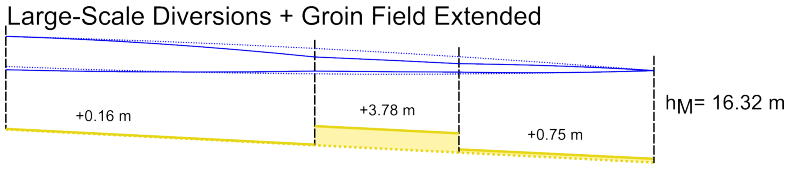

Figure 5.10: Analytical Model Large-Scale Diversions & Extended Groin Field.

Groin fields are a common tool to ensure navigation. Narrowing of the river leads to higher flow velocities in the fairways which contributes to higher sediment transport capacities and hence incising bed levels. On the other hand, construction of groins leads to a higher hydraulic roughness that might lead to higher water levels and consequently, risk of flooding, if the bed incision does not compensate for backwater effects.
The large-scale diversions were combined with the groin fields. The result are similar to a superposition of both cases. However, due to different developments of the backwater curves, deviations become visible. The upstream deposition could also be an erosive reach depending on the chosen parameters, e.g. for longer groins.

Remark:
An additional analysis with varying diversion efficiencies was carried out to get more insight into the corresponding impact on the morphological equilibrium, see section C.4 on p. 164.

6 | Model Outcome Sediment Diversions

In this chapter both analytical and numerical results will be presented and compared. Therefore, key numbers were extracted from the numerical outcome such as:

- **Deposition Rate**
  The annual, width-averaged deposition rate of the reach from Reserve (rkm 223) to Venice (rkm 16)

- **Dredging SWP - HoP**
  The dredging volumes of the dominant reach from Venice (rkm 16) to East Jetty (rkm -30) are ought to give a good insight into the influence of changes in water and sediment input on the settling process in the area of salt water influence.

- **Sediment Diversion**
  For land-building purposes we are especially interested in the amount of sediment that is conveyed through the implemented sediment diversions.

- **Diversion Efficiency**
  When planning a sediment diversions one strives for high sediment diversion efficiency. In this case, the efficiency does not have a direct economic meaning but is based on the ratio of sediment-water ratios determined upstream of the diversion in the main channel and in the offtaking branch. However, when considering the construction costs and the amount of created or restored wetland, the diversion efficiency also reveals an economic aspect. For a more detailed analysis, the diversion efficiency of sand and mud fractions determined separately, as well. A sediment diversion efficiency of 1 states that the both main channel and diversion have the same sediment concentration. Although 2D models cannot capture all processes, see also Heer & Mosselman (2004) [34], the obtained values can at least serve for a qualitative comparison.

6.1 Simulation Outcome

6.1.1 Result Overview

Table 6.1: Simulation Outcome

Scenario	Dredging SWP - HoP $[10^6\ t/year]$			Deposition Rate $[10^6\ m^3/year]$		Sediment Diversion $[10^6\ t/year]$	Diversion Efficiency $(Q_{s,\ div}/Q_{w,\ div})/(Q_{s,\ up}/Q_{w,\ up})$						
	10 years	50 years	av. 50 yrs	av. 10 yrs	av. 50 yrs	av. 10 yrs	L1	L2	UBR	MBR	MBA	LBR	LBA
Base Case	12.0	31.9	19.8	18.8	29.7								
Large 01	5.0	35.8	19.8	38.3	26.5	26.1	1.40	1.27					
Large 02	10.0	30.5	19.0	37.0	26.5	19.8	0.97	0.88					
Large 03	5.3	30.8	16.9	38.0	25.5	25.7	1.27	1.15					
Multi 01	9.0	32.5	18.8	41.6	28.5	18.0			0.84	0.91	0.84	0.60	0.89
Multi 02	8.6	37.1	20.3	42.2	29.1	17.6			1.02	1.19	1.11	0.83	1.25
Multi 03	12.5	37.4	22.6	38.7	28.3	13.7			1.03	1.30	1.15	0.92	1.42
35-65	0.2	39.2	15.1	62.1	48.7								
60-40	9.7	28.2	16.6	28.1	34.0								
Base Case	12.0	31.9	19.8	18.8	29.7								
ORCS 01	11.4	38.4	22.9	17.9	30.3								
ORCS 02	12.6	46.0	27.9	13.9	26.6								
ORCS 03	12.5	38.0	22.8	15.2	27.4								
ORCS 04	11.4	38.3	22.9	17.9	30.4								
60-40 + Large 03	2.6	30.6	16.1	42.3	30.4	15.6	1.39	1.30					
Base Case + Large 03	5.3	30.8	16.9	38.0	25.5	25.7	1.27	1.15					
ORCS 01 + Large 03	6.3	42.3	22.8	38.2	26.7	31.5	1.22	1.10					
ORCS 02 + Large 03	6.2	45.1	27.1	34.8	23.6	39.8	1.16	1.00					
ORCS 03 + Large 03	6.4	38.3	22.4	35.3	24.0	32.5	1.20	1.06					
ORCS 04 + Large 03	5.0	34.6	20.1	31.0	24.1	37.1	1.18	1.03					
60-40 + Multi 02	9.0	36.4	19.8	41.9	31.2	8.8			1.29	1.77	1.55	1.14	1.88
Base Case + Multi 02	8.6	37.1	20.3	42.2	29.1	17.6			1.02	1.19	1.11	0.83	1.25
ORCS 01 + Multi 02	10.0	46.7	27.1	43.8	29.5	20.1			0.92	1.08	0.99	0.82	1.23
ORCS 02 + Multi 02	11.9	41.3	26.9	39.5	25.9	24.7			0.76	0.80	0.72	0.60	0.87
ORCS 03 + Multi 02	10.3	37.1	22.8	39.4	26.6	21.0			0.88	0.97	0.88	0.70	1.03
ORCS 04 + Multi 02	12.1	33.8	21.5	35.7	26.6	22.2			0.86	0.95	0.87	0.70	1.02

In order to structure the analysis of the results, several subsequent questions have to be answered:

- How Does the Lower Mississippi River Evolve over 50 Years?
- Do the Simulation Results Agree with the Analytical Solutions?
- Which Diversion Operation Mode is Most Beneficial?
- Which Operation Mode of ORCS is Most Beneficial?
- Which Combination of Diversion and ORCS Operation Mode is Most Beneficial?
- What Is the Impact of Sea-Level Rise and Land Subsidence?
- What Is the Impact of Increased Sediment Loads?
- What Is a Good Design of a Sediment Diversion?
- What Is the Impact of Additional Groin Fields from Head of Passes to Venice?

6.1.2 Interpretation of Results

How does the Lower Mississippi River Evolve over 50 Years?

From table 6.1 and figure 6.1 it becomes clear that the dredging volumes in the lower dredging reach from Venice (rkm 16) to East Jetty (rkm -30) have started to increase after approximately 15 years. Consequently, dredging volumes are roughly three times higher after 50 years than after 10 years.

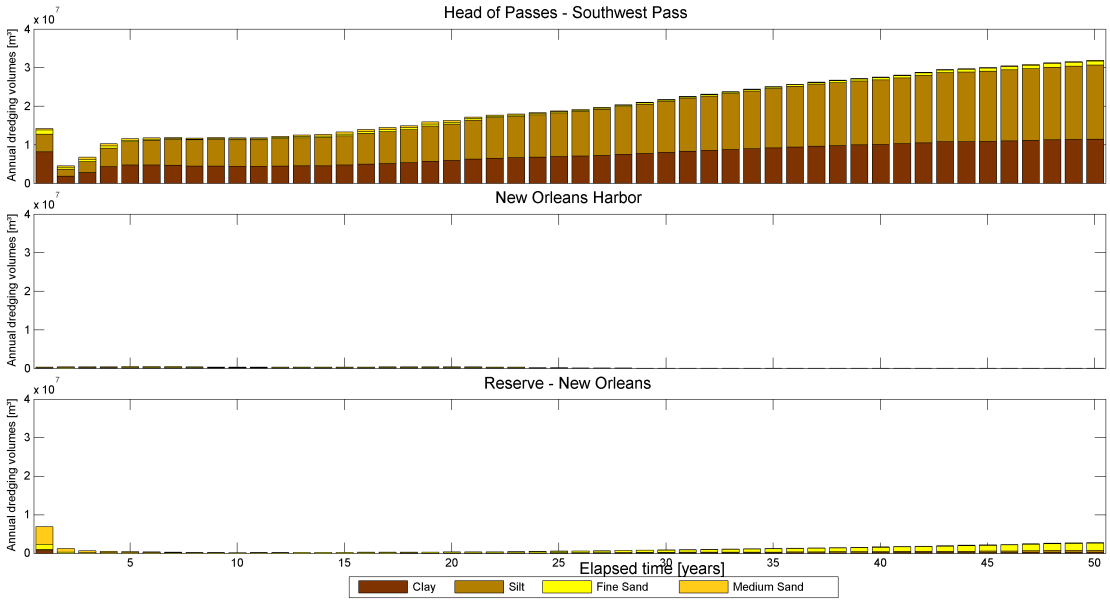

Figure 6.1: Base Case Dredging Volumes after 50 Years.

One reason for this development might be that the defined dredging polygon is at a fixed position, whereas enhanced deposition also occurs aside from this area. After some time of deposition, the amount of water and sediment conveyed through the maintained cross-section of the fairway increases and induces even more deposition.
Hence we can conclude that, as the amount of annual deposition downstream of Venice is higher than the dredging volumes, the river is silting up slowly. Without the model constraints, i.e. fixed discharge distribution and domain, one might even expect a change of course, creation of new crevasses and alterations in flow distribution.
But also in reality, the focus of dredging is on the fairway which has a higher priority than adjacent areas when it comes to effectively making use of available budgets. After some

decades, the operation managers might have to face the problem of increasing dredging volumes, as well.

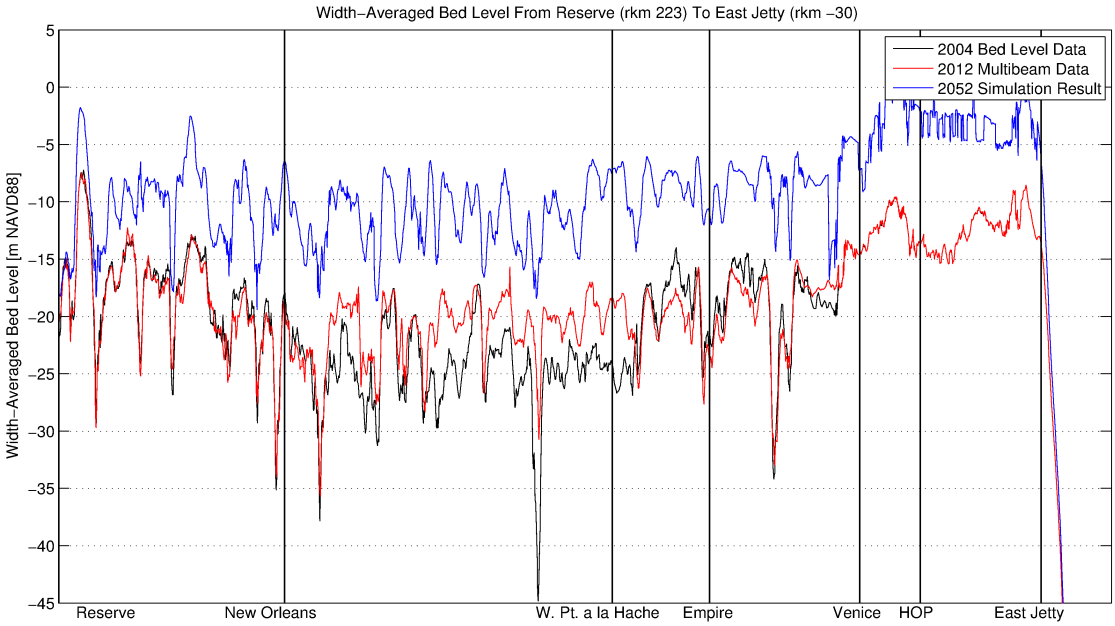

Figure 6.2: Base Case Bed-Level Changes after 50 Years.

Taking a look at the bed-level changes after 50 years in figure 6.2, we find width-averaged depths of approximately 10 to 15 m almost along the entire domain and even less downstream of Venice, where the irregular shape also indicates high dredging activities.

Although the bed level changes show the same tendencies as the bathymetric measurements during a 10-year period, annual deposition rates increase and deposition takes over in the entire domain as the simulations goes on. This observation also agrees with the above given explanation for the dredging volumes.

Do the Simulation Results Agree with the Analytical Solutions?

Table 6.2: Simulation Outcome for Analytical Cases

Scenario	Dredging SWP - HoP $[10^6\ t/year]$			Deposition Rate $[10^6\ m^3/year]$		Sediment Diversion $[10^6\ t/year]$	Diversion Efficiency $(Q_{s,\ div}/Q_{w,\ div})/(Q_{s,\ up}/Q_{w,\ up})$						
	10 years	50 years	av. 50 yrs	av. 10 yrs	av. 50 yrs	av. 10 yrs	L1	L2	UBR	MBR	MBA	LBR	LBA
Base Case	12.0	31.9	19.8	18.8	29.7								
Large 03	5.3	30.8	16.9	38.0	25.5	25.7	1.27	1.15					
Multi 01	9.0	32.5	18.8	41.6	28.5	18.0			0.84	0.91	0.84	0.60	0.89
35-65	0.2	39.2	15.1	62.1	48.7								
60-40	9.7	28.2	16.6	28.1	34.0								
ORCS 04	11.4	38.3	22.9	17.9	30.4								

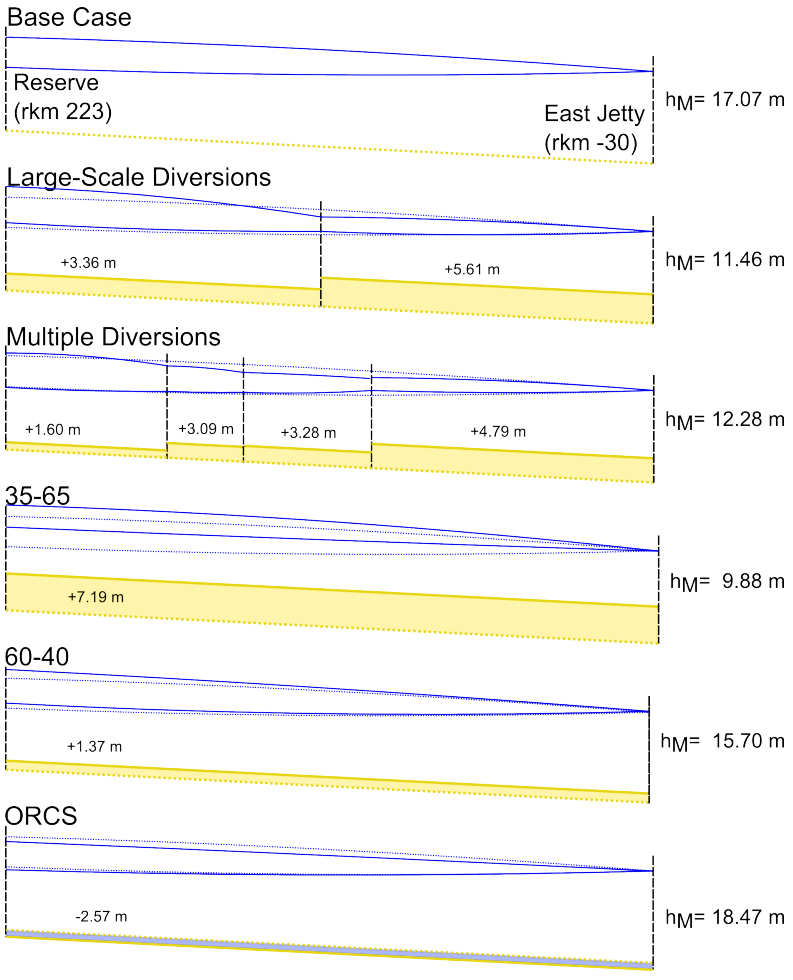

Figure 6.3: Base Case and New Equilibrium Situations for Different Scenarios.

The result of the analytical model represents the new equilibrium situation after several decades to centuries. Moreover, the depositional trend implemented in the numerical model is not considered. By using the $T_{50\%}$ time scale, we can at least check the order of magnitude. For the Large-Scale Diversions, for example, the theoretical bed-level change is in the order of $(38.0 - 18.8) * 10^6\ m^3/year/253000\ m/850\ m * 83\ years \approx 7.4\ m$ for the 10-year average and 2.6 m for the 50-year average. This shows a similar order of magnitude as the analytical equilibrium situation $(3.36 - 5.61\ m)$. However, it must be emphasized that the focus is on finding the same tendencies of each model relative to its Base Case.

From table 6.2 and figure C.15 we find a good correspondence of the analytical model and the simulation results, especially for those after 10 years:

In general, diversions and upstream discharge reduction lead to enhanced deposition as the downstream reach adapts to the decreasing sediment transport capacity. The extreme discharge reduction 35-65, for example, shows the highest annual deposition rates in both simulation and analytical solution. On the other hand, we also find that a pronounced operation of Old River Control Structure leads to higher sediment transport capacities and hence to a lower deposition rate.

The 50-year simulation results show positive effects of extracting water and sediment at ORCS or diversion sites in terms of dredging volumes. However, when looking at the case of extreme discharge reduction, we also find that it has the highest dredging volumes at the end of the simulation and only profits from initially lower dredging volumes as long as the lower dredging reach is not affected by enhanced deposition.

The 50-year deposition rates already show some deviations from the analytical solutions, especially for the sediment diversions. Following the analytical model, deposition rates are expected to be higher than those of the Base Case but after 50 years, we find slightly lower values. Vice-versa, reduction at ORCS leads to higher deposition rates. The difference may be partially explained with length and time-scales as adaptations need more time along the entire domain. However, we also have to take into account the implemented processes, e.g. flocculation, which is not considered by the analytical model: Diversion of sediment takes place at locations upstream of the area of salt water influence, except for periods of low discharge. This way, the diverted sediment cannot be subject to enhanced deposition downstream.

Which Diversion Operation Mode is Most Beneficial?

Table 6.3: Simulation Outcome for Sediment Diversions

Scenario	Dredging SWP - HoP $[10^6\ t/year]$			Deposition Rate $[10^6\ m^3/year]$		Sediment Diversion $[10^6\ t/year]$	Diversion Efficiency $(Q_{s,\ div}/Q_{w,\ div})/(Q_{s,\ up}/Q_{w,\ up})$						
	10 years	50 years	av. 50 yrs	av. 10 yrs	av. 50 yrs	av. 10 yrs	L1	L2	UBR	MBR	MBA	LBR	LBA
Base Case	12.0	31.9	19.8	18.8	29.7								
Large 01	5.0	35.8	19.8	38.3	26.5	26.1	1.40	1.27					
Large 02	10.0	30.5	19.0	37.0	26.5	19.8	0.97	0.88					
Large 03	5.3	30.8	16.9	38.0	25.5	25.7	1.27	1.15					
Multi 01	9.0	32.5	18.8	41.6	28.5	18.0			0.84	0.91	0.84	0.60	0.89
Multi 02	8.6	37.1	20.3	42.2	29.1	17.6			1.02	1.19	1.11	0.83	1.25
Multi 03	12.5	37.4	22.6	38.7	28.3	13.7			1.03	1.30	1.15	0.92	1.42

- Large 01: limit downstream flow to $10,000\ m^3/s$
- Large 02: fixed diversion rate of 45% for all discharge periods, no control structure
- Large 03: progressive diversion rate (75% for highest, 16% for lowest discharge)
- Multi 01: constant diversion ratio of 39%
- Multi 02: constant diversion ratio but diversions closed for $Q < 13,000\ m^3/s$
- Multi 03: progressive diversion rate up to 39% for $Q = 33,000\ m^3/s$

From the simulation outcome, we find that Large 03 leads to the lowest dredging volumes downstream and diverts a relatively high amount of sediment with a good diversion efficiency and a high percentage of sand fractions.
This result also shows the advantage of a pulsed operation compared to a fixed diversion rate, as simulated with Large 02:
The enhanced diversion of water during times with high sediment loads (especially sand fractions) is beneficial for downstream dredging volumes.
Similarly, Multi 02 shows moderate dredging volumes comparable to the Base Case with a good diversion efficiency and guarantees sufficient water depth for navigation as the gates are completely closed for $Q < 13,000\ m^3/s$. Extracting 39% of during lower discharge periods as in Multi 01 does not help to increase the total sediment diversion and puts navigation and the balance of salt and fresh water at stake. Despite high diversion efficiencies, Multi 03 diverts the least amount of water and sediment and causes higher dredging volumes downstream as a consequence from extraction and the sediment load that remains in the main channel.

Which Operation Mode of ORCS is Most Beneficial?

Table 6.4: Simulation Outcome for ORCS Operation Modes

Scenario	Dredging SWP - HoP $[10^6\ t/year]$			Deposition Rate $[10^6\ m^3/year]$		Sediment Diversion $[10^6\ t/year]$	Diversion Efficiency $(Q_{s,\ div}/Q_{w,\ div})/(Q_{s,\ up}/Q_{w,\ up})$						
	10 years	50 years	av. 50 yrs	av. 10 yrs	av. 50 yrs	av. 10 yrs	L1	L2	UBR	MBR	MBA	LBR	LBA
35-65	0.2	39.2	15.1	62.1	48.7								
60-40	9.7	28.2	16.6	28.1	34.0								
Base Case	12.0	31.9	19.8	18.8	29.7								
ORCS 01	11.4	38.4	22.9	17.9	30.3								
ORCS 02	12.6	46.0	27.9	13.9	26.6								
ORCS 03	12.5	38.0	22.8	15.2	27.4								
ORCS 04	11.4	38.3	22.9	17.9	30.4								

- 35-65 : Extreme discharge reduction, $Q \approx 9000\ m^3/s$ annual average discharge
- 60-40 : Discharge reduction at ORCS from 70-30
- ORCS 01: 50% less diversion towards Atchafalaya
- ORCS 02: Separation of river systems
- ORCS 03: Pulsed operation, except for dry periods
- ORCS 04: Pronounced pulsed operation

The above cases for different operation modes of ORCS include extreme cases like Winer (strong discharge reduction) ORCS 02 (separation of river systems, strong discharge increase) that will most likely lead to severe and opposed consequences in both tributaries, Lower Mississippi and Atchafalaya River.
Following the outcome of the analytical solutions, we can expect incising river beds or at least less deposition in the Atchafalaya River for the extreme discharge reduction 35-65. For the scenario of shifting more water to the Lower Mississippi River, the Atchafalaya would tend to silt up.
As the idea of this work is to investigate the effects of sediment diversions on the main channel of the Lower Mississippi River, the extreme discharge reduction 35-65 case can be discarded as not enough water is provided for additional extractions. Furthermore, the simulations showed that ports and industrial complexes along the Lower Mississippi River could be heavily affected.

A relatively small change favoring the Atchafalaya River (60-40) leads to lower dredging volumes but generally higher deposition rates. This case will be evaluated further in combination with sediment diversions to check the impact of such a change in operation mode of ORCS.

The four different cases with increased discharge at ORCS show similar dredging volumes after ten years and somewhat higher volumes for the 50-year period than the Base Case. The deposition rate is below the reference (except for 50-year averages of ORCS 01 and 04 with slightly higher values). The extreme case ORCS 02 with $Q \geq= 13,000\ m^3/s$ reduces the deposition rate from Reserve to Venice. However, a large portion of the transported sediment settles due to interaction with the salt wedge further downstream.

Compared to ORCS 01 and 04, ORCS 03 shows the lowest dredging volume and deposition rate. The latter is also lower than the reference of the Base Case. This can be explained with the non-linear relation between flow velocity and sediment transport: More water is diverted towards the Mississippi and average flow velocities increase. As the sediment transport capacity is usually proportional to the 3rd-to-5th power of the flow velocity, even more sediment can be conveyed.

Consequently, and similar to the large-scale diversions, we find that pulsed operation is the most beneficial operation mode of ORCS for effective wetland restoration. Although the increase in dredging volume has to be considered as a negative effect, we have to consider that changing the upstream operation mode is ought to be accompanied by the construction of new sediment diversions. This way, the additional sediment from the main channel can be extracted and distributed over the wetlands before deposition in the area of salt water influence dominates.

Which Combination of Diversions and Upstream Discharge Changes is Most Beneficial?

Table 6.5: Simulation Outcome for Diversions and ORCS Operation Modes

Scenario	Dredging SWP - HoP $[10^6\ t/year]$			Deposition Rate $[10^6\ m^3/year]$		Sediment Diversion $[10^6\ t/year]$	Diversion Efficiency $(Q_{s,\ div}/Q_{w,\ div})/(Q_{s,\ up}/Q_{w,\ up})$						
	10 years	50 years	av. 50 yrs	av. 10 yrs	av. 50 yrs	av. 10 yrs	L1	L2	UBR	MBR	MBA	LBR	LBA
Base Case	12.0	31.9	19.8	18.8	29.7								
60-40 + Large 03	2.6	30.6	16.1	42.3	30.4	15.6	1.39	1.30					
Base Case + Large 03	5.3	30.8	16.9	38.0	25.5	25.7	1.27	1.15					
ORCS 01 + Large 03	6.3	42.3	22.8	38.2	26.7	31.5	1.22	1.10					
ORCS 02 + Large 03	6.2	45.1	27.1	34.8	23.6	39.8	1.16	1.00					
ORCS 03 + Large 03	6.4	38.3	22.4	35.3	24.0	32.5	1.20	1.06					
ORCS 04 + Large 03	5.0	34.6	20.1	31.0	24.1	37.1	1.18	1.03					
60-40 + Multi 02	9.0	36.4	19.8	41.9	31.2	8.8			1.29	1.77	1.55	1.14	1.88
Base Case + Multi 02	8.6	37.1	20.3	42.2	29.1	17.6			1.02	1.19	1.11	0.83	1.25
ORCS 01 + Multi 02	10.0	46.7	27.1	43.8	29.5	20.1			0.92	1.08	0.99	0.82	1.23
ORCS 02 + Multi 02	11.9	41.3	26.9	39.5	25.9	24.7			0.76	0.80	0.72	0.60	0.87
ORCS 03 + Multi 02	10.3	37.1	22.8	39.4	26.6	21.0			0.88	0.97	0.88	0.70	1.03
ORCS 04 + Multi 02	12.1	33.8	21.5	35.7	26.6	22.2			0.86	0.95	0.87	0.70	1.02

- 60-40 : Discharge reduction at ORCS from 70-30
- ORCS 01: 50% less diversion towards Atchafalaya
- ORCS 02: Separation of river systems
- ORCS 03: Pulsed operation, except for dry periods
- ORCS 04: Pronounced pulsed operation

- Large 03: progressive diversion rate (75% for highest, 16% for lowest discharge)
- Multi 02: constant diversion ratio of 39%, diversions closed for $Q < 13,000\ m^3/s$

The combination of new sediment diversions with different operation modes of ORCS yields a number of interesting results.
First of all, and as expected and indicated before, the downstream dredging volumes show a significant decrease compared to the cases without additional water and sediment extraction. Depending on the operation mode of Old River Control Structure and sediment diversions, the dredging volumes vary from 16 to 27 million tons per year, whereas the Base Case has around 20 million tons per year. This again shows the importance of

choosing a beneficial operation mode and controlled diversions.

The large-scale diversions show good results compared to the Base Case with comparable dredging volumes and deposition rates. In general, the amount of diverted sediment is higher as the diversion ratio is higher (39 vs. 45%). The amount of 56 million tons per year of diverted sediment as anticipated by Parker, however, is not reached. Even the extreme case with altered operation mode of ORCS leads to 40 million tons per year only.

The scenario ORCS 04 + Large 03 yields the most beneficiary combination of low dredging volumes, deposition rates and high diversion with acceptable efficiency.
In case of multiple diversions, ORCS 03 + Multi 02 seems to be a reasonable compromise between dredging volumes, deposition rates and sediment diversion with acceptable diversion efficiencies.

What is the Impact of Increased Sediment Loads?

Table 6.6: Simulation Outcome Geometry and Diversion Angle

Scenario	Dredging SWP - HoP $[10^6\ t/year]$			Deposition Rate $[10^6\ m^3/year]$		Sediment Diversion $[10^6\ t/year]$	Diversion Efficiency $(Q_{s,\ div}/Q_{w,\ div})/(Q_{s,\ up}/Q_{w,\ up})$						
	10 years	50 years	av. 50 yrs	av. 10 yrs	av. 50 yrs	av. 10 yrs	L1	L2	UBR	MBR	MBA	LBR	LBA
Base Case (+82)	12.0			18.8									
Sed + 124	18.9			42.1									
Sed + 178	27.1			73.1									
Sed + 208	34.2			89.5									
Sed + 268	53.5			121.9									

- 82 million tons per year, derived from Allison (2012)
- 124 million tons per year, assumption from Parker (no settling to Reserve)
- 178 million tons per year, amount available at ORCS, Allison (2012)
- 208 million tons per year, sediment load 150 years ago (like Base Case)
- 268 million tons per year, sediment load 150 years ago (no settling to Reserve)

The response of the model domain in terms of dredging volumes and annual deposition rates for increasing sediment concentrations at the upstream boundary is relatively strong after a simulation period of 10 years: An increase with a factor of 1.5 leads to 1.6 times more dredging volumes and 2.25 times higher annual deposition. Reconstructing the 150 year old sediment supply with effectively 2.5 times more sediment would lead to 2.85 times more dredging volumes and even 4.75 times higher deposition.
Increasing the sediment input without any additional measures does not lead to the desired effects. Quite the reverse and as one could expect, severe problems regarding maintenance dredging may arise as the sediment concentrations have increased, whereas the transport capacity of the flow has not.

What is a Good Design of a Sediment Diversion?

Table 6.7: Simulation Outcome Geometry and Diversion Angle

Scenario	Dredging SWP - HoP $[10^6\ t/year]$			Deposition Rate $[10^6\ m^3/year]$		Sediment Diversion $[10^6\ t/year]$	Diversion Efficiency $(Q_{s,\ div}/Q_{w,\ div})/(Q_{s,\ up}/Q_{w,\ up})$						
	10 years	50 years	av. 50 yrs	av. 10 yrs	av. 50 yrs	av. 10 yrs	L1	L2	UBR	MBR	MBA	LBR	LBA
Base Case	12.0			18.8									
Large 03	5.3			38.0		25.7 (13.36)	1.27	1.15					
Large 04	5.5			38.1		25.68 (12.90)	1.22	1.21					
Large 05	5.6			38.1		25.64 (13.05)	1.23	1.19					
Large 06	5.2			38.1		26.07 (13.48)	1.27	1.19					
Large 07	6.0			38.3		26.85 (14.29)	1.34	1.18					
Large 03 01	5.6			38.0		24.81 (12.55)	1.18	1.15					
Large 03 02	5.6			38.1		25.90 (13.19)	1.24	1.20					
Large 03 03	5.6			38.1		26.21 (13.50)	1.27	1.20					
Large 03 04	5.6			38.1		26.35 (13.65)	1.29	1.20					

- Large 03 - original cross-section (1350 x 25 m)
- Large 04 - twice as wide, half as deep (2700 x 12.5 m)
- Large 05 - half as wide (675 x 25 m)
- Large 06 - half as deep (1350 x 12.5 m)
- Large 07 - twice as wide, 1/4 as deep (2700 x 6.25 m)

- Large 03 01 - diversion angle 15°
- Large 03 02 - diversion angle 20°
- Large 03 03 - diversion angle 25°
- Large 03 04 - diversion angle 30°

In order to evaluate design options, cross-sectional areas and diversion angles were tested for diversion efficiency and quantities. In general, Delft3D does not consider the effect of secondary flow on mud fractions. Hence, the impact on sand fractions is expected to be highest.

Large 04 with a wider but shallower cross-section leads to slightly less sediment transport. As expected, especially the sand fraction is affected. This can be explained by the combination of Rouse distribution and vertical velocity profile. The highest concentrations of sand are found near the bed. Hence a large part of the sand cannot be conveyed through

a shallow channel. In case of the mud fractions, we can also find higher concentrations in the upper part of the water column where the flow velocities are higher, as well. Hence, the suspended mud load gets less affected by cross-sectional changes. Although the efficiency of the modified diversion decreases, the efficiency of the left diversions increases in such a way that the total amount of diverted sediment stays the same. This also nicely demonstrates the interdependencies of adjacent diversions.

When we reduce the cross-sectional area by 50%, or, in other words, double the flow velocities (Large 05, 06, 07), we find the highest diversion efficiency for the Large 07 set-up with a 2700 x 6.25 m cross-section. As the efficiency of the modified diversion improves, the other diversion becomes more efficient, as well. This indicates that the combination of generated velocity and Rouse profiles is beneficial for both diversions.

The implementation of different diversion angles leads to the finding that diversions become more efficient for increasing angles. We can conclude that the maximum efficiency is between 30 and 90 °. For a more detailed analysis, additional angles need to be evaluated. However, as the grid resolution is relatively coarse and only two-dimensional, we can also expect some deviations as described by Heer & Mosselmann (2004) [34]. Hence local three-dimensional models are recommended for further investigations.

What is the Impact of Sea-Level Rise and Land Subsidence?

Table 6.8: Simulation Outcome RSLR

Scenario	Dredging SWP - HoP $[10^6\ t/year]$			Deposition Rate $[10^6\ m^3/year]$		Sediment Diversion $[10^6\ t/year]$	Diversion Efficiency $(Q_{s,\ div}/Q_{w,\ div})/(Q_{s,\ up}/Q_{w,\ up})$						
	10 years	50 years	av. 50 yrs	av. 10 yrs	av. 50 yrs	av. 10 yrs	L1	L2	UBR	MBR	MBA	LBR	LBA
Base Case	12.0	31.9	19.8	18.8	29.7								
Base Case RSLR	10.8	27.3	16.8	14.1	26.3								
ORCS 03+Multi 02	10.3	37.1	22.8	39.4	26.6	21.0			0.88	0.97	0.88	0.70	1.03
ORCS 03+Multi 02 RSLR	8.5	27.9	16.2	31.2	22.7	21.5			0.90	0.99	0.92	0.69	1.04

From a simplified, analytical point of view, land subsidence is supposed to cause a morphological response like sediment extraction: As the flow and sediment transport stays unchanged, the removed/subsided volume is filled up by deposition until the equilibrium situation is re-established.

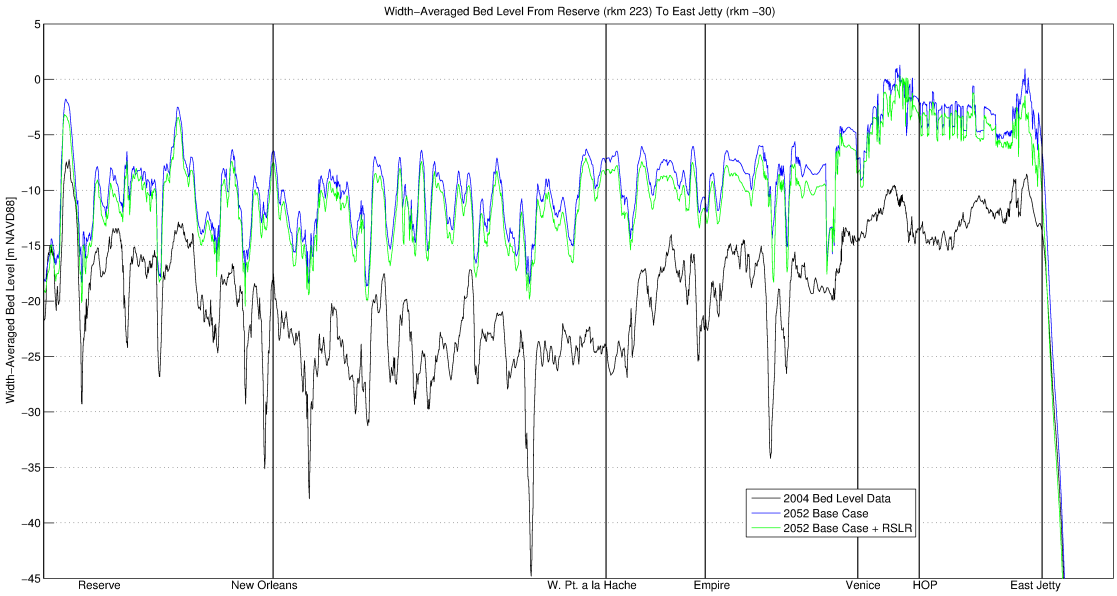

Figure 6.4: 50-Year Bed Level Changes for Base Case with and without RSLR.

However, the implementation of sea-level rise and land subsidence shows a positive effect on downstream dredging volumes. A comparison of the Base Case with and without this feature shows a reduction of 10 - 15% after 10 and 50 years, respectively. Moreover, we also find a reduction of the annual deposition rate which is as large as 25% during the first 10 years and decreases to about 11% during 50 years. Effectively, the deposition

rate is higher because the volume created by the subsidence is not considered. The bed level difference, as presented in figure 6.4, turns out to be in the order of 1 m and therefore corresponds to the cumulative subsidence. The comparison of a scenario with multiple diversions and pulsed operation of ORCS also yields similar results and shows, that the impact on dredging volumes and deposition rates is considerable. Hence, we can conclude that RSLR leads to lower bed levels along the entire Lower Mississippi River and positively affects dredging volumes.

What is the Impact of Additional Groin Fields from Head of Passes to Venice?

In order to reduce dredging volumes, groin fields (beyond the large-scale diversions) could be a good solution.

Table 6.9: Simulation Outcome Extended Groin Fields

Scenario	Dredging SWP - HoP $[10^6\ t/year]$			Deposition Rate $[10^6\ m^3/year]$		Sediment Diversion $[10^6\ t/year]$	Diversion Efficiency $(Q_{s,\ div}/Q_{w,\ div})/(Q_{s,\ up}/Q_{w,\ up})$						
	10 years	50 years	av. 50 yrs	av. 10 yrs	av. 50 yrs	av. 10 yrs	L1	L2	UBR	MBR	MBA	LBR	LBA
Base Case	12.0	31.9	19.8	18.8	29.7								
Base Case Groins	11.4	32.0	19.7	19.1	30.3								

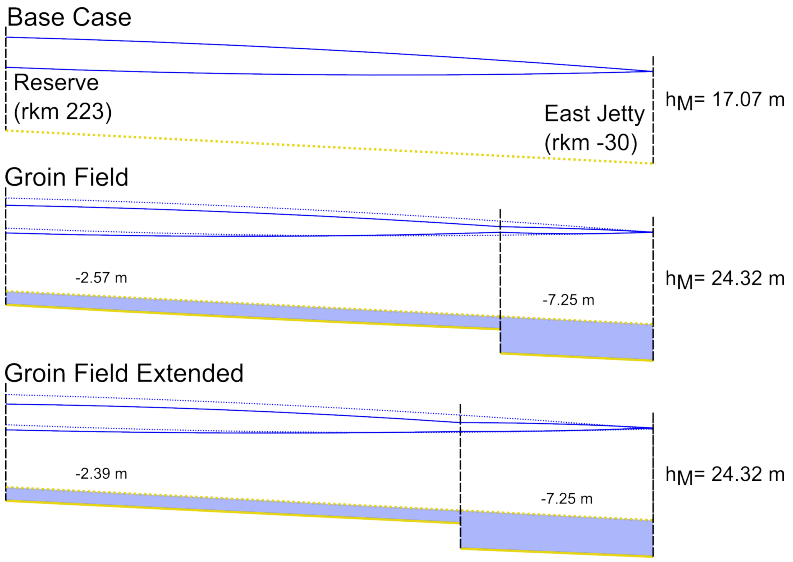

Figure 6.5: Base Case and New Equilibrium Situation for Large-Scale Sediment Diversions and Groin Fields. The figure shows the outcome of the analytical model for different scenarios.

We cannot directly see the impact of the groin fields solely based on the above values. The effect of morphology can be better observed by comparing the local bathymetry as presented in the following figures:

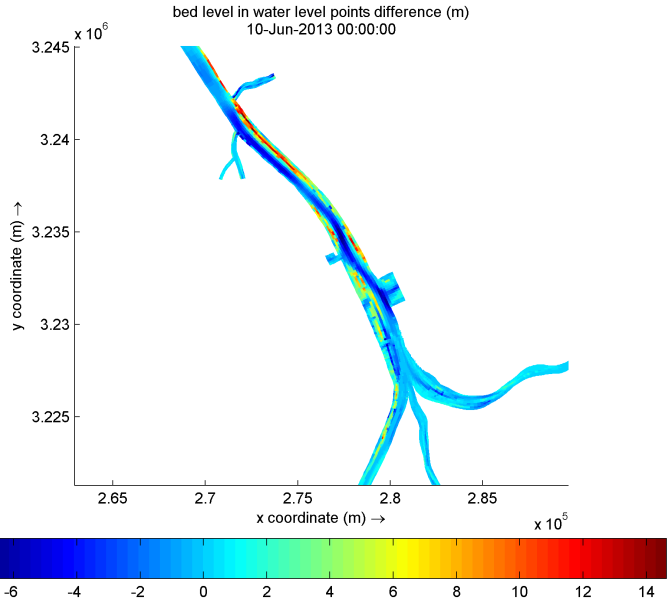

Figure 6.6: Bed Level Difference After 10 Years With And Without Groins. Difference given in meters.

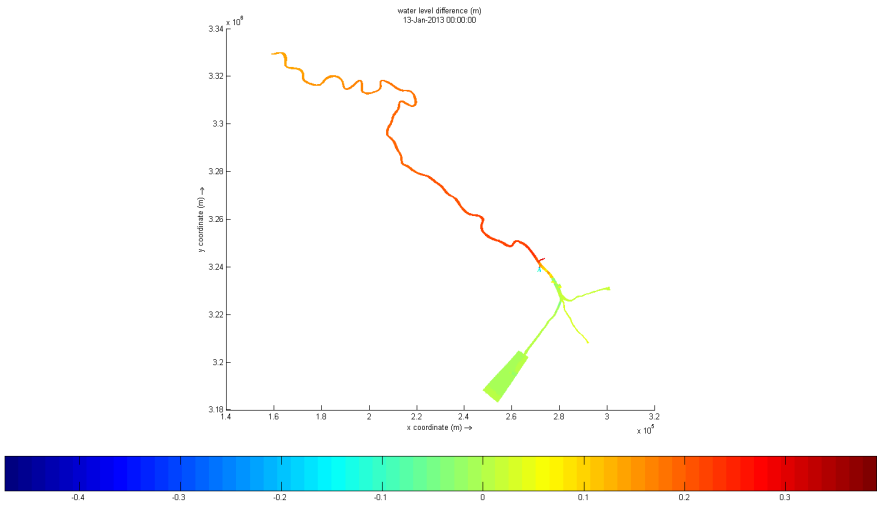

Figure 6.7: Water Level Difference [m] After 10 Years With And Without Groins. Difference given in meters.

The impact of extended groin fields can clearly be seen in the above figures showing bed and water level differences after ten years of simulation. The main channel is about 2-4 m deeper, whereas the adjacent areas show enhanced deposition. This can be explained with the occurring energy losses due to higher resistance and recirculation between the groins. The analytical model does not consider the outer areas but only a general narrowing of the river. The deepening in the main channel corresponds to that model.

The water level shows an increase of around 0.3 m upstream of the extended groin field. Compared to the simple analytical model, this is the opposite result. The deviation of the simulation outcome can also be explained with the fact that the width-averaged bed level is not affected significantly and that the groins generate additional resistance which leads to higher upstream water levels.

7 | Conclusions and Recommendations

7.1 Conclusions

Scientific implications

- The numerical model is able to show the impact of sediment diversions and wetland restoration scenarios on the morphology of the main channel on a decadal time scale.
- Analytical solutions fairly well agree with numerical outcomes regarding the morphological effects of new hydraulic interventions.
- Realistic results with Delft3D for the simulation of salt wedge intrusion in the Lower Mississippi River can only be obtained with a three-dimensional Z-layer model.
- The implementation of sea-level rise and spatially varying land subsidence showed to have some impact on simulation outcomes for long-term simulations.

Location of sediment diversions

- Locations of sediment diversions should be far enough upstream to make use of higher transport capacities and sand concentrations.
- Adjacent sediment diversions show interdependencies that can lead to a general decrease in efficiency.

Design of sediment diversions

- Deep diversion entrances help to capture larger amounts of bed load (sand). However, the amount of captured sediment does also depend on Rouse distribution, flow velocity profile and local geometry.
- The diversion angle showed to give higher diversion efficiencies for values above 30 and below 90°.

Operation of sediment diversions

- Extraction through diversions leads to enhanced deposition upstream of Venice. Within a 50-year period, however, deposition rates normalize and downstream dredging volumes remain relatively stable.
- Operated sediment diversions can capture more flow in case of high river discharges and allow for safe navigation during low river discharges.
- Pulsed operation of sediment diversions is beneficial as it provide more flexibility and a higher land-building capacity and can also contribute to reduced dredging volumes downstream.

Effects of altered upstream water and sediment supply & other interventions

- The system shows to be sensitive to discharge reduction with strong accretion of the upper reach of the main channel and sediment diversions that may convey 50% less sediment per year for an upstream reduction of 10%.
- Pulsed operation at ORCS with higher discharges prevents enhanced deposition, flushes the main channel and, this way, mitigates channel accretion.
- Increasing the sediment concentrations (e.g. flushing of reservoirs, nourishments) mainly contributes to significantly higher deposition in the upper reach, not to wetland restoration.
- Additional groin fields can help to ensure navigability downstream of sediment diversions and thus mitigate negative morphological effects in the main channel.

General Conclusions

- A combination of a pulsed operation of ORCS and large-scale diversions as proposed by Parker et al. seems to be the most effective solution for wetland restoration in the model domain as it leads to similar deposition rates upstream of Venice, only slightly higher dredging volumes in the downstream reach and high sediment diversion, whereas the implementation of multiple diversions seems to be more feasible, as they are already considered in the CPRA Masterplan.
- The application of additional diversions can stabilize local delta regions, but without higher sediment supply from upstream, the diverted amount of sediment is not sufficient for wetland restoration on a larger scale.

7.2 Recommendations

Model Outcome

- The simulation outcomes have shown that it is feasible to operate new sediment diversions without severely affecting the morphology of the main channel. Especially pulsed operation of sediment diversions is beneficial and thus recommended.
- Additional river engineering measures, e.g. groin fields can counteract bed level increase downstream of the diversions. The construction of groin fields and, for example, the presented multiple diversions should be considered in this context in more detailed studies.
- The impacts of the simulated scenarios on the Atchafalaya River have to be taken into account when it comes to decision-making. Extreme alterations will most likely cause strong and opposite effects in this adjacent basin.
- For sophisticated local design studies of sediment diversions, 3D-models are recommended to find optimal settings for each diversion site and to analyze possible interdependencies.

Considerations for future research

- New multibeam data in the reach from Venice (rkm 16) to East Jetty (rkm -30) could bring more insight into dredging activities and the intensity of the settling process induced by salinity. This could further improve the morphological calibration.
- The impact of salt wedge intrusion is a very complex, three dimensional process which should be investigated in more detail.
- Running Delft3D simulations as a three-dimensional morphodynamic Z-layer model with activated salinity might become feasible with upcoming releases and represents a very interesting option for future research on the Lower Mississippi River and other, weakly forced estuarine environments.

Appendices

A | Delta Evolution and Human Interventions

This chapter intends to give an overview over the geological development of the Lower Mississippi River and recent history dominated by river engineering measures.
The different measures and their effects will be explained more in detail followed by a description of actual trends in flow and sediment discharge.

A.1 Geology and Estuarine Classification

In this section, a short introduction is given on the geological evolution starting in the early Holocene around 12,000 BP. At this time the average floodplain south of Baton Rouge was about 24 m lower [59]. The mean water level was even found at 115 to 135 m below present Mean Sea Level. Global warming led to a de-glaciation and consequently to an eustatic sea-level rise that attained values of up to 7 mm/year, decelerated around 7,000 years BP and stabilized at <1 mm/year. [10].
With decelerating sea-level rise and sufficient sediment supply the Mississippi Delta developed a number of individual deltas as old meander belts were abandoned roughly every 1,000 to 1,500 years. The old deltas suffered from sediment shortage and entered a transgressive stage [10, 59]. In general, land building due to sediment supply has to compensate land loss. Consolidation of Holocene and older Pleistocene sediment depositions leads to subsidence rates of approximately 0.12 at the edge of the deltaic plain to 3.00 m per century in the active delta [59].
Present land subsidence rates are up to 23 mm/year [8] which represents a large contribution to the relative sea level rise as the present eustatic sea-level rise is estimated

with approximately 1.5 mm/year. Moreover, human interventions had a severe impact on sediment supply and the latest delta formation processes [20].

In the below figure, the different deltas are presented together with a time line indicating their active phases.

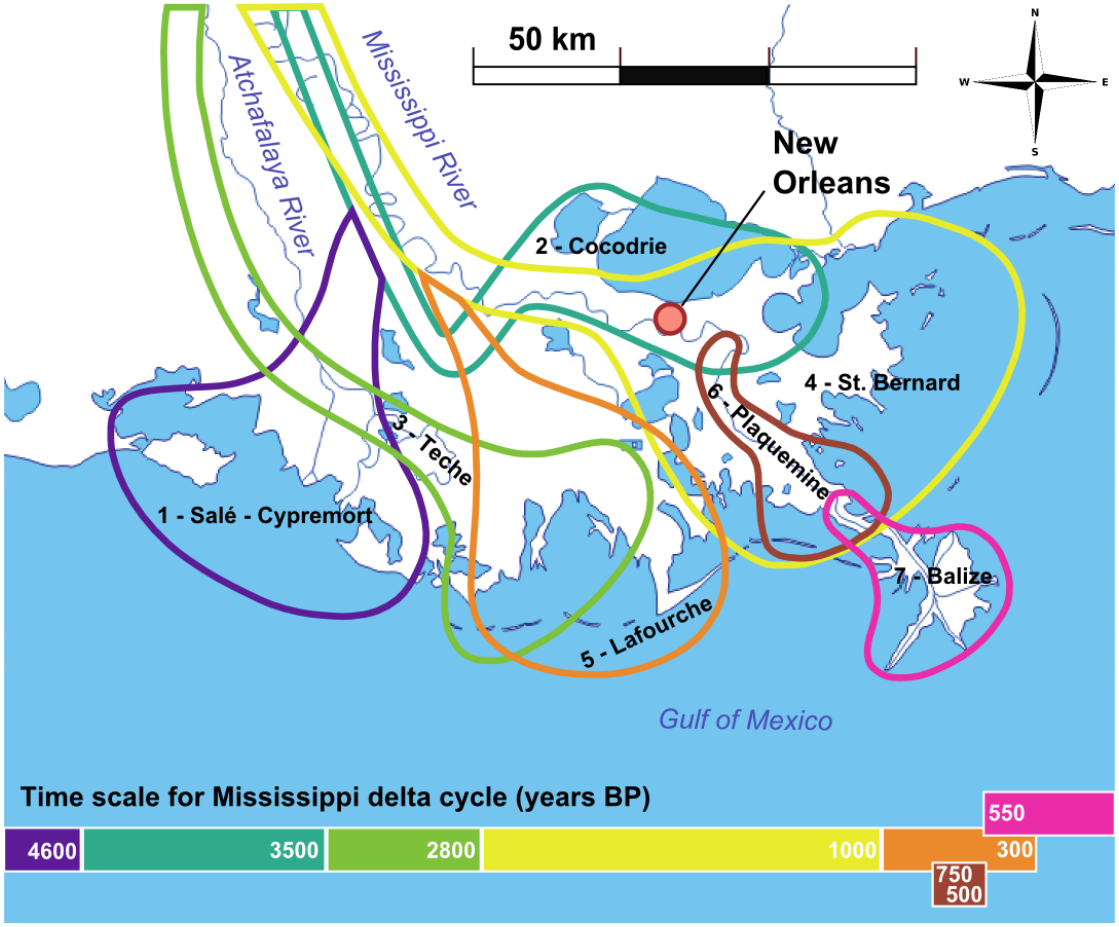

Figure A.1: Holocene Delta Cycle of the Mississippi. The figure shows the delta forming process of the Mississippi River from 8000 BP until today. (BP= before present, defined as 1950)

The Delta in its present form can be classified based on various factors such as the influence of tide, waves and river discharge following the delta classification of Galloway (1975) [32].

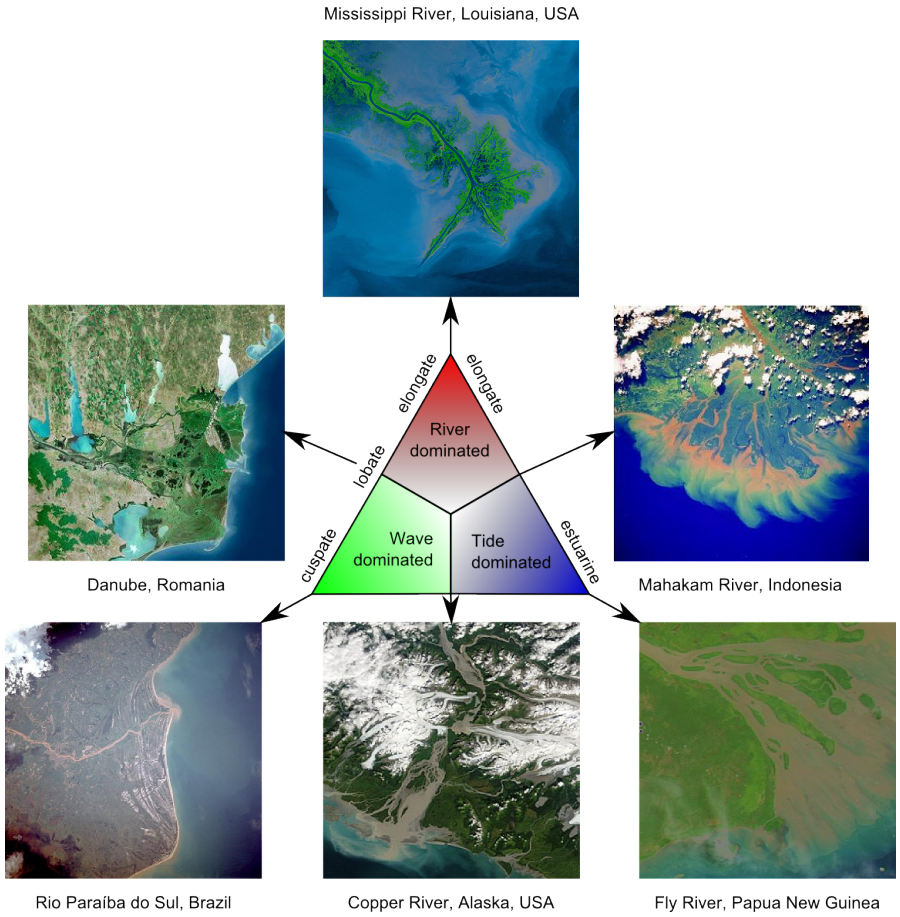

Figure A.2: Delta Classification (Galloway, 1975). The figure shows the satellite images of different deltas, which formed individually due to a combination of sediment availability, tides and wave conditions

The Mississippi River is classified as a fluvially dominated system and thus tends to elongate. This can be explained with small wave and tidal energy fluxes in the Gulf of Mexico that only generate a small distribution of the sediment provided by the river.

A.2 Recent history

The history of river engineering activities at the Lower Mississippi River is extremely short, compared to the geological time scales. The effects of human interventions, however, strongly influence todays appearance of the river.

The first description and mapping of the Mississippi River was carried out by the US-Army Lieutant Ross in 1765. More detailed studies on hydrography followed by Talcott (1838) and Humphreys and Abbot (1861). In 1879, the US Army Corps of Engineers conducted first experiments on bank protection. In the same year, the Mississippi River Commission was established by the US Congress and assigned with the planning of river engineering measures to create stable river banks and a deep channel to control floods and to ensure safe navigation [63].
Although riparian land owners had already started in the beginning of the 17th century to locally build small levees [63], there was no real flood defense system at that time and already in 1882, the entire delta area suffered from a devastating flood event [63].
The reduction of the floodplain area due to ongoing confinements led to increasing levee heights. However, flooding of the Lower Mississippi River area in 1912 and 1913 could not be prevented. A flood in 1927 had the most devastating effect with 67,000 km^2 of inundated area, 200 deaths, 600,000 homeless and about 1.5 billion US-$ damage ("at today's prices"). After this event, the Mississippi River and Tributaries Project was initiated [79]. In the following years, the Lower Mississippi River experienced extensive river training works. Until 1955, artificial cutoffs shortened the river by 331 km. For navigation purposes, bank revetment and groin fields were used. Moreover, due to increasing droughts of the vessels, dredging became another important topic. In order to further improve flood control, levees, floodways, flood water retention structures and reservoirs were constructed. This way, the Lower Mississippi River changed from a freely meandering alluvial river to a highly trained and confined channel. In order to understand their respective impact, the different measures will be explained below in more detail.

A.2.1 Levees

As already mentioned, levees were already applied on a small scale since the 17th century. Original floodplain widths reaching from 30 to 130 km were drastically reduced by levees with heights up to two meters. Consequently, and with ongoing confinements, the levees had to be raised. In the actual stage, the floodplain are between 2 and 24 km wide, whereas the levees reached 12 m in 1973. Due to meandering, several dike systems remained on the floodplains [63].

A.2.2 Old River Control Structure

The Old River Control Structure is an important structure in the Lower Mississippi River, situated between rkm 489 and 510. It distributes the flow between the Atchafalaya River and the Mississippi River. The relation is approximately 30 to 70. Without this control structure, significantly more water would be conveyed through the Atchafalaya River as the natural system tends to leave the downstream Mississippi branch because its distance to the Gulf of Mexico is more than 300 km longer [7].

Figure A.3: Overview of River System Downstream of Old River Control Structure. The figure shows the distances to the Gulf of Mexico. Adapted from: majikphil3.blogspot.de

It was decided to stop the delta evolution process in order to protect industry and communities already present in the Atchafalaya basin. Moreover, also navigation within

the Mississippi River played a significant role. Different controlled hydraulic structures and management strategies led to varying distributions since 1850. In the following, the development of the latitude flow in the Atchfalaya River is shown together with a graphical description of the geomorphological evolution and the human interventions.

Table A.1: Percentage of flow from Red River and Mississippi River conveyed through Atchafalaya River (latitude flow)

Year	Percentage
1850	<10
1900	13
1920	18.1
1940	23.3
1950	30
1973	34.6
1974	34.7
1975	34.9
1976	31.8
1977-1985	30

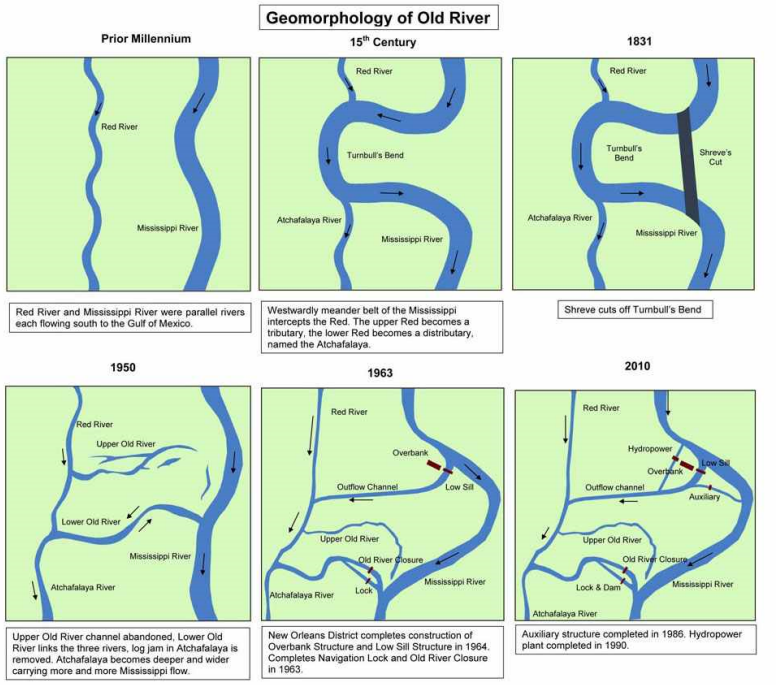

Figure A.4: Development of Old River Control Structure. The figure shows how the Red River/ Atchafalaya has been connected to the Mississippi River by geomorphological evolution and human intervention. Source: Wikipedia Commons

A.2.3 Flood water diversions

The confined channel with their high water levels during floods are a severe threat to the industry, the people and their homes. By constructing spillways it was possible to extract part of the water masses upstream of endangered locations and thus to lower flood stages. In the Lower Mississippi River there are three large flood water diversions:

- **Bonnet Carre Spillway**
  The Bonnet Carre Spillway is a controlled structure on the east bank of the Mississippi at rkm 200 upstream of New Orleans. It was constructed in 1931 and diverts up to $7,100 m^3/s$ to Lake Pontchartrain. The spillway was operated ten times (1937, 1945, 1950, 1973, 1975, 1979, 1983, 1997, 2008 and 2011) [7].

- **Morganza Floodway**
  The Morganza floodway was built in 1954 on the west side of the Mississippi at rkm 450. It diverts up to $17,000 m^3/s$ at $42,000 m^3/s$ at Red River Landing to the Atchafalaya basin. It has been used only once in spring 1973 [78].
  The structure is only opened after the Bonnet Carre Spillway is active and in case the water levels keep rising and become critical [7].

- **Bird's Point - New Madrid Floodway**
  This floodway is located upstream of Old River Control Structure in the state of Missouri and was only used twice, in 1937 and 2011. The floodway diverts at maximum $16,000 m^3/s$ under design flood conditions by flooding a leveed area of $530 km^2$. Downstream, this area can be connected to the Mississippi. The levees at entrance and outflow have to be opened by a controlled detonation [77].

A.2.4 Construction of reservoirs and watershed management

In order to deal with the increased flood stages, reservoirs were build along the LMR. This way, smaller watersheds of the tributaries could be controlled in such a way, that on one hand the downstream stages were reduced and, on the other hand, a minimum navigation depth of 3 m was established in the LMR [63].

A.2.5 Artificial Cutoffs and Channel Alignment

The meandering, natural Mississippi River caused several problems for riparian landowners as it kept shifting continiously. Moreover, with increasing usage of the Mississippi as a waterway, navigational safety and economic aspects became important. Cutting off bends led to shorter transport distances and facilitated navigation.
The alignment of the Lower Mississippi River was carried out in two stages. In stage one, sixteen cutoffs between 1929 and 1945 reduced the length by 243 km upstream of Baton Rouge. In the second stage from 1939 to 1955, another 88km reduction was achieved by cutting off natural chutes. Although 331 km were cut off until 1955, repeated measurements in 1989 showed that the length from the confluence of the Ohio River to the Gulf of Mexico was only 162 km shorter. Obviously, the river changed its length by meandering in not-yet confined reaches to establish a new equilibrium after the bed level gradient was increased artificially [63].

A.2.6 River Bank Revetments

Land loss due to bank retreat was a common problem in the Mississippi Delta. The flood plains provided the largest amount of sediment due to bank caving [27].
Meandering as well as already aligned sections were immobilized with bank revetments since first experiments were carried out in the 1930's with different materials and techinques. Especially the cutbanks of meanders showed a high erodibility and had to be protected with articulated concrete matrasses. Bank revetment played an important role to ensure channel alignment and fixed levee systems [63].

A.2.7 Training dikes (groins)

In order to provide sufficiently deep channels also under conditions with low discharges, groins are an appropriate hydraulic structure. Moreover, they protect the banks by concentrating the flow dynamics in the fairway. In the Lower Mississippi River, whole groin fields were installed in problem reaches. First experiments with permeable groins

showed their inappropriateness due to the lack of accretion of relatively coarse sediment particles [63].

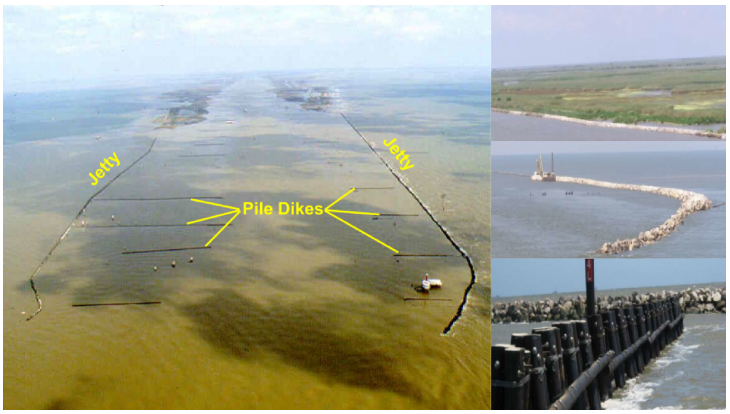

Figure A.5: Southwest Pass Infrastructure Left: Southwest Pass Jetty Structure. Top right: Foreshore Rocks. Middle right: Jetty Structure, Down right: Pile Dikes. Source: [66]

A.2.8 Dredging

The Lower Mississippi River has a strong economic importance to the national economy. Hence, navigability is of special interest. The Mississippi River has to be navigable for sea-going vessels from Southwest Pass up to Baton Rouge and for inland vessels up to Minneapolis. Therefore, the US Corps of Engineers has to maintain a fairway depth of at least 13.70 m (45 ft) and 2.70 m (9 ft), respectively. The dredging reaches of interest are shown in the below figure:

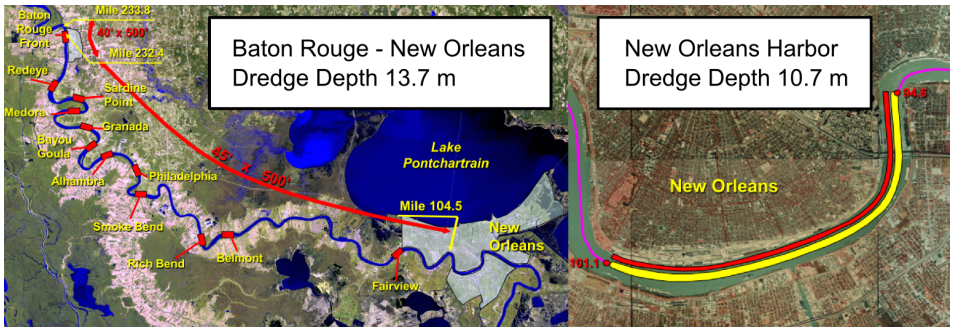

Figure A.6: Deep Draft Dredging Baton Rouge - New Orleans & New Orleans Harbor Source: www.propclubnola.org

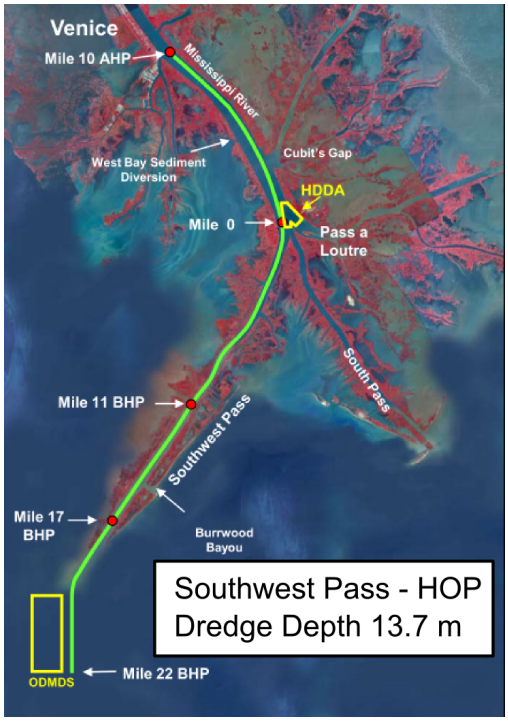

Figure A.7: Deep Draft Dredging Southwest Pass - Head of Passes Source: [66]

As it is crucial to hold the entrance of the Mississippi open, special attention has to be paid to Head of Passes and Southwest Pass where enhanced bed level aggradation can be found mainly due to interaction with salt water intrusion and flocculation of fine particles. Moreover, the infrastructure, e.g. the port of New Orleans has to be maintained, as well. Further upstream, deep draft crossings have to be provided.
It is noted that maintenance dredging is only a temporary measure as it does not influence the upstream transport gradients. Although costly, dredging is conducted on a yearly basis in the Mississippi River. Compared to the economic benefits of navigation on the Mississippi, dredging costs are affordable.

A.3 Response of the river to engineering

As shown in the previous section, there is barely a river section of the Mississippi River that was not subject to river engineering measures. All these activities were conducted

to ensure safety of communities in the Mississippi Valley and to drive forward national prosperity. However, the river reacted to human controls.

Dams and revetments led to a decay of sediment input as upstream sediment is held back and bank caving is suppressed. Big reservoirs were constructed at the Missouri River and at the Arkansas River in the 1950's and 60's, respectively [63]. Kesel (2003) states that *"[...] the construction of artificial levees has reduced water and sediment storage on the flood plain by over 90% [...]"* and that a larger amount of sediment is flushed out to the Gulf of Mexico as the main channel is greatly disconnected from its adjacent wetlands. Figure A.8 shows the disadvantageous vicinity of the birdfoot delta to the shelf break the more favorable situation with a larger and shallow shelf area of the Atchafalya Delta.

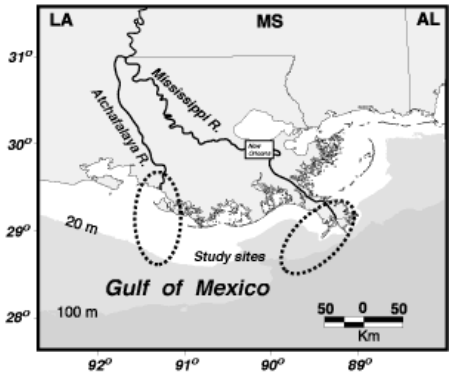

Figure A.8: Sediment Loss due to Shelf Characteristics. The figure shows the Louisiana coast with the shallow shelf at the mouth of the Atchafalaya and the shelf break near the birdfoot delta of the Lower Mississippi Delta. Source: USGS.

Moreover, channel degradation started to migrate upstream from artificial cut-offs, although those effects decelerated in the mid-70's [38, 63].

It is assumed that the total suspended load of the Lower Mississippi River decreased by over 70% since 1850 [37]. These assumptions are also taken into account in the sediment availability study by Blum and Roberts (2009) [10].

The declined sediment input in combination with flow constrictions decreased the sediment supply of the wetlands and hence directly affect land loss rates: From 1913 to 1980, annual land loss rates changed from 17 to 102 km^2 [63].

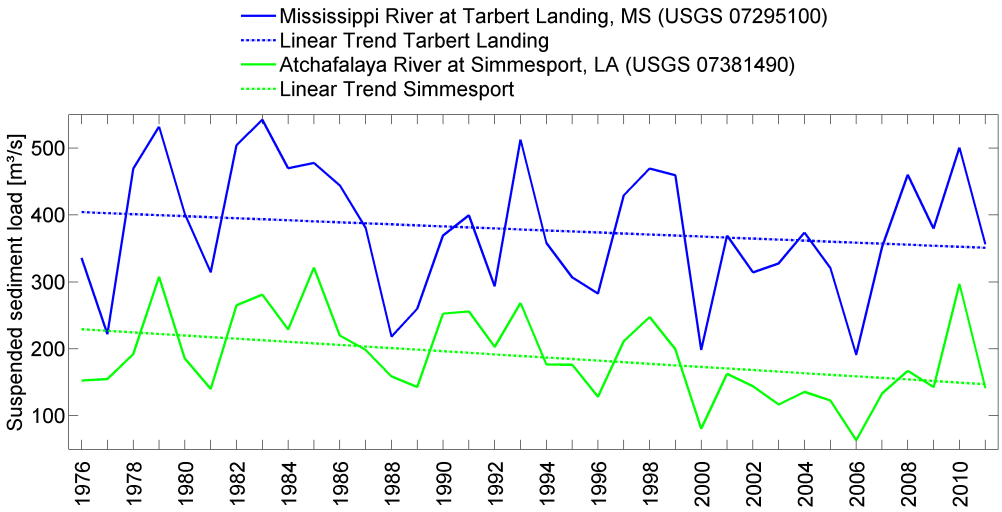

Figure A.9: Suspended Sediment Decline Graph. The figure shows the decreasing suspended sediment loads in the Lower Mississippi River and in the Atchafalaya. Adapted from USGS.

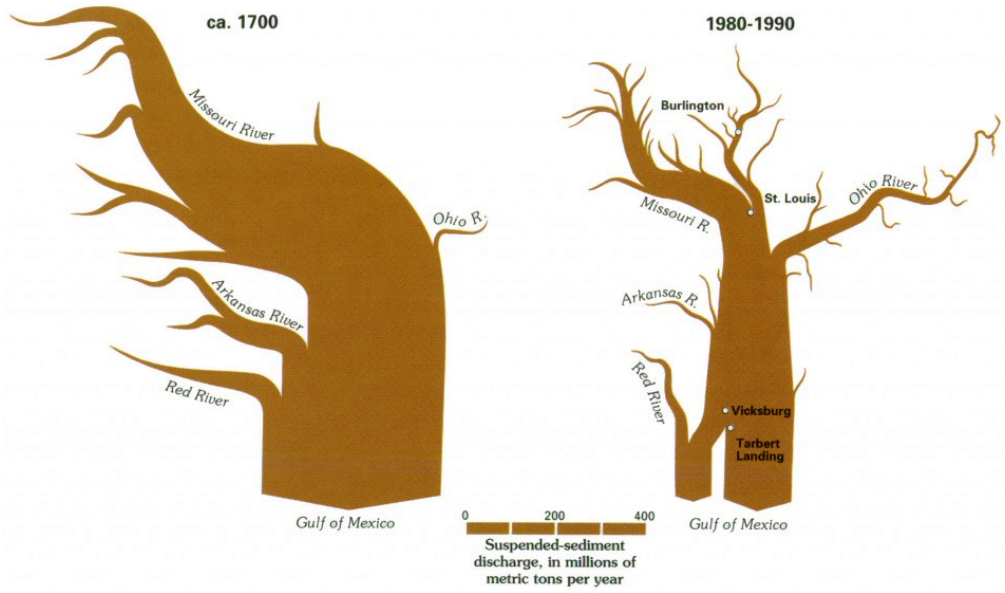

Figure A.10: Suspended Sediment Decline Scheme. The figure shows the decreasing suspended sediment loads in the Mississippi River and in the Atchafalaya. Source: Meade (1995) [44].

B | Theoretical Background

B.1 Conversion to Metric System

As in this work only metric units will be used and some amount of the used data, e.g. local discharge time series, is given in United States customary units, the conversion is presented in the table below.

Table B.1: Conversion - US customary units and metric units.

US customary units	Metric System
35.31467 cubic feet per second (cfs)	1 m^3/s
0.3048 feet (ft)	1 m
1.30795 cubic yards (cu yd)	1 m^3
2.47 acres (a, ac.)	1 ha (hectar)
0.62137 miles	1 km

B.2 Hydrodynamics - Annex

B.2.1 Fundamental Equations

Delft3D uses a set of equations based on the physical principles of conservation of mass and momentum to solve for flow characteristics like water level and velocities. For conservation of mass, the continuity equation for incompressible fluids reads:

$$\frac{\delta u}{\delta x} + \frac{\delta v}{\delta y} + \frac{\delta w}{\delta z} = 0 \tag{B.1}$$

For conservation of momentum (rate of change of momentum = Force) the Reynolds averaged Navier-Stokes (RANS) equations are applied in x-, y- and z-direction, respectively:

$$\frac{\delta u}{\delta t} + \frac{\delta uu}{\delta x} + \frac{\delta uv}{\delta y} + \frac{\delta uw}{\delta z} + \frac{1}{\rho}\frac{\delta \rho}{\delta x} - fv + \frac{1}{\rho}\left[\frac{\delta \tau_{xx}}{\delta x} + \frac{\delta \tau_{xy}}{\delta y} + \frac{\delta \tau_{xz}}{\delta z}\right] = 0 \tag{B.2}$$

$$\frac{\delta v}{\delta t} + \frac{\delta uv}{\delta x} + \frac{\delta vv}{\delta y} + \frac{\delta vw}{\delta z} + \frac{1}{\rho}\frac{\delta \rho}{\delta y} + fu + \frac{1}{\rho}\left[\frac{\delta \tau_{yx}}{\delta x} + \frac{\delta \tau_{yy}}{\delta y} + \frac{\delta \tau_{yz}}{\delta z}\right] = 0 \tag{B.3}$$

$$\frac{\delta w}{\delta t} + \frac{\delta uw}{\delta x} + \frac{\delta vw}{\delta y} + \frac{\delta ww}{\delta z} + \frac{1}{\rho}\frac{\delta \rho}{\delta z} + g + \frac{1}{\rho}\left[\frac{\delta \tau_{zx}}{\delta x} + \frac{\delta \tau_{zy}}{\delta y} + \frac{\delta \tau_{zz}}{\delta z}\right] = 0 \tag{B.4}$$

The terms in the RANS equations represent acceleration of flow (1), advection along the x, y and z direction (2,3,4), pressure gradient in x, y and z direction (5), Coriolis force in x and y and gravitational acceleration in z direction (6) and Reynolds stresses normal and parallel to planes in x, y and z direction.
The number of unknowns in the RANS equations with their additional normal and shear stresses due to small scale motion has to be reduced by means of a turbulence closure

model in order to create a solvable system of equations together with the continuity equation.

Turbulence Closure

As in a laminar case, the shear stress can be related to a velocity gradient and a (turbulent) viscosity. The turbulent viscosity is unknown and can be estimated based on the Prandtl length-scale hypothesis that states that the characteristic velocity of the turbulent motion is proportional to the velocity difference in the mean flow over a distance l_m known as the mixing length. The turbulent shear stress can now be written as:

$$\tau = \rho\overline{x'z'} = -\rho\nu_t\frac{\delta u}{\delta z} \approx -\rho l_m^2\left|\frac{\delta u}{\delta z}\right|\frac{\delta u}{\delta z} \tag{B.5}$$

Near walls, the mixing length l_m is approximated with $l_m = \kappa z$ with the Von Karman constant $\kappa = 0.4$. In the outer region, the mixing length can be taken proportional to the boundary layer, $l_m = 0.09\delta$.

$k-\epsilon$ model

In this work, the $k-\epsilon$ model is used to determine the turbulent viscosity. In its simplest from the model reads

$$\nu_t = C_1\frac{k^2}{\epsilon} \tag{B.6}$$

The $k-\epsilon$ model uses two transport equations, one for turbulent kinetic energy in the flow as a measure for the velocity scale (k) and the other for dissipation containing information about the length scale of the turbulence (ϵ).

$$\frac{Dk}{Dt} = \frac{C_1}{\sigma_k}\nabla_i\left(\frac{k^2}{\epsilon}\nabla_i k\right) + C_1\frac{k^2}{\epsilon}\left\{\nabla_i\overline{v_j}\left(\nabla_i\overline{v_j} + \nabla_j\overline{v_i}\right)\right\} - \epsilon \tag{B.7}$$

$$\frac{D\epsilon}{Dt} = \frac{C_1}{\sigma_\epsilon}\nabla_i\left(\frac{k^2}{\epsilon}\nabla_i\epsilon\right) + C_{p\epsilon}k\left\{\nabla_i\overline{v_j}\left(\nabla_i\overline{v_j} + \nabla_j\overline{v_i}\right)\right\} - C_{d\epsilon}\frac{\epsilon^2}{k} \tag{B.8}$$

with $C_1 = 0.09$, $C_{p\epsilon} = 0.13$, $C_{d\epsilon} = 2.0$, $\sigma_k = 1.0$ and $\sigma_\epsilon = 1.3$.

Together with boundary conditions for k and ϵ, e.g. a logarithmic vertical velocity profile, defined mixing lengths at the wall (Von Karman) and zero gradients for k and ϵ at the surface, k, ϵ and consequently the turbulent viscosity can be determined.
Hence, the continuity equation, the Reynolds averaged Navier-Stokes equations and the $k - \epsilon$ model form a closed system that can be solved by Delft3D.

Boussinesq approximation

In case of small density differences, $\frac{\rho_{max} - \rho_{min}}{\rho_{max}} << 1$, the Boussinesq approximation may be applied. By doing so, the horizontal momentum equations use a constant reference density, ρ_0, instead of the actual densities. For the vertical momentum equation no changes are made.

Hydrostatic approximation

The vertical momentum equation can be simplified by assuming a hydrostatic pressure distribution over the vertical in case of large horizontal length scales compared to vertical ones. By doing so, the momentum equation simplifies to a vertical pressure gradient that solely depends on the density and the gravitational acceleration.

$$\frac{\delta p}{\delta z} = -\rho g \tag{B.9}$$

Coriolis - f-plane approximation

The Coriolis parameter reads $f = 2\Omega sin\phi$, where Ω is the rotation rate of the Earth and ϕ is the latitude. For areas with small variations in f a constant value may be assumed.

B.2.2 Secondary Flow

The Delft3D manual 2011 states that Delft3D considers the the effect of secondary flows on the two dimensional (depth-averaged) momentum equations.

$$tan(\beta) = \frac{sin(\alpha) - f(\theta,\eta)^{-1}\frac{\delta z}{\delta \eta}}{sin(\alpha) - f(\theta,\xi)^{-1}\frac{\delta z}{\delta \xi}} \tag{B.10}$$

where

$$\frac{\delta z}{\delta \eta} and \frac{\delta z}{\delta \xi} \tag{B.11}$$

are bed level slopes in transverse and flow direction, respectively.

B.2.3 Analysis of Roughness Values

Two trends showed up during hydraulic calibration:

- The roughness increased from downstream to upstream
- The roughness increased from high to low discharges

The roughness increased from downstream to upstream.
We can explain the outcome based on the Manning-Strickler formula solved for the Manning coefficient:

$$n = \frac{h^{2/3} i^{1/2}}{v} \tag{B.12}$$

where h is the water depth, i is the water level slope and v is the average flow velocity.

From the above equation it follows that the Manning value depends on the local depth. In case of the Lower Mississippi River the width-averaged depth can simply be

described as increasing in upstream direction from 10-12 m at East Jetty to around 25-29 m at New Orleans. Farther upriver, the depth reduces to around 15-21 m. Of course, the total depth depends on the actual river discharge.
In addition, we have to account for local water level slopes and flow velocities. From the imposed discharge distribution and typical cross-sections we find higher flow velocities between Reserve and New Orleans. Further downstream flow velocities do not change significantly. From the water level data obtained from USACE we can derive the water level slopes which are in the order of $i \approx 2.5 * 10^{-5}$. Especially upstream of New Orleans, the water level slope gets steeper, probably due to higher flow velocities and hence higher energy losses, $i \approx 5.0 * 10^{-5}$.
With the above presented information we can generate an analytical solution for Manning coefficients. For example, we choose the highest discharge period with $Q = 33,000\ m^3/s$:

Table B.2: Analytical Model for Manning Coefficients

	Reserve	New Orleans	East Jetty
h	20	25	10
v	2.0	1.5	1.5
i	5.00E-05	2.50E-05	2.50E-05
n	**0.026**	**0.028**	**0.015**

We find that the Manning coefficients from the hydraulic calibration agree with the analytical model.

The roughness increased from high to low discharges.
At a fixed location, the Manning roughness values change as a result of varying flow velocity, water level slope and depth.
In the formula, all parameters decrease for decreasing discharge. In general, we can conclude that when the water level drops due to lower discharges, the relative inflence of roughness elements on the bed increases and hence the Manning value increases [1].

[1] `http://www.fhwa.dot.gov/bridge/wsp2339.pdf`

B.3 Salinity - Annex

B.3.1 Estuarine Circulation

When fresh water from a river encounters salt water in an estuarine environment, we have to deal with an additional, baroclinic pressure term, caused by a density gradient in horizontal direction. In addition, temperature differences can lead to the same phenomena. Here, however, we focus on the interaction between fresh and salt water.
In the figure below, the process of estuarine circulation is shown. It results from two components: The water level gradient causes an external, barotropic pressure. This way, we can assume a pressure towards the sea that is constant over the vertical.
The internal, baroclinic pressure is directed land inwards, as the sea is saltier and hence denser. However, the vertical distribution is not constant but linearly increases with depth.
The result is a profile which is directed seawards in the upper region and land inwards in the lower region [51], [55].

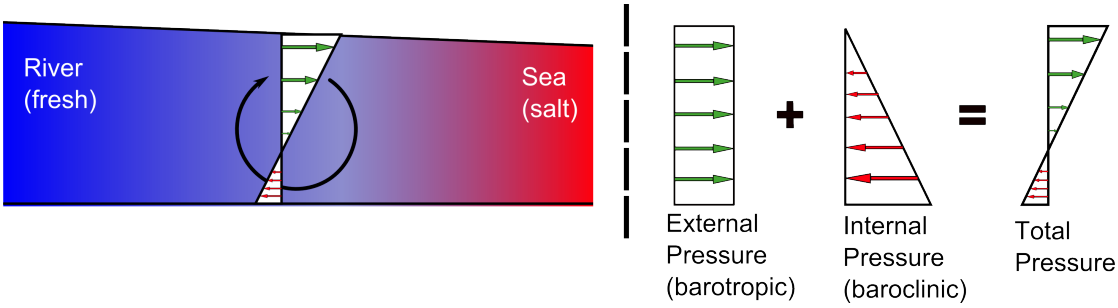

Figure B.1: Estuarine Circulation. Interaction of fresh and salt water.

Of course, other effects might also be found that have an impact on the salt intrusion, e.g. thermal wind, tidal straining or upwelling. However, the concept of estuarine circulation already suffices to explain the interaction of salinity and fine sediment which leads to enhanced deposition. For more details, one is referred to Nguyen (2008) [51] or

de Nijs et al. (2011) [52].
In this section, only the hydraulic effects will be treated. After a general section about morphology, we will focus on this interaction in more in detail.

B.3.2 Forester Filter

The Forester filter is an important feature in Delft3D when it comes to mitigating over- and undershoots (wiggles) through artificial diffusion.
The filter can be activated in the horizontal and in the vertical direction.
In the horizontal direction, the filter helps to keep concentrations of suspended sediment, temperature and salt non-negative. In the vertical direction, the filter has no effect on suspended sediment but only on temperature and salinity.
Moreover, values that exceed the maximum concentration in the system are also reduced by diffusion.[22]
During initial simulations the Forester filters applied in both directions turned out to be essential for numerical stability and reasonable results.

B.3.3 Thatcher-Harleman time lag

Thatcher-Harleman time lags can be specified at any boundary. They determine the return time for concentrations from their value at outflow to their value specified by the boundary condition at inflow.
This way, large jumps between in- and outgoing concentrations can be prevented. The Thatcher-Harleman time lags were applied on the Neumann boundaries that are positioned laterally in the domains of the Gulf of Mexico.
As a result, the lateral boundaries are open and have a minimal impact on the system.

B.3.4 Comparison of Vertical Modeling Techniques

Delft3D offers two possibilities for three-dimensional modeling with curvi-linear grids: The σ-layer model and the Z-layer model. In the following, both options, their imple-

mentation and the outcome will be discussed.
The goal is to find the model that is able to reproduce a realistic salt wedge intrusion. Because this property is most pronounced during low discharges, we first focus on $Q_{nom} = 7000\ m^3/s$.

σ-layer model

The three-dimensional *sigma*-layer Delft3D model comprises ten layers that always show the same relative vertical distribution. The distance was determined based on recommendations by the Delft3D 2012 manual to accurately reproduce the logarithmic velocity profile and thus the transport of salt (and sediment)[22]:

Table B.3: Relative Distribution of Layer Thickness in Percent (Layer 1 = surface layer, Layer 10 = bottom layer)

Layer no.	rel. distribution [%]
1	2
2	3
3	4
4	6
5	8
6	10
7	12
8	15
9	20
10	20

Without additional adaption, the first outcome impressively underlines the shortcomings of the *sigma*-layer model:

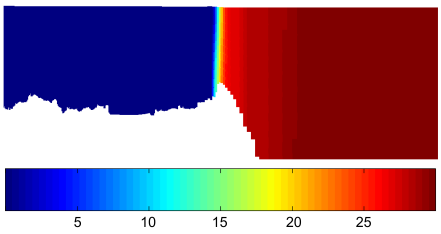

Figure B.2: Result of σ-Layer Model without Anti-Creep.

The σ-layer model shows to develop a strong vertical diffusion which can be explained

by the weakly forced estuary and the steeply falling bottom near the shelf. When the water from the relatively deep shelf reaches the shallower mouth of the river the salt may be evenly distributed over the vertical and form a steep front.
This leads to an unnatural behavior as it is expected that the intruding salt water leads to higher salinity concentrations at the bottom and that the fresh water is conveyed over the salt wedge.
Hence an additional parameter Sigcor =#Y# is used to prevent the upward motion of salt in the shallower riverine section[1] New simulations showed improved performance. However, vertical diffusion still prevented larger salt wedge intrusion. Also adapting background diffusivity and viscosity did not lead to realistic results.

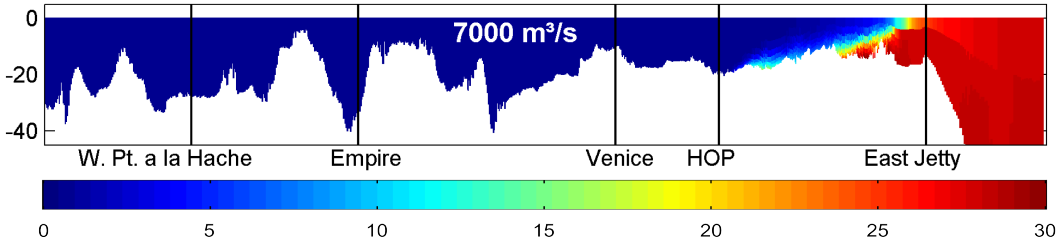

Figure B.3: Result of σ-Layer Model with Anti-Creep. With 10 layers.

Conclusion: The σ-layer model introduces vertical diffusion and, this way, enhances mixing of salt and fresh water over the vertical. Although using anti-creep filter and increased horizontal viscosity the desired stratification could not be established accurately. The intrusion length of the salt wedge was much lower than expected from findings in literature.

[1] "Sigma co-ordinates have a slight disadvantage in case large bottom gradients exist in the model. Owing to truncation errors, artificial vertical diffusion and artificial flow may occur in this case. A counter measure (a so-called anti-creep approach) can be activated to suppress this phenomenon." [22]

Z-layer model

In order to get a more realistic salt wedge behavior, the Z-layer model is applied. The Z-layer model uses strictly horizontal layers. This turns out to be beneficial in case of an estuarine environment with large depth gradients. However, the resolution varies locally and calls for a higher number of layers in shallower areas.

Because we want to model salt wedge intrusion accurately, it was decided to create 30 horizontal layers with the following distribution from bottom to surface [1]:

Table B.4: Distribution of Layer Thickness (1 = bottom layer, 30 = surface layer). Vertical positions of layers are related positive downward to NAVD88=0 m

No.	Thickness [%]	Start [m]	End [m]	Thickness [m]
1	91.000	-688.0	-51.0	637.0
2	1.500	-51.0	-40.5	10.5
3	1.000	-40.5	-33.5	7.0
4	0.750	-33.5	-28.3	5.3
5	0.500	-28.3	-24.8	3.5
6	0.300	-24.8	-22.7	2.1
7	0.230	-22.7	-21.0	1.6
8	0.200	-21.0	-19.6	1.4
9	0.200	-19.6	-18.2	1.4
10	0.200	-18.2	-16.8	1.4
11	0.200	-16.8	-15.4	1.4
12	0.200	-15.4	-14.0	1.4
13	0.200	-14.0	-12.6	1.4
14	0.200	-12.6	-11.2	1.4
15	0.200	-11.2	-9.8	1.4
16	0.200	-9.8	-8.4	1.4
17	0.200	-8.4	-7.0	1.4
18	0.170	-7.0	-5.9	1.2
19	0.150	-5.9	-4.8	1.1
20	0.125	-4.8	-3.9	0.9
21	0.075	-3.9	-3.4	0.5
22	0.075	-3.4	-2.9	0.5
23	0.075	-2.9	-2.4	0.5
24	0.050	-2.4	-2.0	0.4
25	0.050	-2.0	-1.7	0.4
26	0.050	-1.7	-1.3	0.4
27	0.100	-1.3	-0.6	0.7
28	0.200	-0.6	0.8	1.4
29	0.400	0.8	3.6	2.8
30	1.200	3.6	12.0	8.4

[1] **Remark:** In the *sigma*-model layer 1 corresponds to the surface layer while in the Z-model layer 1 refers to the bottom layer.

The result of the Z-layer model with activated Forester filters finally shows a characteristic salt wedge in the Lower Mississippi River.

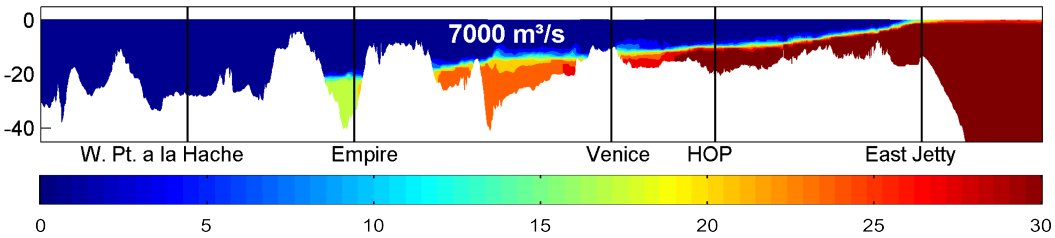

Figure B.4: Result of Z-layer Model. With 30 layers.

Conclusion: The Z-layer model was specifically designed for situations with weak external forcing and large differences. As expected, the salt intrusion is stronger and less mixing over the vertical is observed. Therefore we continue with the Z-layer model.

B.3.5 Need for 3D Modeling of Salt Water Intrusion

In general, denser fluids tend to sink to the ground, whereas lighter fluids rise to the surface. In an estuarine environment this simple principle is also valid. However, the dynamics in the system, in particular the river discharge and the tide, have a large impact on the mixing of the two fluids.

The Delft3D manual [22] states that in case of modeling salinity an estimate should be done on whether the estuary can be classified as being well mixed, partly mixed or strongly stratified. For that purpose, the Estuary number is applied. It comprises information about densities of the fluids, geometry of the estuary, quantity of river flow and tidal properties and reads:

$$E_D = \frac{\rho u_t^3}{\pi \Delta \rho h_0 u_r} \tag{B.13}$$

where:

g	gravitational acceleration	[m/s^2]
h_0	depth at the mouth of the estuary	[m]
u_r	river velocity, i.e. the river flow rate divided by the cross-sectional area at the mouth of the estuary	[m/s]
u_t	amplitude of the profile averaged tidal velocity at the mouth of the estuary	[m/s]
ρ	density of sea water	[kg/m^3]
$\Delta\rho$	density difference between sea water and river water	[kg/m^3]

The Estuary number is the reciprocal expression of the Richardson number. Depending on E_D (Thatcher, 1981), the estuary is strongly stratified, partly stratified or well-mixed:

- $E_D < 0.2$ strongly stratified,
- $0.2 < E_D < 8$ partly mixed,
- $8 < E_D$ well-mixed

The Delft3D manual states that in the partly mixed and strongly stratified cases a 3D computations should be used in principal. Moreover, for strongly stratified flow a $k - \epsilon$ model is recommended [22].

Applying the Estuarine number on the Southwest Pass of the Mississippi with
$u_t = 0.15\ m/s$, $\Delta\rho = 30\ kg/m^3$, $\rho = 1030\ kg/m^3$, $u_r = 1\ m/s$, $h_0 = 20\ m$
results in $E_D \approx 0.002 < 0.2$ which clearly shows that the Mississippi is a strongly stratified estuary.

Conclusion: A three-dimensional model is required.

B.3.6 Upstream Extension

First simulations with the model reaching from Reserve to the Gulf revealed resonance phenomena at the upstream discharge boundary (Reserve). When tidal forcing was applied the water level amplitude at Reserve showed to be a factor 2 to 3 larger than at the mouth of the river. Although it is expected that damping of the tidal signal is rather ineffective due a relatively large water depth of the Mississippi, the tidal amplitude is ought to decay. If the domain has an unfavorable length compared to the tidal wave, for example one quarter of the wave length, resonance might occur. Assuming an average depth of $h = 20\ m$, the propagation velocity in shallow water, $c = \sqrt{gh}$, becomes $c = 14\ m/s$. Together with the length of the domain, $L = 300,000\ m$, the eigenperiod of the domain becomes $T_{Mississippi} = \frac{4\ L}{c} = \frac{4*300,000}{14} \approx 85700\ s$. This rather rough estimate comes very close to the period of the tidal signal, $T = 86400\ s$.
In order to solve for this problem, the model domain is extended approximately 150 kilometers upstream by a coarser, rectangular grid. Its purpose is to generate a reasonable hydraulic behavior. The additional computational time is negligible. The effect of the extension is positive: Instead of increased water level amplitudes, damping mechanisms can be observed.

B.4 Morphology - Annex

B.4.1 Van Rijn 1984 sediment transport formula

For morphodynamic simulation the van Rijn 1984 sediment transport formula was applied. It is suitable for fine sediments in an riverine environment. The formula calculates both suspended sediment and bed load[1].

$$S_b = \begin{cases} 0.053\sqrt{\Delta g D_{50}^3} D_*^{-0.3} T^{2.1}, & \text{for } T < 3.0. \\ 0.100\sqrt{\Delta g D_{50}^3} D_*^{-0.3} T^{2.1}, & \text{for } T \leq 3.0. \end{cases}$$

where T is a dimensionless bed shear stress parameter which can be expressed in terms of the critical bed shear stress according to Shields τ_{bcr} and the effective shear stress $\mu_c \tau_{bc}$.

$T = \frac{\mu_c \tau_{bc} - \tau_{bcr}}{\tau_{bcr}}$

where

$\tau_{bc} = \frac{1}{8}\rho_w f_{cb} q^2$

$f_{cb} = \frac{0.24}{^{10}log(12h/\xi_c)^2}$

$\mu_c = (\frac{18^{10}log(12h/\xi_c)}{C_{g,90}})^2$

with $C_{g,90}$ the grain related Chezy coefficient

$C_{g,90} = 18^{10}log(12h/3D_{90})$

The critical shear stress according to Shields reads

$\tau_{bcr} = \rho_w \Delta g D_{50} \theta_{cr}$

in which θ_{cr} is the Shields parameter which is a function of the dimensionless particle parameter D_*

[1] see Delft3D manual, 11.5.6

$D_* = D_{50}(\frac{\Delta g}{\nu^2})^{1/3}$

The formulation for the suspended sediment transport reads

$S_s = f_{cs} q h C_a$

C_a is the reference concentration, q the depth-averaged velocity, h the water depth and f_{cs} is a shape factor approximated as

$$f_{cs} = \begin{cases} f_0(z_c), & \text{if } z_c \neq 1.2. \\ f_1(z_c), & \text{if } z_c = 1.2. \end{cases}$$

$f_0(z_c) = \frac{(\xi_c/h)^{z_c} - (\xi_c/h)^{1.2}}{(1-\xi_c/h)^{z_c}(1.2-z_c)}$

$f_1(z_c) = (\frac{\xi_c/h}{1-\xi_c/h})^{1.2} ln(\xi_c/h)$

where ξ_c is the reference level or roughness height (can be interpreted as the bed-load layer thickness) and z_c the suspension number.

$z_c = min(20, \frac{w_s}{\beta \kappa u_*} + \phi)$

$u_* = q\sqrt{f_{cb}/8}$

$\beta = min(1.5, 1 + 2(\frac{w_s}{u_*})^2)$

$\phi = 2.5(\frac{w_s}{u_*})^{0.8}(\frac{C_a}{0.65})^{0.4}$

The reference concentration is written as

$C_a = 0.015 \alpha_1 \frac{D_{50}}{\xi_c} \frac{T^{1.5}}{D_*^{0.3}}$

The bed-load transport rate is imposed as bed-load transport due to currents S_{bc}, while the computed suspended load transport rate is converted into a reference concentration equal to $f_{cs} C_a$. The following formula specific parameters have to be specified in the input files of the Transport module (B.9.3):

- calibration coefficient α_1

- dummy argument reference level (bed load thickness) or roughness height ξ_c $[m]$ and settling velocity w_s $[m/s]$.

B.4.2 Engelund-Hansen sediment transport formula

The transport formula of Engelung and Hansen (1967) considers the total sediment load (suspended load and bed load) [2]

$$s = \frac{0.05\alpha u^5}{\sqrt{g}C^3\Delta^2 D_{50}} \tag{B.14}$$

where α is a calibration parameter for Delft3D, u is the averaged flow velocity, C is the Chézy coefficient, Δ is the relative density and D_{50} is the median grain diameter. The Engelund-Hansen formula is only valid, if the following requirements are met: $w_s u_* < 1$, $0.19 < D_{50} < 0.93mm$ and $0.07 < \theta = 6$.

B.4.3 Bed composition model

Delft3D has two options to model sediment composition in river beds. The default comprises a single, uniformly mixed layer. All sediment fractions in this layer are exposed to erosion in the same way. Depositing grains change the local concentrations within the mixed layer but e.g. building up of a cover layer cannot be considered.
The second option is a layered bed stratigraphy (multiple sediment layers). With multiple layers it is possible to keep track of changing bed composition due to deposition. Therefore, a transport layer with a user-defined thickness and additional underlayers are specified. The transport layer receives depositing sediments and forwards the information about the composition to the underlayer below. When the layer thickness of the underlayer is reached, an empty underlayer is created below the transport layer to receive new information about bed composition. Vice versa, erosion only affects the transport layer. In case of complete erosion the top layer is filled up from below as long as there is

[2] see also Delft3D manual, 11.5.2

sediment available [22].

The main advantage of this bed layer model is that for a sufficiently small layer thickness only the sediment is considered that is actually exposed to the flow. In case of deposition of cohesive material on top of fine sand, erosion rates will drop significantly whereas in a single mixed layer a large part of the fine sand may be eroded.

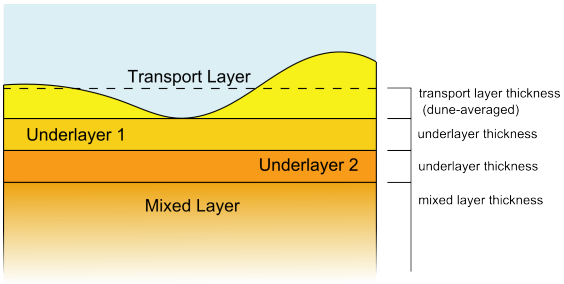

Figure B.5: Bed Layer Model. The figure shows the three main components of the applied bed layer model: The transport layer, a set of underlayers and the mixed layer. Adapted from Mosselman[49].

B.4.4 Exner equation

The Exner equation describes a simple relation between transport gradients and the bed level: The bed level drops for positive sediment transport gradients and grows for negative ones. The one-dimensional Exner equation reads:

$$\frac{\delta z_b}{\delta t} + \frac{\delta q_s}{\delta x} = \frac{\delta z_b}{\delta t} + \frac{\delta q_s}{\delta u}\frac{\delta u}{\delta x} = 0$$

In order to evaluate the initial morphological response of e.g. extraction of discharge and sediment via diversions on the main channel, the Exner equation is a valuable tool.

At the intervention, (theoretical) velocity gradients may go to infinity and initiate a sedimentation/erosion front as the sediment transport capacity suddenly drops/grows. Local alterations also cause backwater curves reaching upstream affecting the transport capacity gradually.

B.4.5 Long-term Morphological Response (Forget-me-nots)

Once a river is brought out of its equilibrium it adapts to the new situation striving towards establishing a new equilibrium. The time scales involved in this process can be in the order of decades and even centuries. The final equilibrium can be obtained from the so called "forget-me-nots", a number of equations derived from the quasi-steady one-dimensional equations for water and sediment discharge.

Table B.5: Forget-me-nots

Intervention	i_1/i_0	h_1/h_0
Water withdrawal	$\frac{Q_0}{Q_0-\Delta Q}$	$1-\frac{\Delta Q}{Q_0}$
Sediment withdrawal	$\left(1-\frac{\Delta Q_{s0}}{Q_{s0}}\right)^{\frac{3}{b}}$	$\left(1-\frac{\Delta Q_{s0}}{Q_{s0}}\right)^{-\frac{1}{b}}$
Long constriction	$\left(\frac{B-\Delta B}{B}\right)^{1-\frac{3}{b}}$	$\left(\frac{B-\Delta B}{B}\right)^{1-\frac{1}{b}}$

For combined extraction of water and sediment and additional changes in width, Crosato [18] provides us with the corresponding equations for equilibrium slope and water level.
In addition, since we have to deal with a hydrograph containing eight different discharge periods with relative duration $p(Q)$, we have to sum up the effect of each period.
At the river mouth, the adapted equations read:

$$\frac{h_{M,\infty}}{h_{M,0}} = \left(\frac{B_0}{B_\infty}\right)^{1-1/b} * \left(\frac{Q_{S,0}}{Q_{S,\infty}}\right)^{1/b} * \left[\frac{\sum\left(p(Q) * Q_{W,\infty}^b\right)}{\sum\left(p(Q) * Q_{W,0}^b\right)}\right]^{1/b} \tag{B.15}$$

$$\frac{i_\infty}{i_0} = \left(\frac{Q_{S,\infty}}{Q_{S,0}}\right)^{3/b} * \left(\frac{B_\infty}{B_0}\right)^{1-3/b} * \left[\frac{\sum\left(p(Q) * Q_{W,0}^{3/b}\right)}{\sum\left(p(Q) * Q_{W,\infty}^{3/b}\right)}\right]^{3/b} \tag{B.16}$$

B.4.6 Length and Time Scales of Interventions

In order to make first estimates about the length of backwater curves and time scales analytical expressions are available.
Derived with the method of characteristics, the celerity of bed disturbances, c_{bed}, can be estimated with the width, b, sediment discharge, q_s, water discharge q, flow velocity u and degree of non-linearity in $q_s(u)$, $b(> 3)$.

$$c_{bed} \approx \frac{bq_s}{h} = b\frac{q_s}{q}u, for Fr << 1 \tag{B.17}$$

Together with the length of the affected river section upstream of the intervention an estimate about the time scale can be made.
For changes over relatively large distances, the half-length of the backwater curve is a relevant parameter which can be approximated with:

$$X_{0.5} \approx \frac{1}{4}\frac{h_0}{i_b} \tag{B.18}$$

The half length represents the upstream distance at which half of the total exponential decay of the water level is found.
The "Time needed for half the total effect at a long distance, L (parabolic model, diffusion)" is then:

$$T_{0.5} = \frac{3i_b L^2 B}{nqs} \tag{B.19}$$

where n represents the power of the transport formula.

For short distances, e.g. the filling of a dredged trench, the following approximations can be applied for celerity of bed disturbances and time scale, respectively:

$$c_{bed} \approx \frac{bq_{s0}}{(1 - Fr_0^2)h_0}, for Fr << 1 \tag{B.20}$$

$$T \approx \frac{h_0 L}{bq_{s0}} \tag{B.21}$$

B.4.7 Settling Velocity (van Rijn (1993))

The fall velocities of grains with different diameters can be approximated with the formulae from van Rijn (1993) [82]:

Table B.6: Fall velocities after van Rijn (1993)

$w_s = \frac{\Delta g D^2}{18\nu}$	for $1 < D \leq 100\mu m$
$w_s = \frac{10\nu}{D}\left(\sqrt{1 + \frac{0.01\Delta g D^3}{\nu^2}} - 1\right)$	for $100 < D \leq 1000\mu m$
$w_s = 1.1\sqrt{\Delta g D}$	for $D > 1000\mu m$

We can simply calculate the fall velocities for the sediment fractions, e.g. for the sand fraction. With $D = 200\ \mu m = 0.0002\ m$, $\nu = 1 * 10^{-6} m^2/s$ and $\Delta = 1.65$ the corresponding equation for $100 < D \leq 1000\ \mu m$ yields a fall velocity of $w_s = 0.0257\ m/s \approx 2.6\ cm/s$.

The other fractions have smaller diameters, so the first formula is applied for silt $D \approx O(16\ \mu m)$ and clay $D \approx O(2$
$mum)$. This results in very small fall velocities of 0.023 cm/s for silt and 0.00036 cm/s for clay corresponding to 82.8 cm/hour and 1.3 cm/hour, respectively.
A rough estimate considers a particle near the surface at the upstream boundary. The Mississippi is still 255 km long, the flow velocity is assumed to be 1 m/s and the depth 25 m. Hence the particle needs more than 3 days until it arrives at the mouth. Without taking into account gradient transport due to turbulence, cohesion or flocculation due to salt water, the silt particle settles after 1 day and 6 hours at a distance of 109 km from the upstream boundary, whereas the clay particle would deposit after more than 80 days, i.e., effectively, it would be flushed out into the Gulf of Mexico. This is also what can be observed to some amount in reality, but estuarine effects play an important role in settling processes and dominate around Head of Passes.

B.4.8 Bed Slope Effects (Koch and Flokstra (1980))

Delft3D includes formulations to cope with bed-slope effects on bed load transport. In general, two bed slopes, parallel (x) and perpendicular (y) to the initial transport direction, are considered. With a factor, α_s, the magnitude of the bed load transport, S_b'', can be corrected for bed slope effects.

$$S'_{b,x} = \alpha_s S''_{b,x} \tag{B.22}$$

$$S'_{b,y} = \alpha_s S''_{b,y} \tag{B.23}$$

In this work, the formulation of Koch and Flokstra (1980) as extended by Talmon et al. (1995) yields the correction factor, α_s .

$$\alpha_s = 1 + \alpha_{bs} \frac{\delta z}{\delta s} \tag{B.24}$$

where α_{bs} (keyword ALFABS) is a user-defined calibration parameter.
Moreover, the bed load direction changes from the original direction, φ_T to the final direction φ_s:

$$tan(\phi_s) = \frac{sin(\varphi_T) + \frac{1}{f(\theta)} \frac{\delta z_b}{\delta y}}{cos(\varphi_T) + \frac{1}{f(\theta)} \frac{\delta z_b}{\delta x}} \tag{B.25}$$

with

$$f(\theta) = A_{sh} \theta_i^{B_{sh}} \left(\frac{D_i}{H} \right)^{C_{sh}} \left(\frac{D_i}{D_m} \right)^{D_{sh}} \tag{B.26}$$

This leads to four additional tuning parameters A_{sh} (Ashld), B_{sh} (Bshld), C_{sh} (Cshld) and D_{sh} (Dshld).

B.4.9 Mud

As the Mississippi is also called "The Big Muddy" it becomes quite clear that mud is a relevant topic. In the following, a short overview is given including definition and description of physical small-scale processes based on Winterwerp (2012) [85] and the Pegasos Project [54].

Definition of Mud

First of all, mud comprises several minerals, organic matter and water. One could even add living organisms and gas to this list. The morphological model focuses on the sediment fractions. In fact, all fractions, sand, silt and clay can be part of mud where the mud fractions are most relevant. An important property of mud is its cohesive nature due to clay particles.

Flocculation

The process of flocculation depends on processes that go down to pore water chemistry. The salt water introduces cations (positively charged atoms or molecules) that act as binding agents between fine sediment particles. In addition, organic material (e.g. cellulose, lipids, proteins) also tends to flocculation due to van der Waals forces and bipolar forces/ bi-polarity. Moreover, bound water is an important part of those flocs with 90 to 98% under natural conditions.

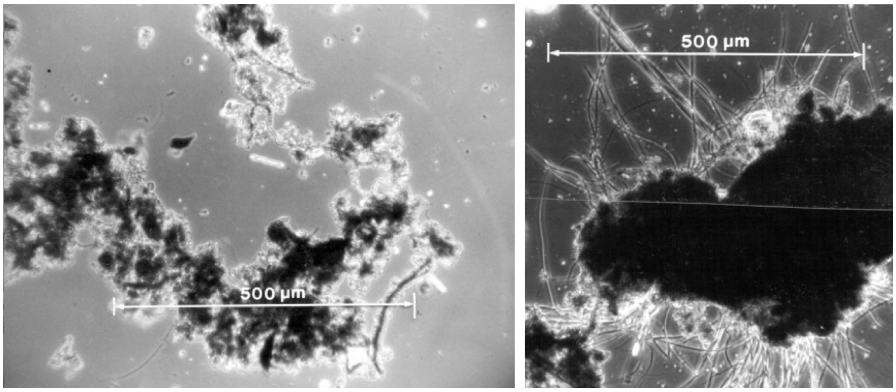

Figure B.6: Flocculated Mud. The figure shows the dimension of flocculated mud particles. Source: Winterwerp (2012) [85].

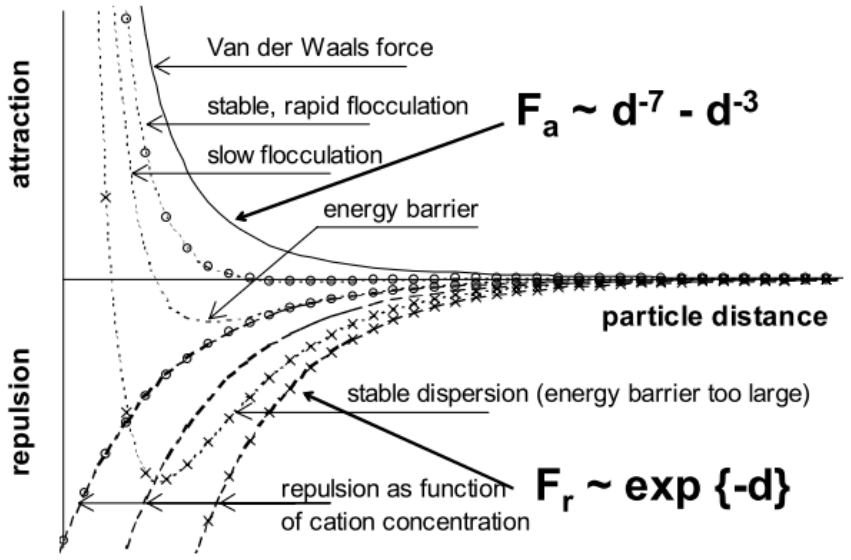

Figure B.7: Attracting and repulsing forces acting on mud particles. The figure shows that flocculation of cohesive mud fractions depends on the distance of single particles and the sediment diameter. The attraction due to van der Waals forces is counteracted by the cation concentration which can even lead to a stable dispersion. Source: Winterwerp (2012) [85].

Cohesive Beds

In general, beds can be assumed cohesive with clay contents around 5 to 10% or a mud content around 30 to 40%. In such a case the bed becomes more resistant to erosive processes. Based on measurements, the implemented bed composition shows such a percentage of mud already for the New Orleans area with an increasing portion of mud in downstream direction (see 2.11, p. 22). We can hence consider the bed in this reach as cohesive. When looking at the clay fractions, we find percentages of over 5% already at the upstream boundary. This implies that the river bed in the entire reach could be defined as being cohesive. Taking into account the linear increase of clay fractions and mud in general in downstream direction, it can be assumed that the cohesive effect will also be enhanced correspondingly. From this consideration, the decision was made to linearly vary the critical shear stresses along the domain in order to calibrate for decadal bed level changes (see 2.6.5, p. 31).

Settling: Comparison of Fall Velocity by Winterwerp (2012)

The fall velocities of sand and mud particles can easily vary by a factor 1000. However, flocculated mud particles are much bigger than an individual grain and hence significantly increase the fall velocity. Winterwerp gives an example for a concentration of 1 g/l with:

Sand, $D_{50} = 110\ \mu m$, $w_s = 9\ mm/s$

Mud (Kaolinite), $D_{50} = 3\ \mu m$, $w_s = 0.01\ mm/s$

Flocs of kaolinite (with 3 mg CF803 organic flocculant), $D_{50} = 100\ \mu m$, $w_s = 3\ mm/s$

Moreover, as flocs consist to a large amount of water, the relative density at the bed is around $\Delta\rho_{floc} = 50\ kg/m^3$ instead of $\Delta\rho = 1600\ kg/m^3$.

Erosion of Mud Fractions

Once the flocs have settled onto the river bed, they might contribute to non-erodible consolidated layers as shown by Nittrouer (see figure 2.10), p. 21). However, depending on internal structure and shear stress acting on the surface, bed erosion can occur as one of four distinctive modes and due to their corresponding physical processes:

Table B.7: Erosion of Mud Fractions, Winterwerp (2012)

Erosion Mode	**Physical Process**
Entrainment	Turbulent Mixing
Floc Erosion	Floc Rupture
Surface Erosion	Drained Failure
Mass Erosion	Undrained Failure

B.4.10 Partheniades-Krone formulation (Partheniades, 1965)

As demonstrated before, cohesive forces introduce a different behavior of the mud fractions. Hence, we cannot apply the van Rijn formulation for non-cohesive sediments (sand fractions). Instead, Delft3D makes use of the transport formula of Partheniades-Krone. Their solution to cohesive transport comprises critical bed shear stresses for both sedimentation and erosion. This way, a threshold is created that prevents immediate erosion or deposition of a particle [22].
The formula is activated, if

- the critical shear stress for erosion is exceeded by the bed shear stress (erosion) or
- if the critical shear stress for deposition exceeds the bed shear stress (deposition)

$$E^{(l)} = m^{(l)} S\left(\tau_{cw}, \tau_{cr,e}^{(l)}\right) \tag{B.27}$$

$$D^{(l)} = w_s^{(l)} c_b^{(l)} S\left(\tau_{cw}, \tau_{cr,d}^{(l)}\right) \tag{B.28}$$

$$c_b^{(l)} = c^{(l)}\left(z = \frac{\Delta z_b}{2}, t\right) \tag{B.29}$$

where
$E^{(l)}$: Erosion flux $[kgm^{-2}s^{-1}]$
$M^{(l)}$: User-defined erosion parameter EROUNI $[kgm^{-2}s^{-1}]$
$S\left(\tau_{cw}, \tau_{cr,e}^{(l)}\right)$: Erosion step function

$$S\left(\tau_{cw}, \tau_{cr,e}^{(l)}\right) = \begin{cases} \left(\frac{\tau_{cw}}{\tau_{cr,e}^{(l)}} - 1\right), & \text{if } \tau_{cw} < \tau_{cr,e}^{(l)}. \\ 0, & \text{if } \tau_{cw} \geq \tau_{cr,e}^{(l)}. \end{cases} \tag{B.30}$$

$D^{(l)}$: Deposition flux $[kgm^{-2}s^{-1}]$
$s_s^{(l)}$: Fall velocity (hindered) $[m/s]$
$c_b^{(l)}$: Average sediment concentration in the near bottom computational layer

$S\left(\tau_{cw}, \tau_{cr,d}^{(l)}\right)$: Deposition step function

$$S\left(\tau_{cw}, \tau_{cr,d}^{(l)}\right) = \begin{cases} \left(1 - \frac{\tau_{cw}}{\tau_{cr,d}^{(l)}}\right), & \text{if } \tau_{cw} < \tau_{cr,d}^{(l)}. \\ 0, & \text{if } \tau_{cw} \geq \tau_{cr,d}^{(l)}. \end{cases} \tag{B.31}$$

τ_{cw}: Maximum bed shear stress due to current and waves
$\tau_{cr,e}^{(l)}$: user-defined critical erosion shear stress TCEUNI N/m^2
$\tau_{cr,d}^{(l)}$: user-defined critical deposition shear stress TCDUNI N/m^2

Superscript (l) implies that this quantity applies to sediment fraction (l).
The calculated erosion or deposition flux is applied to the near bottom computational cell by setting the appropriate sink and source terms for that cell. Advection, particle settling, and diffusion through the bottom of the near bottom computational cell are all set to zero to prevent double counting these fluxes.

B.5 Important Aspects for River Diversions

B.5.1 Sediment Concentration Profile - Rouse Distribution

Vertical sediment concentration profiles commonly follow the Rouse distribution:
We can assume that - except for a constant settling velocity - the sediment particles act like passive tracers. This way, we can rewrite the (stationary) transport equation

$$w_s \bar{c} + D_{zz} \frac{\delta \bar{c}}{\delta z} = 0 \tag{B.32}$$

using the Reynolds analogy and replace eddy diffusivity by a parabolic vertical turbulent viscosity.

$$D_{zz} \approx \nu_t = \kappa u_* z \left(1 - \frac{z}{h}\right) \tag{B.33}$$

Integration of the stationary transport equation gives the Rouse distribution for vertical sediment concentration:

$$\bar{c} = c_0 * \left(\frac{h - z}{z}\right)^{\frac{w_s}{\kappa u_*}} \tag{B.34}$$

where $\frac{w_s}{\kappa u_*}$ is the Rouse parameter showing the relation between settling velocity and vertical mixing due to turbulence.

B.5.2 Asymmetrical Approach Conditions

In case of asymmetrical approach conditions, the effect of secondary flows might have a significant impact on water and sediment distribution. Water flowing through a bend is subject to centrifugal forces. This requires a transverse water-level slope which finally results in a secondary circulation as shown in figure B.8. The secondary flow also affects the transverse bed level and the bed composition. Segregation of sediment leads to a

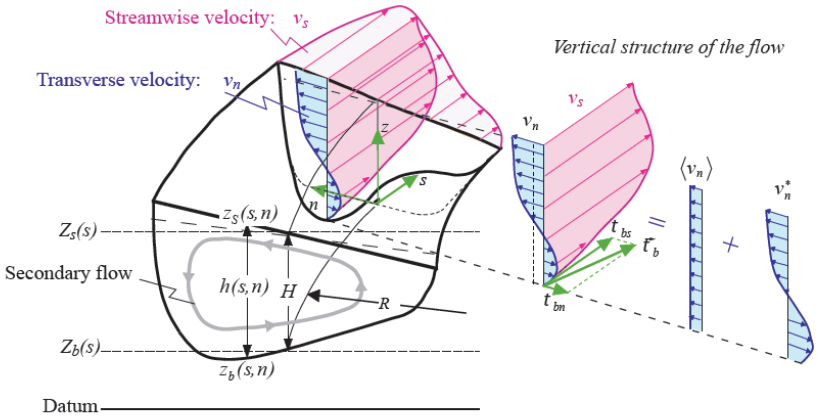

Figure B.8: Flow Through a Bend. From Lecture Flow in River Bends 2011, Bram van Prooijen , Courtesy of Blanckaert.

coarsening towards the outer bend and the outer bend is deepening until an equilibrium is reached between secondary flow and transverse bed level slope.
Diversions at inner bend might suffer enhanced deposition at the entrance due to helical flow. However, in case of sediment diversions, this might even be intended.

B.5.3 Flow resistance - Distance to the sea

The distribution of water and sediment do not only depend on local flow patterns but also on the downstream characteristics of the distributaries. For example, backwater curves or different flow resistance has an impact on the diversion.

B.5.4 Bulle Effect

The Bulle effect can be described as a curvature-induced spiral flow that develops due to the geometry of the offtaking branch. The flow at the bottom has lower velocities and hence can easily be diverted whereas the surface flow is faster and tends to remain in the main channel. From the Rouse profile we find that most of the sediment is transported near the bottom and, indeed, Rouse (1926) found that relatively more sediment enters the diversion. The strength of this effect still depends on the discharge relation, the width-

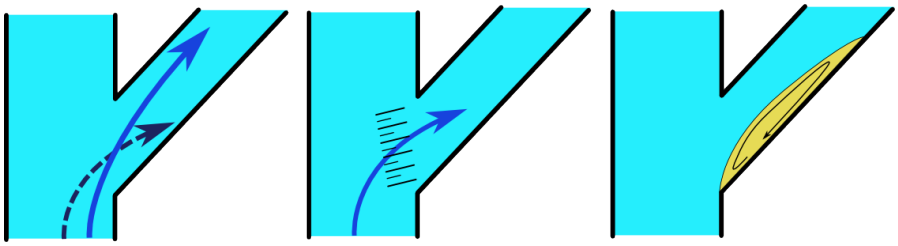

Figure B.9: Hydraulic Effects at a Diversion Site. Left: Bulle effect. Middle: Gravity pull. Right: Flow Separation. Adapted from Melman (2012) [45]

to-depth ratio of the diversion and the local geometry and angle at the bifurcation. Due to the Bulle effect deposition occurs at the outer bank of the diversion [45].

B.5.5 Gravity Pull along Bed Slopes

Transverse bed slopes that were, for example, created by helical flow lead to an attraction of sediment. In particular, bed load transport is affected. Depending on the orientation of the secondary flow and hence on the bed slope more sediment is conveyed to the main channel or the diversion [45].

B.5.6 Flow Separations

In numerical simulations, Heer & Mosselman (2004) found that the roundness of the upstream wall angle is important for the flow field and that it is difficult to set up a grid that reproduces the observed pattern and also meets the requirements of orthogonality and smoothness. This way, numerical errors or unwanted flow detachment might occur and limit the validity of the model [34].
However, this effect also occurs in reality for sharp transitions between main channel and diversion. The resulting eddy reaches from the detachment point at the bifurcation to a reattachment point somewhere downstream of the diversion and - due to gradient transport mechanisms - is supplied with sediment from the diverting flow. Inside the eddy structure, the sediment is accumulated in the center and deposits. This may influence the cross-sectional area and hence the discharge distribution [45].

C | Model Validation and Further Analysis

C.1 Mud Parameters

- **Critical shear stress for erosion, $\tau_{crit,ero}$**

  After an initial analysis of the effects of critical shear stresses, it was decided to stick to the settings for the critical shear stress for erosion, which is $\tau_{crit,ero} = 1\ N/m^2$ outside the region of salt water influence. This limited the erosion of mud in the upper reach from Reserve (rkm 223) to New Orleans (rkm 165) and thus led to a stable bed without obstructing erosional processes too much along the rest of the domain. In the region of salt water influence, the critical shear stress for erosion was set to $\tau_{crit,ero} = 1000\ N/m^2$, which leads to a fixation of settled mud fractions in the corresponding regions and during the presence of the salt wedge (discharge-dependent area of influence).

  The above described settings led to a reasonable behavior and allowed for choosing settling velocities and critical shear stress for deposition to be the governing parameters of the calibration procedure.

- **Critical shear stress for deposition, $\tau_{crit,dep}$**

  The critical shear stress for deposition was chosen to be quite small and constant over the entire domain during the calibration of the suspended sand transport.

  This led to erosion upstream of Belle Chasse, low dredging volumes and, consequently, high outflow concentrations at, e.g. Southwest Pass.

  In order to get realistic bed level changes and dredging volumes, especially in the

region of salt water influence, this parameter had to be tuned, as well.
Several simulations were run to evaluate the effect of different settings. It was decided to try constant as well as linearly increasing values from Reserve to the tip of the salt wedge. Also from the tip of the salt wedge down to East Jetty, the critical shear stress for deposition was chosen to be linearly increasing to mimic flocculation and enhance deposition.

- **Settling velocities, $w_{s,silt}$ and $w_{s,clay}$**
  The two mud fractions silt an clay were initially set up with the settling velocities following the estimate from van Rijn 1993 (Delft3D Manual, 11.3.1 [22]). This also contributed to low deposition. During calibration it turned out that the settling velocities had to be increased significantly to achieve realistic deposition. The reason for that is that the critical shear stresses only act as thresholds and deposition becomes insensitive for high critical shear stresses. The only parameter left that influences settling is the settling velocity.
  The increase of settling velocity can aso be justified from a physical point of view: The flocculation process leads to particle sizes much larger than a single mud particle. As shown in the Annex (B.4.9, p. 137), these particles can even have settling velocities similar to sand fractions. Unfortunately, spatially varying settling velocities are only feasible for simulations including salinity. As the two-dimensional modeling of a salt wedge in a weakly forced estuarine environment turned out to produce unrealistic results, this is no option.
  Instead, it was decided to use higher values for the entire domain. Of course, this might lead to inaccuricies, but the negative effects are mitigated: Usually, there is less deposition of mud in the upper reach, whose bed is dominated by sand and that is not affected by the influence of salinity.
  In the lower reach, where salinity is present, the settling can now be tuned more effectively by means of the critical shear stresses used as calibration parameters.
  The settling velocities were chosen to be: $w_{s,silt} = 10^{-3}\ m/s$ for silt and $w_{s,clay} = 10^{-4}\ m/s$ or, alternatively, $w_{s,silt} = w_{s,clay} = 10^{-3}\ m/s$, which effectively represents a single mud fraction. Following the US Interagency Committee on Water Resources, $10^{-3}\ m/s$ can be found for medium to coarse silt fractions [81]. In this model, the settling velocity also has to account for enhanced settling due to flocculation which justifies the increase to $10^{-3}\ m/s$ also of smaller fractions.

C.2 Model Validation

C.2.1 Hydraulic Validation

Only little data is available to validate the hydraulic model. In the year 2011, Allison [6] made ADCP measurements around Bonnet Carrè Spillway, which is situated near the upstream boundary of the model domain.
Four different measurements at three locations where chosen, because they were taken during high to medium flow and, this way, could be compared to velocities during the periods of constant discharge with $Q_{nom} = 28,000\ m^3/s$ and $Q_{nom} = 24,000\ m^3/s$.

Conclusion:
Taking into account the deviations and uncertainties in discharge and the simplifications that a two-dimensional model implies, reasonable results were obtained for the depth-averaged transversal velocities.

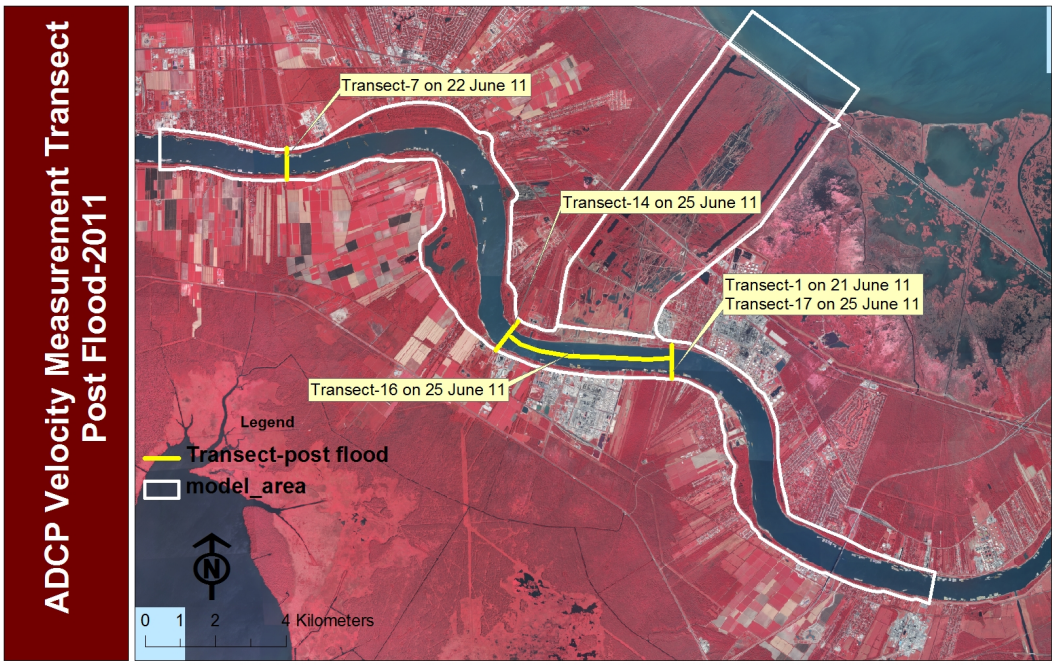

Figure C.1: Locations of Transects. ADCP Measurements by Allison in 2011.

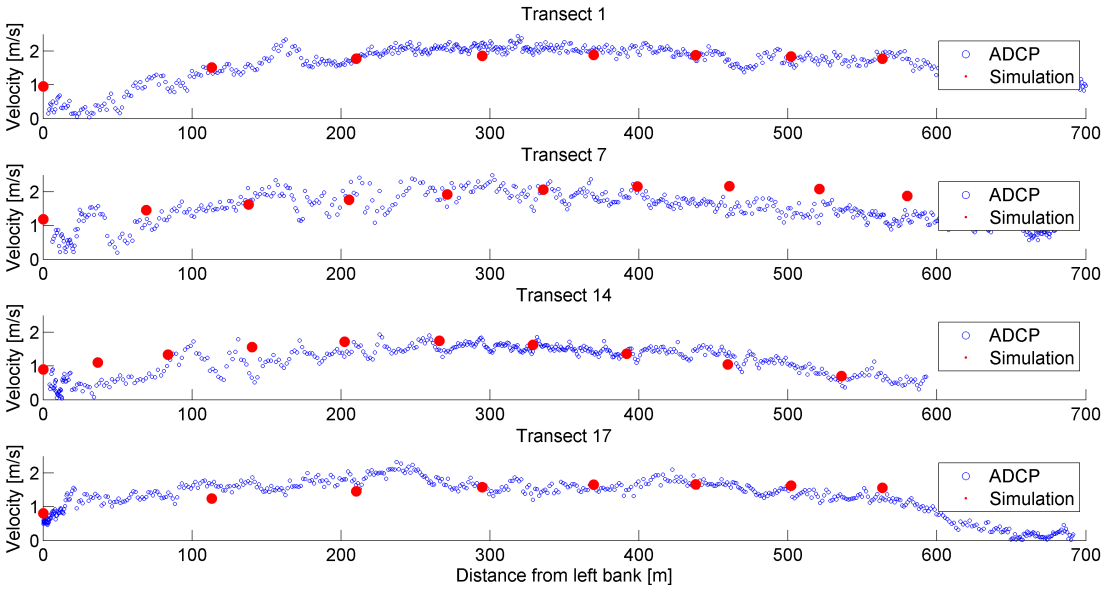

Figure C.2: Results of Hydraulic Validation. ADCP Measurements by Allison in 2011.

C.2.2 Validation of Sand Transport

The sand transport through a cross-sectional area at Myrtle Grove (rkm 95) can be compared to measurements carried out in April and May 2011 by Allison [1].

Table C.1: Myrtle Grove Suspended Sediment Comparison.

			Q_w $[m^3/s]$		Q_{sand} $[tons/day]$			Q_{mud} $[tons/day]$			Total Load $[tons/day]$		
No.	Location	Date	meas.	sim	meas.	sim	dev. [%]	meas.	sim	dev. [%]	meas.	sim	dev. [%]
10	MGup	10.10.2008	11910	11500	1006	1130	**12**	111410	194840	**75**	112416	195970	**74**
9	MGbend	06.05.2009	20728	21500	37985	25044	**-34**	175711	264730	**51**	213696	289774	**36**
13	MGbend	09.04.2009	19312	21500	71335	25044	**-65**	224535	264730	**18**	295870	289774	**-2**
6	MGdown	06.05.2009	20530	21500	29444	22722	**-23**	165601	275710	**66**	195045	298432	**53**
17	MGdown	05.04.2009	19142	21500	81592	22722	**-72**	275776	275710	**0**	357368	298432	**-16**
5	MGup	15.04.2010	22484	21500	44977	42851	**-5**	168271	259230	**54**	213248	302081	**42**
7	MGup	04.05.2009	20105	21000	26824	42851	**60**	167648	259230	**55**	194472	302081	**55**
14	MGup	07.04.2009	20162	21500	97118	42851	**-56**	259344	259230	**0**	356462	302081	**-15**
15	MGup	15.05.2010	20416	21500	49531	42851	**-13**	274062	259230	**-5**	323593	302081	**-7**
20	MGup	11.05.2010	18604	21500	49502	42851	**-13**	500229	259230	**-48**	549731	302081	**-45**
2a	MGup	31.03.2011	28260	26300	190874	126650	**-34**	102955	288470	**180**	293829	415120	**41**
11a	MGup	14.05.2011	34830	26300	155541	126650	**-19**	343099	288470	**-16**	498640	415120	**-17**
2b	MGup	31.03.2011	28260	31800	190874	263900	**38**	102955	298880	**190**	293829	562780	**92**
11b	MGup	14.05.2011	34830	31800	155541	263900	**70**	343099	298880	**-13**	498640	562780	**13**

Figure C.3: Myrtle Grove Suspended Sediment Comparison. The figure shows measured and simulated discharges, total suspended loads, sand load in suspension and mud transport for the area around Myrtle Grove, rkm 93 to 99.

C.3 Sensitivity Analysis

Various aspects were considered in order to evaluate the sensitivity of the numerical model:

- Simulation without Impact of Salt Wedge (constant $\tau_{crit,\ dep}$)
- Reduced Fall Velocity of Mud Fraction
- Tidal Signal at East Jetty
- Upstream Neumann Boundary for Sediment
- Simulation of Dunes
- Dredging Parameters and Strategies
- Multiple Sand Fractions & Spatially Varying Median Grain Size
- Sediment Transport Equations
- Bed Layer Model
- Analysis of Filling of Deep Pits
- Analysis of Discharge Variability

C.3.1 Simulation Without Impact of Salt Wedge

The salt wedge is modeled by a spatially varying, discharge-dependent critical shear stress for deposition. This leads to increased settling in areas with high values of $\tau_{crit,dep} = 1000\ N/m^2$ making sure that this term is not getting involved. With a constant critical shear stress for deposition of $\tau_{crit,dep} = 1000\ N/m^2$ over the entire model domain (as imposed by Bos (2011) [12] in a smaller model) we end up with more deposition upstream of Venice but also with too little deposition below Venice.
This way, the dredging volumes for Southwest Pass and Head of Passes are reduced to less than 20%. It can be concluded that we cannot model the estuarine environment with an intruding salt wedge without spatially varying critical values for deposition as intended. (sim 42)

C.3.2 Reduced Fall Velocity of Mud Fraction

The usage of a locally higher critical shear stresses for deposition leads to increased settling. However, flocculation of mud particles is not included. Especially the very small clay particles are still treated as single grains with a very low fall velocites. This way, too much suspended sediment does not settle within the model.
The effect of flocculation leads to large structures with fall velocities comparable to those of the imposed sand fraction (1 to 2.5 cm/s). Unfortunately, it is not possible to determine a spatially varying fall velocity of grains without modeling salinity. As shown before, two-dimensional modeling of salinity would not lead to acceptable results.
A way to deal with the limitations of the model is to impose an overall increased fall velocity for at least the clay fraction.
When the settling velocities of silt and clay are equal, we get a realistic amount of deposition downstream of Venice. Because the fall velocity is still relatively small with $w_s = 0.1 cm/s$ and there is no increased critical shear stress for deposition in the upstream part of the model, the morphological effect is small.
Conclusion: The combination of increased critical shear stress for deposition and fall velocity gives reasonable results for the estuarine environment of the Mississippi River in a two-dimensional model.
(sim 24 compared to sim 29: Upstream dredging volumes are identical, whereas Southwest Pass - Head of Passes increases by 50%!)

C.3.3 Tidal Signal at East Jetty

Similar to the three-dimensional salinity model, we can also apply a tidal boundary at Southwest Pass with a sinusoidal amplitude of 30 cm. However, a ten-year simulation revealed that the morphological impact of such a measure is negligible. Although there is a flow reversion in the birdfoot delta, other modeled processes seem to have a dominating effect, especially the modeling of the salt wedge. From this simulation it was concluded to keep constant downstream water levels for the two-dimensional morphological model. (sim 31)

C.3.4 Upstream Neumann Boundary for Sediment

Delft 3D offers the possibility to define upstream Neumann boundaries for mud and sand fractions. This implies that the amount of introduced material corresponds to the local equilibrium concentration. This option is especially recommendable to avoid extreme bed level changes near the upstream boundary.

First, only the mud fractions will be affected. As the imposed mud concentrations were derived from suspended sediment samples with a relatively high uncertainty (factor 2-4), a model was tested with a Neumann boundary at Reserve (rkm 223). Comparison of sediment transport rates led to the conclusion that there is a negligible difference. This also indicates that the concentrations from literature fairly well agree with the calibrated hydraulic model. (Compare sim 22 to sim 2)
As already shown for the mud fractions, it is also possible to introduce an equilibrium concentration at the upstream boundary for sand fractions. A comparison of simulations with imposed concentrations from literature and equilibrium concentration led to slight differences that can be neglected. (Compare sim 25 to sim 2)

C.3.5 Simulation of Dunes

Dunes influence the amount of dredging as they create higher bed level elevations. In Delft3D, bed forms and their effect can be considered by including simulated dune heights in volume computations of dredging activities.
As the dune height is not a uniform value the effective bed level can be increased by only a fraction of the dune height. In the model, the default is chosen with 0.5 (Keyword AlphaDuneHeight=0.5) [22].
After dredging has been carried out, the dunes will be removed by setting their height to zero (Keyword UseDunes = true) [22].
No interaction of tide and dunes were observed (Compare sim 34 to sim 35). Dunes lead to an increase in dredging volume at Southwest Pass - Head of Passes by 30% (Compare sim 32 to sim 34).

C.3.6 Dredging Parameters and Strategies

There is a number of options when dredging the Lower Mississippi River. The dredging polygon does not follow the grid, so we have to determine which cells have to be included and which not. The keyword is "Inpolygon". Here we can define, whether a cell has to be completely inside the polygon or if the cell center or even a corner is sufficient to be considered as part of the polygon.
We want to check the difference between the standard option, Inpolygon=2 for cell centers and Inpolygon=3 for cell corners. The sensitivity mainly depends on the grid size and the differences in depth of adjacent cells.
For the maximum dredging area (Inpolygon=3), the dredging volume increases by 25%. (Compare sim 17 to sim 2)

Another aspect is the dredging schedule. With the default values, the model continuously removes material above the specified dredge depth (plus clearance) during all discharge periods. However, when we limit dredging activities to discharges smaller or equal to $Q = 20,000 m3/s$ the dredging volumes stay almost unchanged (The dredging at New Orleans Harbor drops from 7.0E+05 to 4.0E+05). (Compare sim 21 to sim 2) We therefore continue with continuous dredging.

C.3.7 Multiple Sand Fractions & Spatially Varying Median Grain Size

In the first models, we only used a single sand fraction. Splitting up this fractions into two fractions with different median grain size diameters allows for a variation of the median grain diameter of sand along the domain.
Unfortunately, since we use cohesive fractions, hiding and exposure mechanisms cannot be modeled with Delft3D. Normally, this is another common reason to apply multiple sand fractions.
The effect of two sand fractions showed to be negligible in the downstream areas, where mud dominates. In the upstream region with higher sand concentrations, however, dredging volumes dropped to about 30%. (Compare sim 23 to sim 17)

C.3.8 Sediment Transport Equations

In this work we intend to use the formulation of van Rijn 1984 (see section B.4.1 on p. 129). However, it is always wise to check the performance of other transport formulae. Here, we chose the approach of Engelund-Hansen and van Rijn 1993 and 2004. The corresponding equation can be found in the Delft3D Manual [22]. Results:

- Engelund-Hansen: The sand is completely modeled as bed load. The transport through the cross-sections reveals a strong accretion upstream of West Point a la Hache. At Venice, the original model showed 15% sand fractions, whereas Engelund-Hansen leads to less than 2%. Clearly, this drastic decrease of sand is not representative. We can conclude that Engelund-Hansen does not lead to satisfying results without additional calibration. However, the bed levels upstream seem to be more realistic as they show less erosion. In general, the formula could be acceptable, if there was less settling of sand. However, the Engelund-Hansen formula only considers total loads and highly influences dredging volumes upstream. (Compare sim 40 EH to sim 40)
- Van Rijn 1993: Similar to Engelund-Hansen, sand only plays a role upstream of West Point a la Hache
- Van Rijn 2004: Similar to Engelund-Hansen, sand only plays a role upstream of West Point a la Hache. The dredging volumes are comparable to those from sim 40.

C.3.9 Bed Layer Model

In case of graded sediment and caused by the differences in mass, grain size and shape, sorting processes take place. However, the morphological model only considers grain size in general as the other parameters are not available. Sediment sorting processes do not only take place along the thalweg but also on a smaller scale due to local flow patterns. In the model, the initiation of motion of a grain depends on its diameter. If the critical shear stress acting on the grain is exceeded and there is no additional resistance by

other grains (hiding and exposure mechanisms), it is displaced. Especially in bends, a transverse sediment sorting process can be observed. When modeling several sediment fractions in a single bed layer in Delft3D, problems may arise as the bed composition "competes" with changes in bed level to eliminate transport gradients (pers. comm. Kees Sloff, 20.07.2013). In first simulations with a single layer high deposition was observed in the outer bends while the inner bends incised. From this, it was concluded that the transverse sorting processes induced by the transverse velocity gradient dominated. In order to avoid this strong effect, a bed layer model with multiple sediment layers was introduced.

During morphological calibration it showed that different settings regarding number and thickness of bed layers strongly influence local bed levels. Below, three simulations with different settings are compared. (sim 11c, b & d).

Table C.2: Settings for multiple bed layer model

Transport layer thickness [m]	No. underlayers	Underlayer thickness [m]
5.0	2	2.50
1.0	2	0.50
0.4	2	0.20

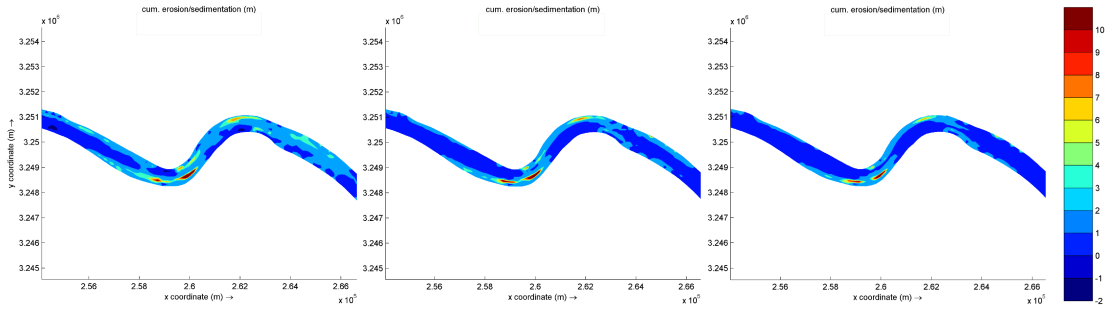

Figure C.4: Multiple Layers. Simulation results.

Conclusion: Thinner transport layers lead to reduced sedimention and erosion due to transverse sorting processes.

Tests with a high resolution of bed layers did not show a large deviation, so that the above setting appears to be reasonable. Simulation were carried out with 50 underlayers and a small value for the top layer thickness (0.2m). The dredging volumes stayed almost identical compared to a bed layer model with only 4 underlayers and a top layer thickness of 0.2 m. (Compare sim 22 to sim 11)

C.3.10 Analysis of Filling of Deep Pits

During the morphological calibration, fast filling of initially deep pits in river bends was observed. This was reduced by introducing the bed layer model and higher suspended loads.
However, there was still a trend for deposition within these areas. This phenomenon can be explained by the fact that the model cannot consider and resolve all processes that may play a relevant role. First of all, the bed composition is rather simple, whereas in reality a large stratigraphic inhomogeneity of old and new river beds consisting of erodible and non-erodible material exists due to meandering of the Mississippi River. Moreover, the turbulent processes in deep pits are three-dimensional, especially when steep slopes to the adjacent areas are found (pers. comm. Sloff 11.09.2013).
In order to artificially increase the local shear stress, a higher Manning value of 0.04 was applied in areas deeper than 35m NAVD. The result after almost one year can be seen below.

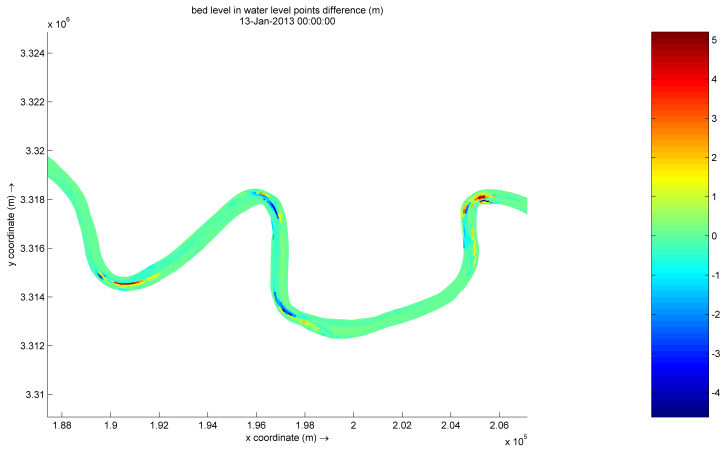

Figure C.5: Dredging Volumes. Result of Simulation 40.

Although the increase in roughness has quite some impact with up to 5 meters of bed level difference, the approach was discarded because it also led to the same amount of accretion and there was no clear reaction. Moreover, changing the roughness also influences the water level and the flow field (higher water level with lower velocities). This might have counteracted the increase in local shear stress.

C.3.11 Analysis of Discharge Variability

Single floodyears of the Mississippi River show a variability that might lead to morphological deviations compared to the "average" 2009 flodyear that normally is repeated in the quasi-steady simulation. At first sight, this seems to be contradictory to the fact, that an average floodyear is used whose sand transport has been calibrated and validated for low, medium and high discharges. Nevertheless, due to the non-linear relation between flow velocity and sediment transport, floodyears with a pronounced flood peak might have had a significantly higher impact on bed level changes in that particular reach of the Lower Mississippi River.

Table C.1 on p. 149 clearly shows this non-linear trend. For low flows ($Q_{eff} = 11,500 m^3/s$), sand transport is only around $1,000$ $tons/day$. For medium discharges ($Q_{eff} = 21,500$ m^3/s) we already find around $40,000$ $tons/day$. For the two highest discharges, ($Q_{eff} = 26,300$ m^3/s) and ($Q_{eff} = 31,800$ m^3/s), the flow deviates by 20% while the sediment transport difference is over 200% (from $127,000$ to $264,000$ $tons/day$).

Consequently, the deviation in bed level change can be interpreted as missing variability of different floodyears. When looking at discharge data, this variability becomes obvious. Although the floodyear 2009 can also be interpreted as an average year in terms of both water discharge and sediment transport for the 2003/4 to 2012/13 period, there has been a continuous variation of years with low discharges (2007, 2012) and floodyears including pronounced flood peaks (2008, 2010, 2011).

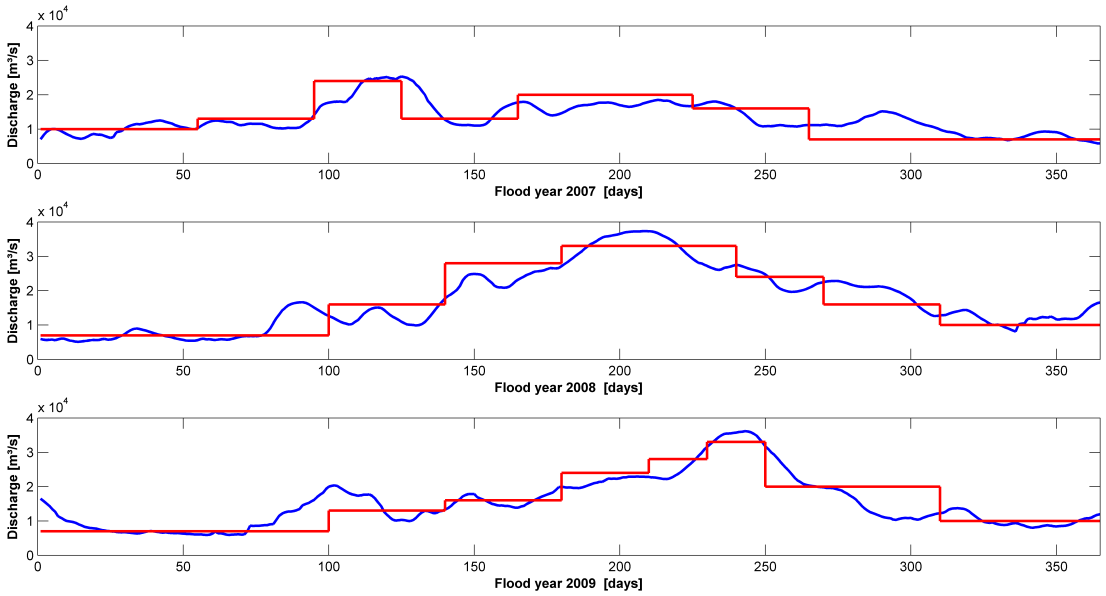

Figure C.6: Three Floodyears. The figure shows the hydrographs of the floodyears 2007 to 2009. The discretization of the years 2007 and 2008 uses the same settings for discharge, simulation period and morphogical acceleration factor as the already applied 2009 discretized floodyear. Source hydrographs: Rating curves 2004-2013, Allison(2013) [2].

A comparison of two simulations is made: sim 157 with a repeating single discretized floodyear 2009 and sim 173 with three repeating discretized floodyears 2007 to 2009 as shown in figure C.6.

Bed Level Change:

From the bed level changes over a period of ten years we only see small deviations.

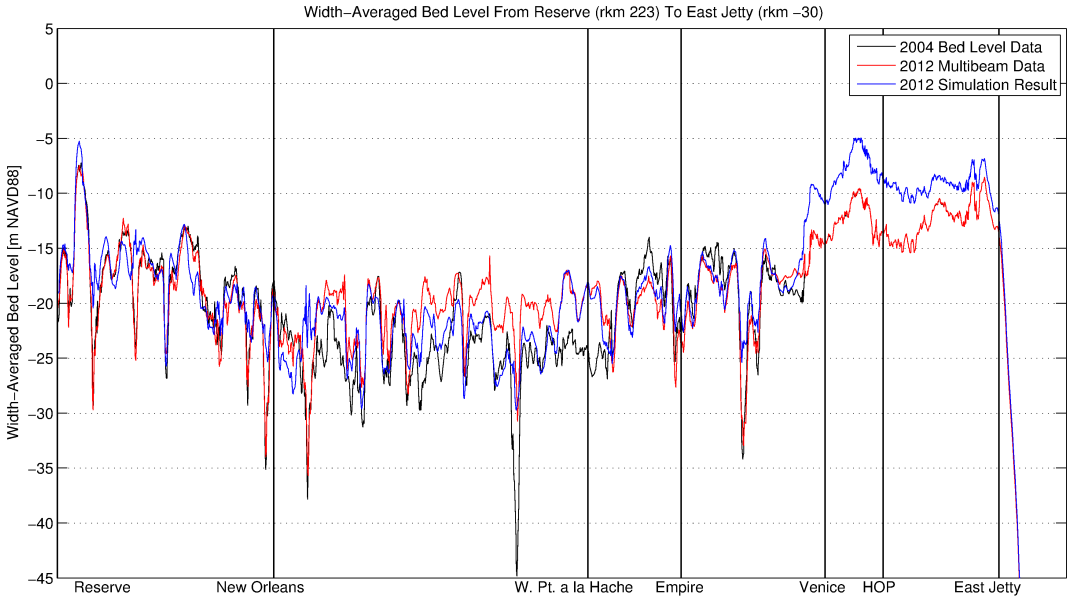

Figure C.7: Bed Level Change in 10 Years with Single Floodyear.

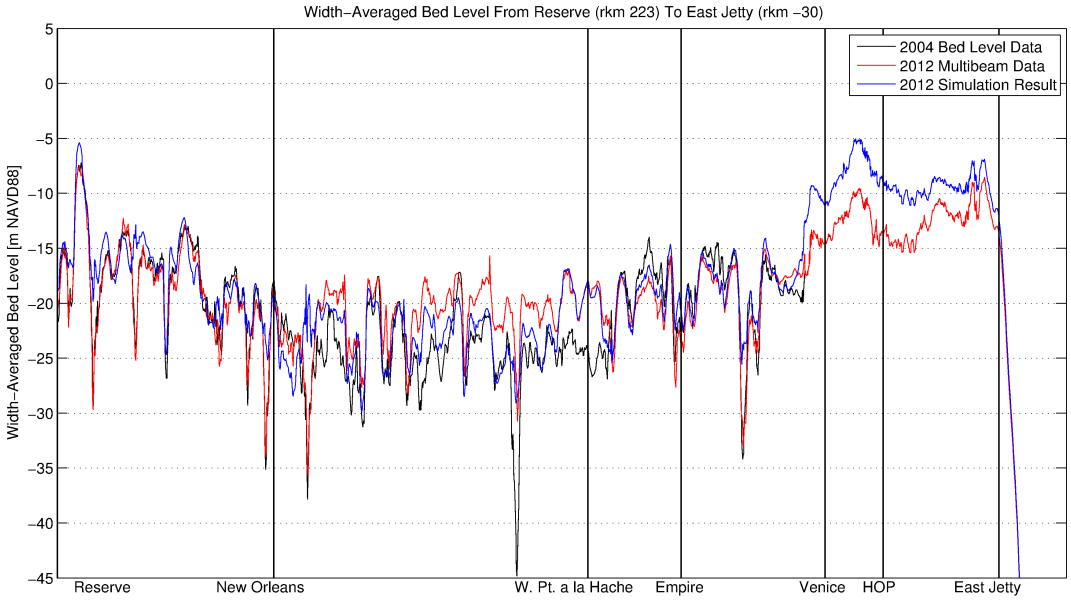

Figure C.8: Bed Level Change in 10 Years with Three Floodyears.

When looking at the output data, sim 157 had 14.2 million tons per year of deposition from Reserve to Venice. The deposition for sim 173 is slightly stronger and comes close to the total annual deposition rate 16.4 compared to 17.5 million tons per year. However, the correlation between measurements and simulation reveals that sim 157 better corresponds to the field data.

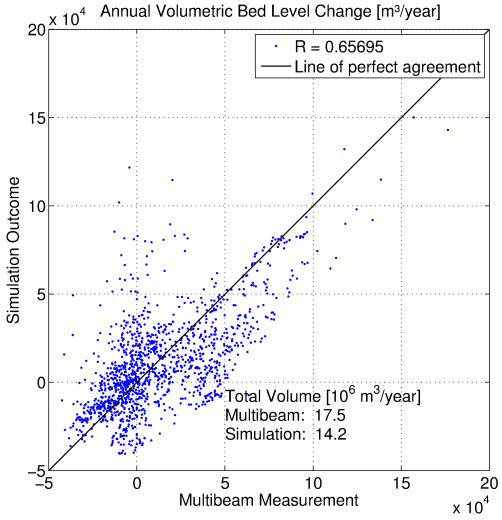

Figure C.9: Bed Level Change in 10 Years with Single Floodyear.

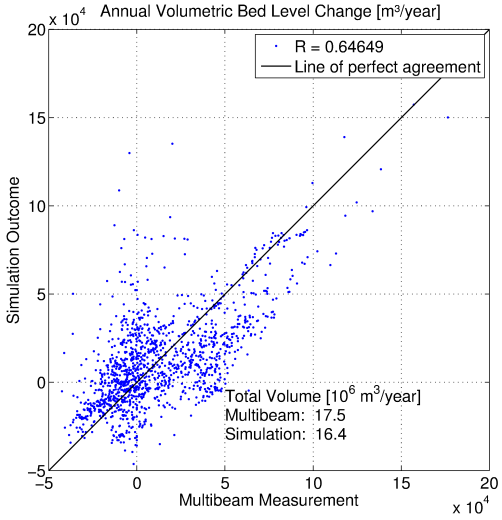

Figure C.10: Bed Level Change in 10 Years with Three Floodyears.

Sediment Transport:

The 10-year average sediment transport through cross-sections along the domain shows that (1) the upper reach from Reserve to New Orleans is relatively stable, (2) the deposition downstream of New Orleans is mainly caused by sand fractions as they show the strongest decrease, (3) deposition of mud from West Point a la Hache to East Jetty becomes stronger due to simulated salt wedge effects. The simulation with three floodyears shows a slightly lower sand transport at New Orleans which indicates that the upper reach from Reserve to New Orleans is depositing somewhat more.

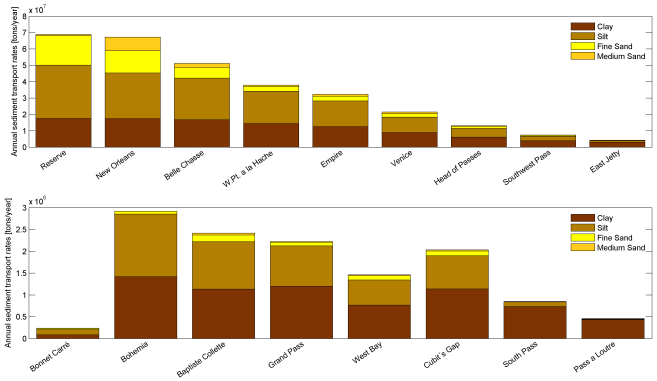

Figure C.11: 10-Year Average Sediment Transport Rates Through Cross-Section along Domain for Single Floodyear.

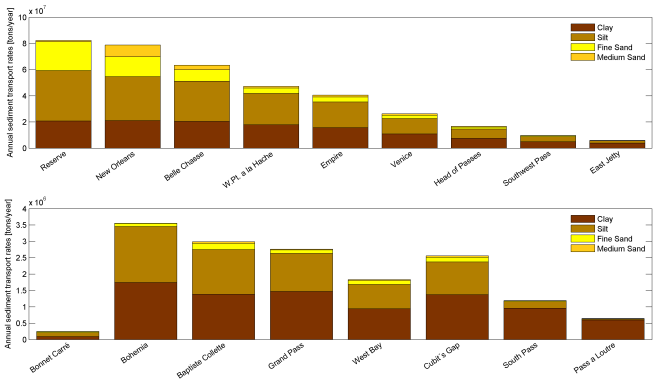

Figure C.12: 10-Year Average Sediment Transport Rates Through Cross-Section along Domain for Three Floodyears.

Dredging Volumes:

The different years lead to a larger variability in dredging volumes. However, there is no significant deviation. In the last year, the dredging volumes are almost equal.

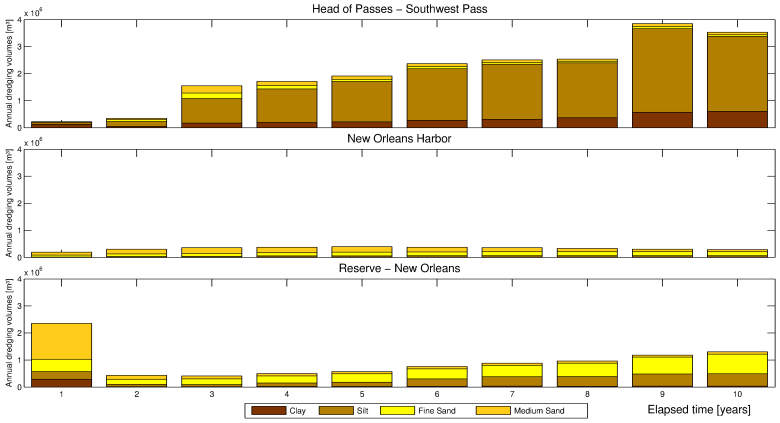

Figure C.13: Dredging Volumes for Simulation with Single Floodyear.

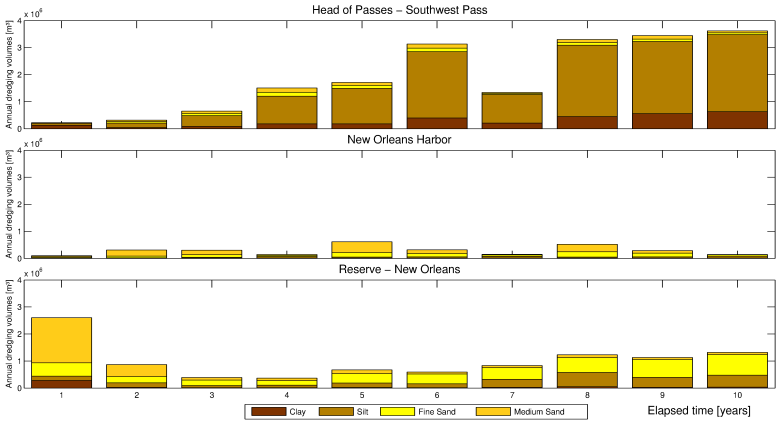

Figure C.14: Dredging Volumes for Simulation with Three Floodyears.

Conclusion:

Simulations with three discretized floodyears to consider annual variability only show minor deviations from simulations with a single floodyear. Increasing the number of floodyears leads to a strong increase in model complexity. Hence, we continue with the standard setup of a single discretized floodyear 2009.

C.4 Analysis of Analytical Diversion Efficiency

In the analytical model for the morphological equilibrium that was used before, the sand load in the channel always corresponds to the sediment transport capacity. Due to the non-linear relation of water and sediment transport, we find a diversion efficiency of 1.4 in the analytical model.
Depending on cross-sectional geometry, diversion angle and operation mode, diversion efficiencies of sand fractions vary between 1 and 1.8 in the numerical simulation. In general, the total efficiency is lower with values from 1 to 1.3.
The United States Army Corps of Engineers requires a diversion efficiency of at least 1.8 to avoid negative side effects on the main channel (pers. comm. Ehab Meselhe, 04.11.2013)
We can also evaluate the effect of varying diversion efficiencies of the analytical model. The range was chosen to be from 0.8 to 2.1 which represents inefficient extraction and an almost total extraction of sediment, respectively. Based on the results, we can answer the following questions:

- What are the effects of varying diversion efficiencies?
- How are time scales influenced by varying diversion efficiencies?
- What is the necessary efficiency to ensure sufficient navigational depth?

What are the effects of varying diversion efficiencies?
Contrary to the analytical models that consider equilibrium transport in the main channel (in this case: diversion efficiency 1.4), changing the efficiency leads to changes in downstream bed slope. For efficiencies smaller than 1.4, we find increasing bed slopes downstream, whereas the bed slope decreases for efficiencies larger than 1.4. When looking at equation 5.2, we find that changes in water and sediment extraction do not balance each other any more: High diversion of sediment leads to smaller sediment discharge and, consequently, bed slopes downstream and vice-versa.
The effect on the downstream water levels is inverse, see also equation 5.1: The higher the diversion efficiency the less sediment is transported downstream and, consequently, the deeper the river incises.

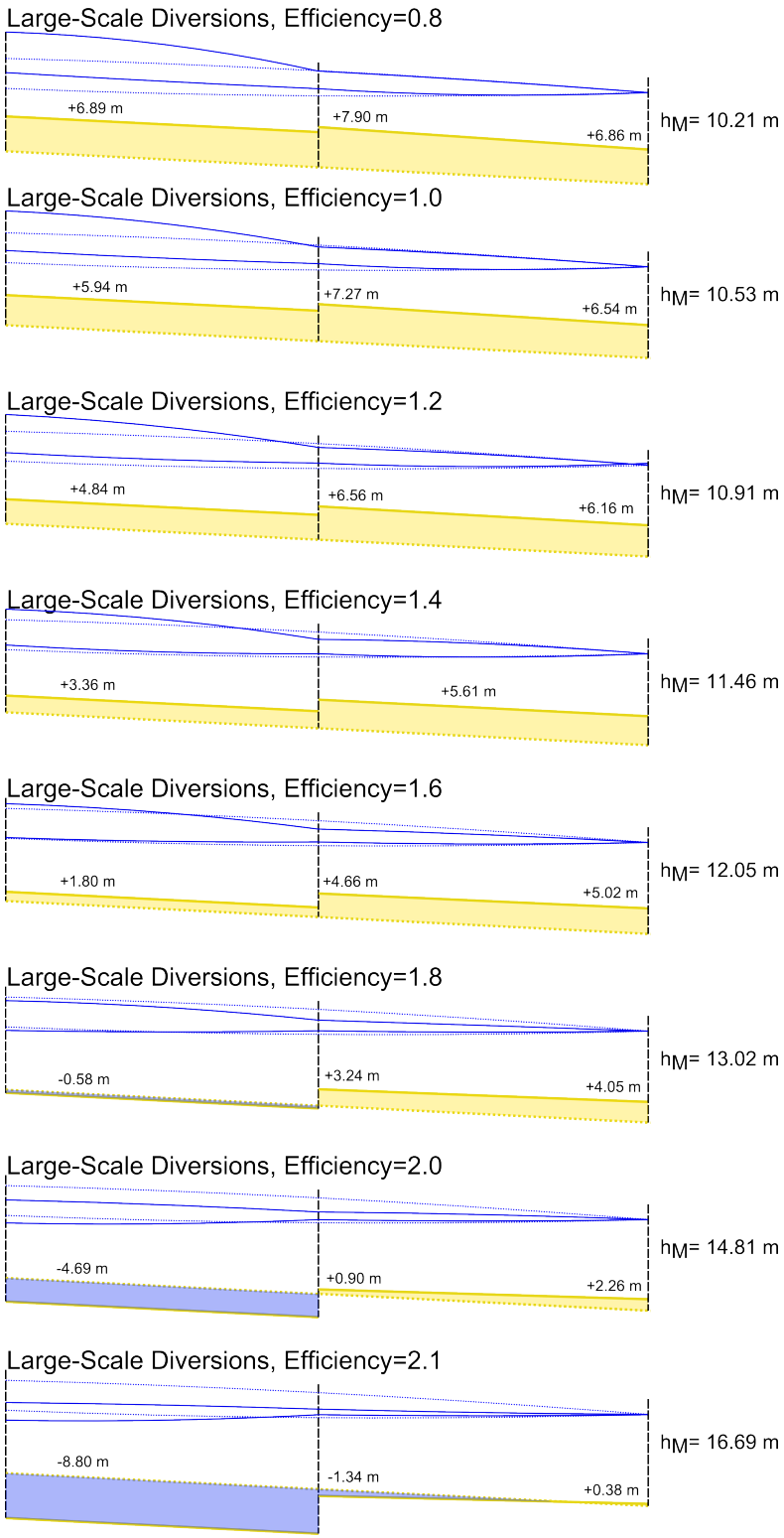

Figure C.15: Equilibrium Situations of Large-Scale Diversions for Different Diversion Efficiencies.

How are time scales influenced by varying diversion efficiencies?

A comparison of time scales for morphological changes downstream for varying diversion efficiencies was carried out. Besides the general decrease in equilibrium depth, higher diversion efficiencies show a positive effect in terms of smaller annual deposition rates as the time scales increase.

Table C.3: Time Scales for Varying Diversion Efficiencies

Diversion Efficiency	Downstream Time Scale [years]
0.8	29
1.0	31
1.2	33
1.4	36
1.6	40
1.8	47
2.0	61
2.1	77

What is the necessary efficiency to ensure sufficient navigational depth?

The analytical model with a diversion efficiency of 1.8 as recommended by USACE leads to the smallest changes in upstream direction. The upstream water depth nicely corresponds to the initial water depth with 12.22 m. This shows that the navigational circumstances are kept approximately constant upstream of the diversions.

By further increasing the efficiency, the downstream accretion can be counteracted and even inversed. However, efficiencies above 2 are highly unlikely for large-scale diversions as this would imply an almost complete extraction of the available sediment. Consequently, in order to achieve a similar morphological response, multiple diversions with lower total conveyance need higher diversion efficiencies.

Remark:

In general, we have to consider that especially mud fractions cannot be extracted with efficiencies much larger than 1 as they are well distributed over the entire water column and width. The effect of mud and enhanced settling is not included in the analytical model and might especially affect bed level changes downstream of the diversion sites.

References

[1] Allison, M.A. (2011). Water and Sediment Surveys of the Mississippi River Channel Conducted at Myrtle Grove and Magnolia in Support of Numerical Modeling (October 2008-May 2011) . *Report to the State of Louisiana Office of Coastal Protection and Restoration*. 38, 149

[2] Allison, M.A. (2013). Rating curves for the Lower Mississippi River from 2004 to 2013. *Not in press*. 159

[3] Allison, M.A. & Meselhe, E.A. (2010). The Use of Large and Sediment Diversions in the Lower Mississippi River (Louisiana) for Coastal Restoration. *Journal of Hydrology 387 (2010), pp. 346 -360*. 18, 19, 42

[4] Allison, M.A. & Vosburg, B. (2011). Stakeholder Meeting Presentation 27 July 2011 - A Summary of Field Data Collection at the Myrtle Grove Diversion Site in the Myrtle Grove Diversion Site in Support of Numerical Modeling. Online: (`http://www.lca.gov/Library/FileDownload.aspx?ProdType=2&id=3081`)., [Accessed 03-September-2013]. 46

[5] Allison, M.A., Dema, C.R., Ebersole, B.A., Kleiss, B.A., Little, C.D., Meselhe, E.A., Powell, N.J., Pratt, T.C. & Vosburg, B.M. (2012). A Water and Sediment Budget for the Lower Mississippi-Atchafalaya River in Flood Years 2008-2010: Implications for Sediment Discharge to the Oceans and Coastal Restoration in Louisiana. *Journal of Hydrology 432-433 (2012), pp. 84-97*. 1, 11, 12, 23, 61

[6] Allison, M.A., , Vosburg, B.M., T., R.M. & Meselhe, E.A. (2013). Mississippi River Channel Response to the Bonnet CarrÃľ Spillway Opening in the 2011

Flood and its Implications for the Design and Operation of River Diversions. *Journal of Hydrology 477 (2013), pp. 104-118*. 3, 29, 147

[7] Americas Wetland Resources (2013). Louisiana River Control. Online: (`http://www.americaswetlandresources.com/background_facts/detailedstory/LouisianaRiverControl.html`)., [Accessed 28-May-2013]. 107, 109

[8] Ayres, S. (2012). Atlas of U.S. Army Corps of Engineers Historic Daily Tide Data in Coastal Louisiana. *Final Report to the LCA Science & Technology Program, 22 pp.*. 67, 68, 103

[9] Bindoff, N.L., Willebrand, J., Artale, V., Cazenave, A., Gregory, J., Gulev, S., Hanawa, K., Le QuÃĽrÃĽ, C., Levitus, S., Nojiri, Y., Shum, C.K., Talley, L.D. & Unnikrishnan, A. (2007). Observations: Oceanic Climate Change and Sea Level Rise. *In: Climate Change 2007: The Physical Science Basis. Contribution of Working Group I to the Fourth Assessment Report of the Intergovernmental Panel on Climate Change [Solomon, S., D. Qin, M. Manning, Z. Chen, M. Marquis, K.B. Averyt, M. Tignor and H.L. Miller (eds.)]. Cambridge University Press, Cambridge, United Kingdom and New York, NY, USA*. 67

[10] Blum, M.D. & Roberts, H.H. (2009). Restoration Sedimentology. *Nature Geoscience, Vol. 2 (July 2009), pp. 488-491*. 2, 53, 65, 103, 113

[11] Blum, M.D. & Roberts, H.H. (2009). Restoration Sedimentology - Supplementary Information. *Nature Geoscience, www.nature.com/naturegeoscience*.

[12] Bos, M.F.M. (2011). The Morphological Effects of Sediment Diversions on the Lower Mississippi River. *MSc Thesis, Delft University of Technology*. 11, 150

[13] Bosboom, J. & Stive, M.J.F. (2012). Coastal Dynamics I. *Lecture Notes CIE4305, Delft University of Technology*.

[14] Bundesministerium fuer Umwelt und Naturschutz (2004). Flussgebietseinheit Rhein - Anlage 4. Online: `http://www.bmu.de/fileadmin/bmu-import/files/pdfs/allgemein/application/pdf/wrrl_bericht_umsetzung_anlage04.pdf`, [Accessed 28-May-2013]. 1

[15] Burchard, H. & Baumert, H. (1998). The Formation of Estuarine Turbidity Maxima due to Density Effects in the Salt Wedge. A Hydrodynamic Process Study. *Journal of physical oceangraphy, Feb 1998 (309-321).* 27

[16] Burchard, H. & Hetland, R.D. (1993). The Importance of Suppression of Turbulence by Stratification on the Estuarine Turbidity Front. *Estuaries 16 (1), 113-125*. 27

[17] Burchard, H. & Hetland, R.D. (2010). Quantifying the Contributions of Tidal Straining and Gravitational Circulation to Residual Circulation in Periodically Stratified Tidal Estuaries. *Journal of Physical Oceanography 40:6, 1243-1262, Online publication date: 1-Jun-2010.*. 27

[18] Crosato, A. (2012). River Morphodynamics - Morphological Response at the Reach Scale. *Lecture Notes LN0381 , UNESCO IHE, Delft, The Netherlands*. 70, 133

[19] CWPPRA (2013). Coastal Wetlands Planning, Protection and Restoration Act. Online: (`http://lacoast.gov/new/About/Default.aspx`)., [Accessed 17-July-2013]. 3, 39, 40

[20] Day, J.W., Boesch, D.F., Clairain, E.J., Kemp, G.P., Laska, S.B., Mitsch, W.J., Orth, K., Mashriqui, H., Reed, D.J., Shabman, L., Simenstad, C.A., Streever, B.J., Twilley, R.R., Watson, C.C., Wells, J.T. & Whigham, D.F. (2007). Restoration of the Mississippi Delta: Lessons from Hurricanes Katrina and Rita. *Science Magazine, v. 315, pp. 1679-1684*. 104

[21] Dean, R.G., Wells, J.T., Fernando, J. & Goodwin, P. (2012). River Diversions: Principles, Processes, Challenges and Opportunities - A Guidance Document. *U.S. Army Corps of Engineers, State of Louisiana, U.S. Geological Service*. 43

[22] Deltares (2012). Delft3D-FLOW User Manual, Version 3.15.25157 - Simulation of Multi-Dimensional Hydrodynamic Flows and Transport Phenomena, including Sediments. Online: (`http://oss.deltares.nl/documents/183920/185723/Delft3D-FLOW_User_Manual.pdf`)., [Accessed 28-May-2013]. xv, 8, 9, 29, 122, 123, 124, 126, 127, 132, 140, 146, 152, 154

[23] Dokka, R.K., Sella, G.F. & H., D.T. (2006). Tectonic Control of Subsidence and Southward Displacement of Southeast Louisiana with respect to Stable North America. *Geophysical Research Letters 33: L23308.*. 67

[24] Donnell, B.P., Letter, J.V.J. & Teeter, A.M. (1991). The Atchafalaya River Delta. *Report 11, Two Dimensional Modeling, Technical Report HL-82-15, US Army Engineer Waterways Experiment Station, Vicksburg, MS.*.

[25] Edmonds, D.A. (2012). Restoration Sedimentology. *Nature Geoscience, Vol. 5 (November 2012), pp. 758-759*. 41

[26] EPA (2013). United States Environmental Protection Agency - Wetlands Definitions. Online: (`http://water.epa.gov/lawsregs/guidance/wetlands/definitions.cfm`)., [Accessed 17-July-2013]. 39

[27] Filippo, S. (2010). Mississippi River Sediment Avaiability Study: Summary of Available Data. Online: (`http://www.dtic.mil/cgi-bin/GetTRDoc?AD=ADA527428`)., [Accessed 28-May-2013]. 110

[28] Fisk, H.N. (1944). Geological Investigation of the Alluvial Valley of the Lower Mississippi River. *US Army Corps of Engineers, Mississippi River Commission, Vicksburg, MS, 78 pp.*.

[29] Fisk, H.N. (1955). Sand Facies of Recent Mississippi Delta Deposits. *World Petroleum Congress, 4th, Rome, Proc. sec. 1, pp. 377-398*.

[30] Frazier, D.E. (1967). Recent Deltaic Deposits of the Mississippi River: Their Development and Chronology. *Gulf Coast Assoc. Geol. Socs. Trans, v. 17, pp. 377-398*.

[31] Galler, J.J. & Allison, M.A. (2008). Estuarine Controls on Fine-Grained Sediment Storage in the Lower Mississippi and Atchafalaya Rivers. *Geological Society of America Bulletin 120, (386-398)*. 21

[32] Galloway, W.E. (1975). Process Framework for Describing the Morphologic and Stratigraphic Evolution of Deltaic Depositional Systems. *Broussard, M. L., Editor, Deltas: Models for Exploration, Houston Geological Society, (1975), pp. 87-98*. 104

[33] Google Earth (2013). Version 7.1.1.1888, Louisiana, United States of America. Online: (http://www.earth.google.com)., [Accessed 13-May-2013]. 1, 7

[34] Heer, de, A. & Mosselman, E. (2004). Flow Structure and Beload Distribution at Alluvial Diversions. Online: (http://www.deltares.nl/xmlpages/TXP/files?p_file_id=21164)., [Accessed 09-July-2013]. 42, 43, 77, 91, 144

[35] Keown, M.P., Dardeau, E.A. & Causey, E. (1981). Characterization of the Suspended Sediment Regime and Bed Material Gradation of the Mississippi River Basin. *US Army Corps of Engineers, Lower Mississippi Valley Div., Potamology Program (P-1), 2 volumes*.

[36] Keown, M.P., Dardeau, E.A. & Causey, E. (1986). Historic Trends in the Sediment Flow Regime of the Mississippi River. *Water Resources Res., 22: pp. 1555-1564*.

[37] Kesel, R.H. (1988). The Decline in the Suspended Load of the Lower Mississippi River and its Influence on Adjacent Wetlands. *Environ Geol Water Sci Vol. 11, No. 3, pp. 271-281*. 113

[38] Kesel, R.H. (2003). Human Modifications to the Sediment Regime of the Lower Mississippi Flood Plain. *Geomorphology 56 (2003), pp. 325-334*. 113

[39] Kim, W., Mohrig, D., Twilley, R., Paolo, C. & Parker, G. (2008). Land Building in the Delta of the Mississippi River: Is it Feasible? *Chapter 10. In, R.R. Twilley (ed.), Coastal Louisiana Ecosystem Assessment & Restoration (CLEAR) Program: A tool to support coastal restoration. Volume IV. Final Report to Department of Natural Resources, Coastal Restoration Division, Baton Rouge, LA. Contract No. 2512-06-02.*. 2, 53, 67

[40] Kim, W., Mohrig, D., Twilley, R., Paolo, C. & Parker, G. (2008). Modeling of Land Building in the Mississippi Delta: A Template for Reconstruction. Online: (http://hydrolab.illinois.edu/people/parkerg/_private/MississippiAAAS-GP-Feb08Comp.ppt)., [Accessed 09-July-2013]. 3, 48

[41] Kolker, A.S., Miner, M.D. & Weathers, H.D. (2012). Depositional Dynamics in a River Diversion Receiving Basin: The Case of the West Bay Mississippi River Diversion. *Estuarine, Coastal and Shelf Science 106 (2012), pp. 1-12*.

[42] Lely, M.S. (2007). Hydraulic Roughness in Sediment-Laden Flow. *MSc Thesis, Delft University of Technology*. 27

[43] Little, C.D. (2010). Mississippi River Geomorphology and West Bay Diversion. *2nd Joint Federal Interagency Conference, Las Vegas, NV, June 27 - July 1, 2010, pp. 1-12*.

[44] Meade, R.e. (1995). Contaminants in the Mississippi River. *1987-92. Reston, VA: US Geological Survey, Circular 1133, 1995*. 114

[45] Melman, F.C.R., Mosselman, E., Jiminez Osorio, J.L. & Montes Arboleda, A. (2012). Numerical Exploration of Navigability in Anabranches around a Large Fluvial Island. *River Flow 2012 - Murillo (Ed.), Taylor & Francis Group, London, pp. 749 - 754.*. 43, 144

[46] Meselhe, E.A., Georgiou, I., Allison, M.A. & McCorquodale, J.A. (2012). Numerical Modeling of Hydrodynamics and Sediment Transport in Lower Mississippi at a Proposed Delta Building Diversion. *Journal of Hydrology 472-473 (2012) pp. 340 - 354.*. 20, 46

[47] Mossa, J. (1996). Sediment Dynamics in the Lowermost Mississippi River. *University of Florida, FL, Engineering Geology 45, pp. 457-479*. 21, 22

[48] Mosselman, E. (2004). Morphology of River Bifurcations: Theory, Field Measurements and Modelling. Online: (`http://www.deltares.nl/xmlpages/TXP/files?p_file_id=21216`)., [Accessed 09-July-2013].

[49] Mosselman, E. (2012). River Dynamics. *Lecture Notes CT5311, Delft University of Technology, Delft, The Netherlands*. 132

[50] National Research Council (1987). National Academies Press, Washington, D.C., 160 pp. *Responding to Changes in Sea Level: Engineering Implications.*. 67

[51] Nguyen, A.D. (2008). Salt intrusion, Tides and Mixing in Multi-Channel Estuaries. *Dissertation, UNESCO-IHE, Taylor & Francis/ Balkema, Leiden, the Netherlands*. 121

[52] Nijs, de, M., Pietrzak, J.D. & Winterwerp, J.C. (2011). Advection of the Salt Wedge and Evolution of the Internal Flow Structure in the Rotterdam Waterway. *Journal of physical oceangraphy, 41 (Jan 2011)*. 27, 122

[53] Parker, G. (2009). Modeling the Morphodynamics of the Lower Mississippi River as a Quasi-Bedrock Stream. Online: (`http://www.wun.ac.uk/sites/default/files/mississippimodelbedrockwun-09.pdf`)., [Accessed 28-May-2013]. 20, 21

[54] Pegasos Project (2013). Dynamics of Mud Transport. Online: (`http://www.pegasoproject.eu/wiki/Dynamics_of_mud_transport`)., [Accessed 28-May-2013]. 137

[55] Pietrzak, J. (2012). Stratified Flows. *Lecture Notes CIE 5302, Delft University of Technology, Delft, The Netherlands*. 121

[56] Reed, D.J. (2009). A new Approach to River Managment: Action for a Sustainable Coastal Landscape. *Universities Council on Water Resources, Journal of Contemporary Water Research and Education (March 2009), Issue 141, pp. 35-38*.

[57] Restore Or Retreat (2013). Third Delta Conveyance. Online: (`http://www.restoreorretreat.org/solution_third_delta_conveyance.php`)., [Accessed 28-May-2013]. 52

[58] Restore the Mississippi River Delta (2012). Coastal Masterplan 2012. Online: (`http://www.mississippiriverdelta.org/restore-the-delta/public-policy/2012-coastal-master-plan/`)., [Accessed 17-Oct-2013]. 40

[59] Saucier, R.T. (1984). Quartenary Geology of the Lower Mississippi Valley. *Arkansas Archeological Survey, Research Series No.6*. 103

[60] Sherwood, Gagliano, Karen & Wicker (2009). Third Delta Conveyance Channel: A New Branch for The Mississippi River. Presentation at The Diversion Summit Bourbon Orleans Hotel New Orleans, La. March 3-5, 2009. Online: (`http://155.76.244.234/lcast/pdfs/09mar/Gagliano%20-%20Third%20Delta%20Conveyance%20Channel.pdf`)., [Accessed 28-May-2013]. 52

[61] Shinkle, K.D. & Dokka, R.K. (2004). Rates of Vertical Displacement at Benchmarks in the Lower Mississippi Valley and the Northern Gulf Coast. *NOAA Technical Report NOS/NGS 50., 135 pp.*. 67

[62] Shinkle, K.D. & Dokka, R.K. (2004). Rates of Vertical Displacement at Benchmarks in the Lower Mississippi Valley and the Northern Gulf Coast, NOAA Technical Report NOS/NGS 50. Online: (`http://www.ngs.noaa.gov/heightmod/NOAANOSNGSTR50.pdf`)., [Accessed 28-May-2013]. 14

[63] Smith, L.M. & Winkley, B.R. (1996). The Response of the Lower Mississippi River to River Engineering. *Engineering Geology 45 (1996) pp. 433-455*. 2, 106, 107, 109, 110, 111, 113

[64] Snedden, G.A., Cable, J.E., Swarzenski, C. & Swenson, E. (2007). Sediment Discharge into a Subsiding Louisiana Deltaic Estuary through a Mississippi River Diversion. *Estuarine, Coastal and Shelf Science 71 (2007), pp. 181-193*.

[65] Soileau, C.W., Garrett, B.J. & Thibodeaux, B.J. (1989). Drought Induced Saltwater Intrusion on the Mississippi River. *Proceedings of Coastal Zone 1989 Conference, ASCE*. 17, 18, 27

[66] Spraul, M. (2012). Mississippi River - Baton Rouge to the Gulf. Online: (`http://www.propclubnola.org/events/2012Convention/presentations/Mississippi`)., [Accessed 28-May-2013]. 111, 112

[67] Spraul, M. (2012). New Orleans District - Dredging Schedule, FY 2012. Spraul, Michelle, Operations Manager, USACE, New Orleans District. Online: (`http://operations.usace.army.mil/nav/11OctWEDA/11_Oct_2011_MVD.pdf`)., [Accessed 28-May-2013]. 33

[68] Spraul, M. (2013). FY 2013 Maintenance Dredging Mississippi River, Baton Rouge to the Gulf, Deep Draft Crossings. Spraul, Michelle, Operations Manager, USACE, New Orleans District. Online: (`http://www2.mvn.usace.army.mil/od/FY%2013%20MS%20DEEP%20DRAFT1.pdf`)., [Accessed 28-May-2013]. 33

[69] Spraul, M. (2013). FY 2013 Maintenance Dredging Mississippi River, Baton Rouge to the Gulf, Southwest Pass. Spraul, Michelle, Operations Manager, USACE, New

Orleans District. Online: (http://www2.mvn.usace.army.mil/od/FY%2013%20SWP.pdf)., [Accessed 28-May-2013]. 33

[70] Spraul, M. (2013). New Orleans District - Dredging Schedule, FY 2013. Spraul, Michelle, Operations Manager, USACE, New Orleans District. Online: (http://operations.usace.army.mil/nav/12octWEDA/FY13MVN_DredgingSchedule_EasternChapter.pdf)., [Accessed 28-May-2013]. 33

[71] State of Louisiana (2013). LouisianaâĂŹs Comprehensive Master Plan for a Sustainable Coast. Online: (http://www.lacpra.org/assets/docs/2012%20Master%20Plan/Final%20Plan/2012%20Coastal%20Master%20Plan.pdf)., [Accessed 17-Oct-2013]. 40, 46

[72] The New York Times (1991). Corps of Engineers Struggles to Alter Mississippis Fate. Online: (http://155.76.244.234/lcast/pdfs/09mar/Gagliano%20-%20Third%20Delta%20Conveyance%20Channel.pdf)., [Accessed 28-May-2013]. 53

[73] Thorne, C., Harmar, O., Watson, C., Clifford, N., Biedenharn, D. & Measures, R. (2008). Current and Historical Sediment Loads in the Lower Mississippi River. *Final Report, European Research Office of the U.S. Army, London, England, pp. 181-193*. 2

[74] United States Army Corps of Engineers (2003). Hydrodynamic and Sediment Transport Modeling of Deltaic Sediment Processes. *Dissertation, Department of Civil and Environmental Engineering, Louisiana State University, Baton Rouge.*.

[75] United States Army Corps of Engineers (2009). Water Resource Policies and Authorities Incorporating Sea-Level Change Considerations in Civil Works Programs. *Circular No. 1165-2-211.*. 67

[76] United States Army Corps of Engineers (2011). Water Resource Policies and Authorities Incorporating Sea-Level Change Considerations in Civil Works Programs. *Circular No. 1165-2-212., 32 pp.*. 67

[77] United States Army Corps of Engineers (2013). Bird's Point - New Madrid Floodway. Online: (http://www.mvm.usace.army.mil/Readiness/bpnm/bpnminfo.asp)., [Accessed 4-April-2013]. 109

[78] United States Army Corps of Engineers (2013). Morganza Floodway. Online: (`http://www.mvn.usace.army.mil/bcarre/morganza.asp`)., [Accessed 4-April-2013]. 109

[79] United States Army Corps of Engineers (2013). The Mississippi Drainage Basin. Online: (`http://www.mvn.usace.army.mil/Missions/MississippiRiverFloodControl/MississippiRiverTributaries/MississippiDrainageBasin.aspx`)., [Accessed 28-May-2013]. 106

[80] United States Army Corps of Engineers (2013). Water Level Data from River Gages. Online: (`http://www2.mvn.usace.army.mil/eng/edhd/wcontrol/miss.asp`)., [Accessed 28-May-2013]. 15, 24

[81] US Interagency Committee on Water Resources, Subcommittee on Sedimentation (1957). Some Fundamentals of Particle Size Analysis. *Report no. 12, St. Anthony Falls Hydraulic Laboratory, Minneapolis, Minnesota*. 146

[82] Vriend, de, H.J., Havinga, H., Prooijen, van, B.C., Visser, P.J. & Wang, Z.B. (2011). River Engineering. *Lecture Notes CT4345, Delft University of Technology, Delft, The Netherlands*. 135

[83] Winer, H.S. (2011). Re-Engineering the Mississippi River as a Sediment Delivery System. *Journal of Coastal Research: Special Issue 59: pp. 229 - 234.*. 46, 50, 51, 52

[84] Winterwerp, J.C. (2008). Stratification Effects by Cohesive and Noncohesive Sediment. *Journal of Geophysical Research: Oceans (1978 - 2012) Volume 106, Issue C10, pages 22559 - 22574, 15 October 2001*.

[85] Winterwerp, J.C. (2012). Cohesive Sediment. *Presentation Coastal Dynamics II CIE4309, Delft University of Technology, Delft, The Netherlands*. 137, 138

Declaration

I hereby declare that this thesis and the work reported herein was composed by and originated entirely from me. Information derived from the published and unpublished work of others has been acknowledged in the text and references are given in the list of sources.

Delft, 30.10.2013